5 Frequency-Domain Lifetime Measurements

In the preceding chapter we described the theory and instrumentation for measuring fluorescence intensity decays using time-domain measurements. In the present chapter we continue this discussion, but describe frequency-domain fluorometry. In this method the sample is excited with light that is intensity modulated at a high frequency comparable to the reciprocal of the lifetime. When this is done, the emission is intensity modulated at the same frequency. However, the emission does not precisely follow the excitation, but rather shows time delays and amplitude changes that are determined by the intensity decay law of the sample. The time delay is measured as a phase angle shift between the excitation and emission, as was shown in Figure 4.2. The peak-to-peak height of the modulated emission is decreased relative to the modulated excitation, and provides another independent measure of the lifetime.

Time-resolved measurements, whether performed in the time domain or in the frequency domain, provides information about intensity decay of the sample. Samples with multiple fluorophores typically display multi-exponential decays. Even samples with a single fluorophore can display complex intensity decays due to conformational heterogeneity, resonance energy transfer, and transient effects in diffusive quenching or fluorophore–solvent interactions, to name just the most common origins. The goal of the time-resolved measurement is to determine the form of the intensity decay law, and to interpret the decay in terms of molecular features of the sample.

Intensity decays can be single-exponential, multi-exponential, or non-exponential. Irrespective of the complexity of the decay, one can always define a mean or apparent decay time. For a single exponential decay in the time domain the actual lifetime is given by this the time when the intensity decays to 1/e of its initial value. For a multi-exponential decay, the 1/*e* time is typically not equal to any of the decay times. In the frequency domain an apparent lifetime (τ_ϕ) determined from the phase angle (ϕ_ω) or the apparent lifetime (τ_m) determined from the modulation (m_ω, eqs. 4.5 and 4.6). The apparent lifetimes are characteristic of the sample, but do not provide a complete description of the complex intensity decay. The values of τ_ϕ and τ_m need not be equal, and each value represents a different weighted average of the decay times displayed by the sample. In general, the apparent lifetime depends on the method of measurement. The earlier literature on time-resolved fluorescence often describes apparent lifetimes. At present, there are relatively few reports of only the mean decay times. This is because the mean lifetimes represent complex weighted averages of the multi-exponential decay. Quantitative interpretation of mean decay times is usually difficult and the results are often ambiguous.

Prior to 1983, frequency-domain fluorometry allowed determination of mean lifetime, but was not able to resolve complex intensity decays. This limitation was the result of phase-modulation fluorometers, which only operated at one, two, or three fixed light modulation frequencies. The resolution of a complex decay requires measurements at a number of modulation frequencies that span the frequency response of the sample. While several variable-frequency instruments were described prior to 1983, these were not generally useful and were limited by systematic errors. The first generally useful variable frequency instrument was described in the mid 1980s.[1–2] These instruments allowed phase and modulation measurements from 1 to 200 MHz. These designs are the basis of currently available instruments. Frequency-domain fluorometry is now in widespread use,[3–9] and instruments are commercially available. Frequency-domain fluorometers are now routinely used to study multi-exponential intensity decays, and non-exponential decays resulting from resonance energy transfer, time-dependent solvent relaxation, and collisional quenching.

In this chapter we describe the instrumentation for FD measurements and the theory used to interpret the experimental data. We will describe examples that illustrate the

applications of the FD method for the resolution of complex decay kinetics. We describe the present state-of-the-art instrumentation, which allows FD data to be obtained to 10 GHz, depending upon the photodetector and associated electronics. We will describe the newer simple FD instrumentation based on laser diodes (LD) or light-emitting diodes (LED) as the excitation source.

The objective of both the time- and frequency-domain measurements is to recover the parameters describing the time-dependent decay. Assume that the sample is excited with a δ-function pulse of light. The resulting time-dependent emission is called the impulse response function, which is often represented by the multi-exponential model:

$$I(t) = \sum_i \alpha_i e^{-t/\tau_i} \tag{5.1}$$

In this expression the values of α_i are the pre-exponential factors and the τ_i values the decay times.

If the emission decays with a single decay time (Figure 5.1), it is rather easy to measure the decay time with good accuracy. If the single decay time is long relative to the excitation pulse, then log $I(t)$ decays linearly versus time, and the decay time is easily obtained from the slope. The more difficult task is recovery of multiple decay times, which is illustrated for two widely spaced decay times in Figure 5.1 (5 and 20 ns). In this case, log $I(t)$ does not decay linearly with time. Unfortunately, decay times of the emission from macromolecules are often more closely spaced than the fivefold difference shown in Figure 5.1, and resolution of the decay times becomes increasingly difficult as the decay times become more closely spaced. If the decay times are spaced by 20% (e.g., 5 and 6 ns or 10 and 12 ns), it is difficult to visually distinguish a single-exponential decay from a double-exponential decay. In fact, such closely spaced decay times cannot usually be resolved using TD or FD measurements. It is generally difficult to resolve sums of exponentials because the parameters describing the decay are highly correlated. Hence, one requires a high signal-to-noise ratio, or equivalently a large number of photons, to recover the multiple decay times with reasonable confidence.

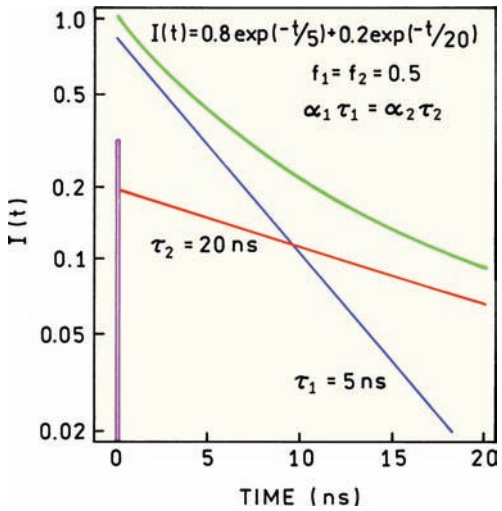

Figure 5.1. Impulse response function for decay times of 5 and 20 ns, and for a multi-exponential decay with the same decay times.

It is valuable to understand how a multi-exponential decay is related to the steady-state intensity of the same sample. The fraction of the intensity observed in the usual steady-state measurement due to each component in the multi-exponential decay is

$$f_i = \frac{\alpha_i \tau_i}{\sum_j \alpha_j \tau_j} \tag{5.2}$$

The contribution of any decay component to the steady-state intensity is proportional to the ατ product for this component. This can be understood by visualizing the area under an intensity decay, which is proportional to the ατ product (Figure 5.1).

Intensity decays are routinely analyzed in terms of the multi-exponential model. However this does not mean that the values of α_i and τ_i have any physical meaning. The multi-exponential model is very powerful and able to account for almost any decay law. Depending upon the sample, the values of α_i and τ_i may have direct or indirect molecular significance. For a mixture of two fluorophores, each of which displays a single decay time, τ_i are the decay times of the two fluorophores, and f_i are the fractional contributions of each fluorophore to the total emission. In many circumstances there is no obvious linkage between the α_i and τ_i values and the molecular features of the sample. For instance, non-exponential decays occur due to transient effects in quenching, or due to distributions of donor–acceptor distances. These intensity decays can usually be satisfactorily fit by the multi-exponential model, for such decays it is difficult to relate the values of α_i and τ_i to the molecular parameters of the sample.

5.1. THEORY OF FREQUENCY-DOMAIN FLUOROMETRY

In frequency-domain fluorometry the excitation source and measurements are rather different than for time-domain

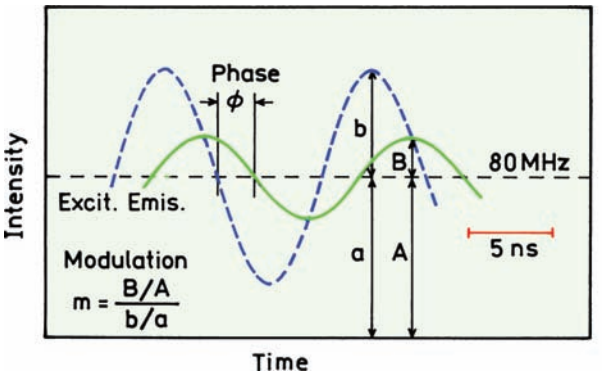

Figure 5.2. Definitions of the phase angle and modulation of emission. The assumed decay time is 5 ns and the light modulation frequency is 80 MHz.

measurements. In time-domain measurements the excitation source is a pulsed light source. In frequency-domain measurements the excitation is an intensity-modulated light source.[3] Because of the time lag between absorption and emission, the emission is delayed in time relative to the modulated excitation (Figure 5.2). The delay is measured as a phase shift ϕ_ω between the excitation and emission, where ω is the modulation frequency in radians/s. The finite time response of the sample also results in demodulation of the emission by a factor m_ω. The finite lifetime of the excited state prevents the emission from precisely following the excitation. This results in a decrease in the peak-to-peak amplitude of the modulated emission, which is measured relative to the modulated excitation (Figure 5.2).

The phase shift and modulation of the emission depend on the relative values of the lifetime and the light modulation frequency. This is shown in Figure 5.3 for a decay time of 5 ns and modulation frequencies of 2.5, 25, and 250 MHz. As the light modulation frequency increases, the phase shift of the emission increases and the modulation of the emission decreases. The dependence of the phase angle ϕ and modulation m on the light modulation frequency is used to recover the intensity decay of the sample.

The origin of the phase shift and demodulation can be understood by considering the time-dependent excitation intensity and the time of intensity decay of the fluorophore. Figure 5.4 shows a 10-ns intensity decay superimposed on the modulated excitation. Consider the fluorophores that are excited when the intensity is at its maximum (t = 0). If the modulation frequency is 2.5 MHz, a full cycle is 400 ns long. On this timescale the intensity decay is barely visible. For this reason the emission closely follows the excitation with a minimal phase shift and nearly complete modulation. Now consider modulation at 250 MHz, where a cycle is 4

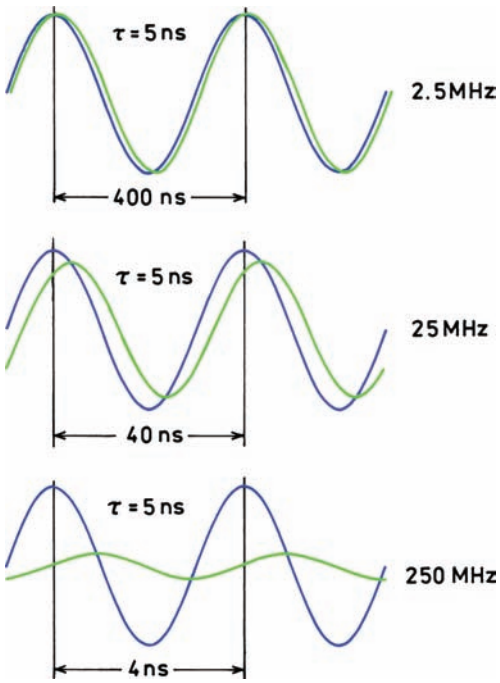

Figure 5.3. Emission of a 5-ns decay time fluorophore in response to sinusoidally modulated excitation at 2.5, 25, and 250 MHz.

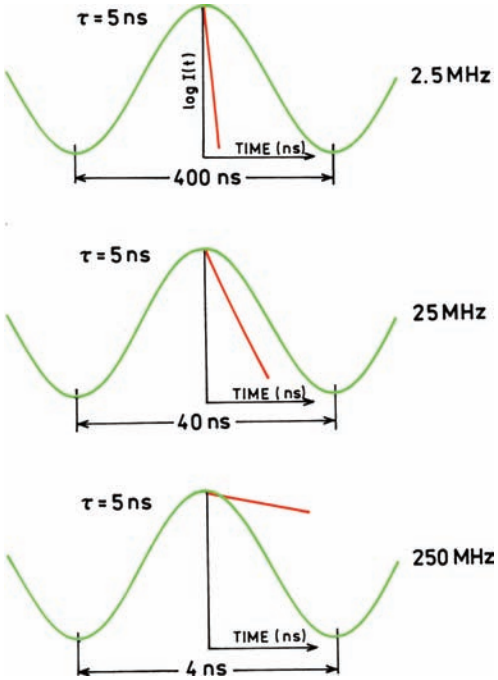

Figure 5.4. Comparison of a 5-ns intensity decay with light modulation frequencies of 2.5, 25, and 250 MHz. The time axis of the inserts are the same as for the modulated intensity.

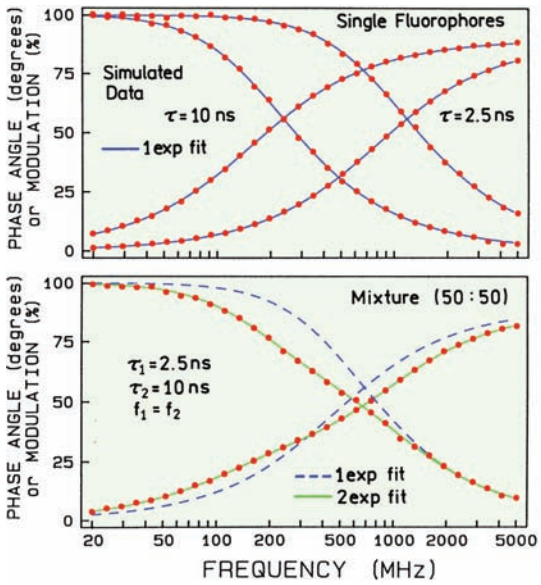

Figure 5.5. Simulated frequency-domain data for single- (top) and double- (bottom) exponential decays. The phase angle increases and the modulation decreases with increasing modulation frequency. The datapoints indicate the simulated data. **Top**: The solid lines show the best fits to a single decay time. **Bottom**: The dashed and solid lines show the best single- and double-exponential fits, respectively.

ns long. In this case the molecules excited at the peak of the intensity continue to emit during the entire modulation cycle. This results in an averaging of the decay across the peaks and valleys of the excitation. This averaging results in the phase shift and decrease in modulation of the emission. At an intermediate modulation frequency of 25 MHz some averaging occurs, but to a lesser extent than at 250 MHz.

In FD measurements the phase angle and modulation are measured over a wide range of frequencies. These data are called the frequency response of the sample. The characteristic features of the frequency response of a sample are illustrated in Figure 5.5 (top) for a single exponential decay. As the light modulation frequency is increased the phase angle increases from 0 to 90°. At first glance the 90° phase angle limit is counterintuitive. For a time delay of the type available from an optical delay line, the phase shift can exceed 90° and reach any arbitrary value. For a single exponential or multi-exponential decay, the maximum phase angle is 90°. Hence the phase angle displayed by any sample is some fraction of 90°, independent of the modulation frequency. Only under special circumstances can the phase angle exceed 90° (Chapter 17).

The modulation of the emission also depends on the modulation frequency of the incident light. As the frequency increases the modulation decreases from 1.0 to 0. The modulation of the emission is zero when the frequency is much larger than the emission rate. In presenting frequency-domain data, the modulation frequency on the *x*-axis (Figure 5.5) is usually described in cycles/s (Hz or MHz). The circular modulation frequency ($\omega = 2\pi$ x Hz) in radians/s is used for calculations.

The shape of the frequency response is determined by the number of decay times displayed by the sample. If the decay is a single exponential (Figure 5.5, top), the frequency response is simple. One can use the phase angle or modulation at any frequency to calculate the lifetime. For a single-exponential decay, the phase and modulation are related to the decay time (τ) by

$$\tan \phi_\omega = \omega\tau \tag{5.3}$$

and

$$m_\omega = (1 + \omega^2\tau^2)^{-1/2} \tag{5.4}$$

The derivation of eqs. 5.3 and 5.4 is given in Section 5.11. For the 10-ns decay time, the phase shift at 20 MHz is 51.5°, and the emission is demodulated by a factor of 0.62 relative to the excitation. At a modulation frequency of 100 MHz the phase angle increases to 81°, and the modulation decreases to 0.16. Most samples of interest display more than one decay time. In this case the lifetimes calculated from the value of ϕ_ω or m_ω, measured at a particular frequency, are only apparent values and are the result of a complex weighting of various components in the emission (Section 5.10). For such samples it is necessary to measure the phase and modulation values over the widest possible range of modulation frequencies.

The frequency response has a different shape for a multi-exponential decay (Figure 5.5, bottom). In this simulation the assumed decay times are 2.5 and 10 ns. The shape of the frequency response is used to determine the form of the intensity decay. This is generally accomplished using nonlinear least-squares procedures.[10–13] The fitting procedure is illustrated by the solid and dashed lines in Figure 5.5. For the single-exponential decays shown in the top half of the figure, it is possible to obtain a good match between the data (●) and the curves calculated using the single-exponential model (solid line). For a double-exponential decay, as shown in the bottom half of the figure, the data cannot be matched using a single-decay time fit, represented by the dashed lines. However, the complex frequency response is accounted for by the double-exponential model,

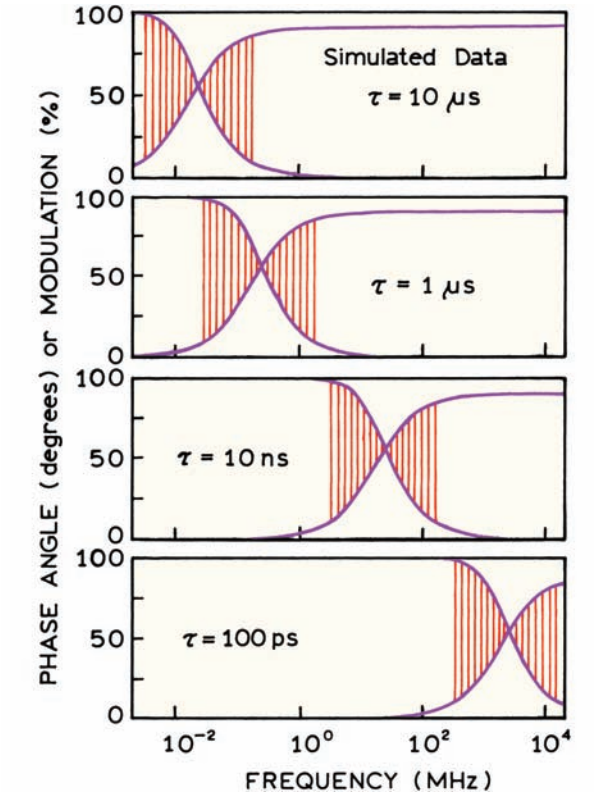

Figure 5.6. Relationship between the decay time and the useful range of light modulation frequencies.

represented by the solid lines, with the expected decay times (2.5 and 10 ns) and fractional intensities ($f_1 = f_2 = 0.5$) being recovered from the least-squares analysis.

The range of modulation frequencies needed to recover the intensity decay depends on the lifetimes. The useful modulation frequencies are those where the phase angle is frequency dependent, and there is still measurable modulation (Figure 5.6). Most fluorophores display lifetimes near 10 ns, so that modulation frequencies are typically near 2–200 MHz. If the decay time is near 100 ps, higher modulation frequencies near 2 GHz are needed. For longer decay times of 1 to 10 μs the modulation frequencies can range from 10 kHz to 1 MHz. As the modulation frequency increases, the modulation of the emission decreases. Hence it becomes more difficult to measure the phase angles as they approach 90°.

5.1.1. Least-Squares Analysis of Frequency-Domain Intensity Decays

The procedures used to analyze the frequency-domain data are analogous to those used for TCSPC. The frequency-domain data are usually analyzed by the method of nonlinear least squares.[10–13] The measured data are compared with values predicted from a model, and the parameters of the model are varied to yield the minimum deviations from the data. The phase and modulation values can be predicted for any decay law. This is accomplished using sine and cosine transforms of the intensity decay $I(t)$:

$$N_\omega = \frac{\int_0^\infty I(t) \sin \omega t \, dt}{\int_0^\infty I(t) \, dt} \tag{5.5}$$

$$D_\omega = \frac{\int_0^\infty I(t) \cos \omega t \, dt}{\int_0^\infty I(t) \, dt} \tag{5.6}$$

where ω is the circular modulation frequency (2π times the modulation frequency in Hz). The denominator $J = \int_0^\infty I(t) \, dt$ normalizes the expression for the total intensity of the sample. These expressions are valued for any intensity decay law, whether the decay is multi-exponential or non-exponential. Non-exponential decay laws can be transformed numerically. For a sum of exponentials the transforms are[12–13]

$$N_\omega = \sum_i \frac{\alpha_i \omega \, \tau_i^2}{(1 + \omega^2 \tau_i^2)} \Big/ \sum_i \alpha_i \tau_i \tag{5.7}$$

$$D_\omega = \sum_i \frac{\alpha_i \tau_i}{(1 + \omega^2 \tau_i^2)} \Big/ \sum_i \alpha_i \tau_i \tag{5.8}$$

For a multi-exponential decay $J = \Sigma_i \alpha_i \tau_i$, which is proportional to the steady-state intensity of the sample. Because of this normalization factor one can always fix one of the amplitudes (α_i or f_i) in the analysis of frequency-domain data. The calculated frequency-dependent values of the phase angle ($\phi_{c\omega}$) and the demodulation ($m_{c\omega}$) are given by

$$\tan \phi_{c\omega} = N_\omega / D_\omega \tag{5.9}$$

$$m_{c\omega} = (N_\omega^2 + D_\omega^2)^{1/2} \tag{5.10}$$

In the least-squares analysis the parameters (α_i and τ_i) are varied to yield the best fit between the data and the calcu-

lated values, as indicated by a minimum value for the goodness-of-fit parameters χ_R^2:

$$\chi_R^2 = \frac{1}{\nu}\sum_{\omega}\left[\frac{\phi_\omega - \phi_{c\omega}}{\delta\phi}\right]^2 + \frac{1}{\nu}\sum_{\omega}\left[\frac{m_\omega - m_{c\omega}}{\delta m}\right]^2 \quad (5.11)$$

where ν is the number of degrees of freedom. The value of ν is given by the number of measurements, which is typically twice the number of frequencies minus the number of variable parameters. The subscript c is used to indicate calculated values for assumed values of α_i and τ_i, and $\delta\phi$ and δm are the uncertainties in the phase and modulation values, respectively. Unlike the errors in the photon-counting experiments (Chapter 4), these errors cannot be estimated directly from Poisson statistics.

The correctness of a model is judged based on the values of χ_R^2. For an appropriate model and random noise, χ_R^2 is expected to be near unity. If χ_R^2 is sufficiently greater than unity, then it may be correct to reject the model. Rejection is judged from the probability that random noise could be the origin of the value of χ_R^2.[10,11] For instance, a typical frequency-domain measurement from this laboratory contains phase and modulation data at 25 frequencies. A double-exponential model contains three floating parameters (two τ_i and one α_i), resulting in 47 degrees of freedom. A value of χ_R^2 equal to 2 is adequate to reject the model with a certainty of 99.9% or higher (Table 4.2).

In practice, the values of χ_R^2 change depending upon the values of the uncertainties ($\delta\phi$ and δm) used in its calculation. The effects of selecting different values of $\delta\phi$ and δm has been considered in detail.[12–13] The fortunate result is that the recovered parameter values (α_i and τ_i) do not depend strongly on the chosen values of $\delta\phi$ and δm. The parameter values can be expected to be sensitive to $\delta\phi$ and δm if the data are just adequate to determine the parameter values, that is, at the limits of resolution.

For consistency and ease of day-to-day data interpretation we use constant values of $\delta\phi = 0.2°$ and $\delta m = 0.005$. While the precise values may vary between experiments, the χ_R^2 values calculated in this way indicate to us the degree of error in a particular data set. For instance, if a particular data set has poor signal-to-noise, or systematic errors, the value of χ_R^2 is elevated even for the best fit. The use of fixed values of $\delta\phi$ and δm does not introduce any ambiguity in the analysis, as it is the relative values of χ_R^2 that are used in accepting or rejecting a model. We typically compare χ_R^2 for the one-, two-, and three-exponential fits. If χ_R^2 decreases twofold or more as the model is incremented, then the data probably justify inclusion of the additional decay time. According to Table 4.3, a ratio of χ_R^2 values of 2 is adequate to reject the simpler model with a 99% certainty. It should be remembered that the values of $\delta\phi$ and δm might depend upon frequency, either as a gradual increase in random error with frequency, or as higher-than-average uncertainties at discrete frequencies due to interference or other instrumental effects. In most cases the recovered parameter values are independent of the chosen values of $\delta\phi$ and δm. However, caution is needed as one approaches the resolution limits of the measurements. In these cases the values of the recovered parameters might depend upon the values chosen for $\delta\phi$ and δm.

The values of $\delta\phi$ and δm can be adjusted as appropriate for a particular instrument. For instance, the phase data may become noisier with increasing modulation frequency because the phase angle is being measured from a smaller signal. One can use values of $\delta\phi$ and δm which increase with frequency to account for this effect. In adjusting the values of $\delta\phi$ and δm, we try to give equal weight to the phase and modulation data. This is accomplished by adjusting the relative values of $\delta\phi$ and δm so that the sum of the squared deviations (eq. 5.11) is approximately equal for the phase and modulation data.

Another way to estimate the values of $\delta\phi$ and δm is from the data itself. The phase and modulation values at each frequency are typically an average of 10 to 100 individual measurements. In principle, the values of $\delta\phi$ and δm are given by the standard deviation of the mean of the phase and modulation, respectively. In practice we find that the standard deviation of the mean underestimates the values of $\delta\phi$ and δm. This probably occurs because the individual phase and modulation measurements are not independent of each other. For simplicity and consistency, the use of constant values of $\delta\phi$ and δm is recommended.

In analyzing frequency-domain data it is advisable to avoid use of the apparent (τ_ϕ) or modulation (τ_m) lifetimes. These values are the lifetimes calculated from the measured phase and modulation values at a given frequency. These values can be misleading, and are best avoided. The characteristics of τ_ϕ and τ_m are discussed in Section 5.10.

5.1.2. Global Analysis of Frequency-Domain Data

Resolution of closely spaced parameters can be improved by global analysis. This applies to the frequency-domain data as well as the time-domain data. The use of global analysis is easiest to visualize for a mixture of fluorophores

each displaying a different emission spectrum. In this case the intensity decay at each wavelength (λ) is given by

$$I(\lambda,t) = \sum_{i=1} \alpha_i(\lambda)\, e^{-t/\tau_i} \tag{5.12}$$

where the values of $\alpha_i(\lambda)$ represent the relative contribution of the *i*th fluorophore at wavelength λ. The frequency response is typically measured at several wavelengths resulting in wavelength-dependent values of the phase angle $\phi_\omega(\lambda)$ and the modulation $m_\omega(\lambda)$. In this case the values of N_ω^λ and D_ω^λ depend on the observation wavelength, and are given by

$$N_\omega^\lambda = \sum_i \frac{\alpha_i(\lambda)\omega\tau_i^2}{1+\omega^2\tau_i^2} \Big/ \sum_i \alpha_i(\lambda)\tau_i \tag{5.13}$$

$$D_\omega^\lambda = \sum_i \frac{\alpha_i(\lambda)\omega\tau_i}{1+\omega^2\tau_i^2} \Big/ \sum_i \alpha_i(\lambda)\tau_i \tag{5.14}$$

The wavelength-dependent data sets can be used in a global minimization of χ_R^2:

$$\chi_R^2 = \frac{1}{\nu}\sum_{\lambda,\omega}\left[\frac{\phi_\omega(\lambda) - \phi_{c\omega}(\lambda)}{\delta\phi}\right]^2 + \frac{1}{\nu}\sum_{\lambda,\omega}\left[\frac{m_\omega(\lambda) - m_{c\omega}(\lambda)}{\delta m}\right]^2 \tag{5.15}$$

where the sum now extends over the frequencies (ω) and wavelengths (λ). Typically the values of τ_i are assumed to be independent of wavelength and are thus the global parameters. The values of $\alpha_i(\lambda)$ are usually different for each data set, that is, are non-global parameters. The data are normalized at each wavelength, allowing one of the amplitudes at each wavelength to be fixed in the analysis.

It is important to estimate the range of parameter values that are consistent with the data. As for TCSPC, the asymptotic standard errors (ASEs) recovered from least-square analysis do not provide a true estimate of the uncertainty, but provide a significant underestimation of the range of parameter values which is consistent with the data. This effect is due to correlation between the parameters, which is not considered in calculation of the asymptotic standard errors. Algorithms are available to estimate the upper and lower bounds of a parameter based on the extent of correlation.[14–16] If the analysis is at the limits of resolution we prefer to examine the χ_R^2 surfaces. This is accomplished just as for the time-domain data. Each parameter value is varied around its best fit value, and the value of χ_R^2 is minimized by adjustment of the remaining parameters. The upper and lower limits for a parameter are taken as those which result in an elevation of the F_χ value expected for one standard deviation ($P = 0.32$) and the number of degrees of freedom (Section 5.7.1).

5.2. FREQUENCY-DOMAIN INSTRUMENTATION

5.2.1. History of Phase-Modulation Fluorometers

The use of phase-modulation methods for measurements of fluorescence lifetimes has a long history.[17] The first lifetime measurements were performed by Gaviola in 1926 using a phase fluorometer.[18] The first suggestion that phase angle measurements could be used for measuring fluorescence lifetimes appears to have been made even earlier in 1921.[19] The use of phase delays to measure short time intervals appears to have been suggested even earlier, in 1899.[20] Hence, the use of phase shifts for timing of rapid processes has been recognized for 100 years. Since the pioneering measurements by Gaviola[18] a large number of phase-modulation instruments have been described. These include an instrument by Duschinky in 1933,[21] and an instrument of somewhat more advanced design described by Szymonowski[22], on which many of Jablonski's early measurements were performed. Phase fluorometers have been described by many research groups.[23–53] The first generally useful design appeared in 1969.[41] This instrument used a Debye-Sears ultrasonic modulator[42–43] to obtain intensity-modulated light from an arc lamp light source. The use of the Debye-Sears modulator has been replaced by electrooptic modulators in current FD instruments. However, an important feature of this instrument[41] is the use of cross-correlation detection (Section 5.11.2). The use of this radio frequency mixing method simplified measurement of the phase angles and modulation values at high frequencies, and allowed measurement of the phase angle and modulation with relatively slow timing electronics.

The primary technical factor limiting the development of frequency-domain fluorometers was the inability to obtain intensity-modulated light over a range of modulation frequencies. Debye-Sears modulators are limited to operating at the frequency of the crystal, or multiples thereof.

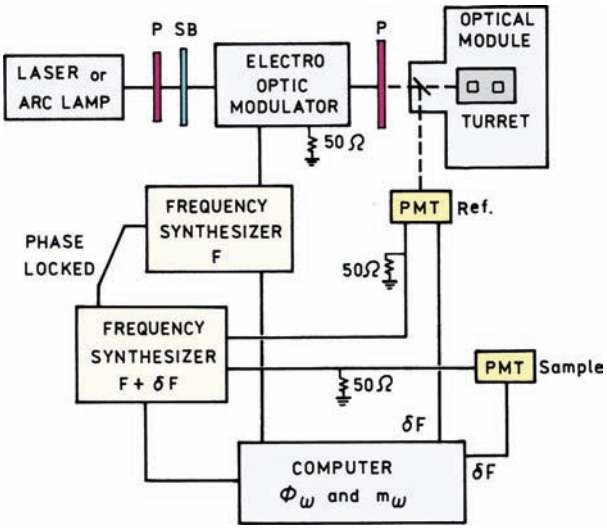

Figure 5.7. Schematic representation of the variable-frequency phase-modulation fluorometer. P, polarizer; SB, Soliel-Babinet compensator; F, frequency; δF, cross-correlation frequency; PMT, photomultiplier tube.

Consequently, the early phase-modulation fluorometers operated at only one to three fixed modulation frequencies. The limited data these instruments provided were adequate for measuring mean decay times, or for detecting the presence of a complex decay. However, the data at a limited number of modulation frequencies were not generally useful for resolution of the parameters describing multi- or non-exponential decays.

As has occurred for TCSPC, pulsed-laser diodes (LDs), and light-emitting diodes (LEDs) are becoming the preferred excitation source. The output of the LDs and LEDs can be modulated directly by the electrical input. This eliminates the need for the electrooptic modulator, which adds cost and complexity to the FD instruments.

5.2.2. An MHz Frequency-Domain Fluorometer

Frequency-domain fluorometers are now in widespread use. Most designs are similar to that shown in Figure 5.7. The main differences are the laser light source, the light modulator, and the associated radio-frequency electronics. Without the use of LDs or LEDs it is difficult to obtain light modulation over a wide range of frequencies. Amplitude modulation of laser sources over a continuous range of frequencies to 200 MHz is possible with electrooptic modulators. Light can also be modulated with acoustooptic modulators. However, acoustooptic modulators provide modulation at discrete resonances over a limited range of frequencies.[54–56] Most electrooptic modulators have long narrow optical apertures, and electrooptic modulators are not easily used with arc lamp sources. Initially, only laser sources seemed practical for use with electrooptic modulators. Surprisingly, it is now possible to use electrooptic devices to modulate arc lamps to 200 MHz, which is done in commercial FD instruments. The operational principles of the modulators and the electronic parts needed to construct such an FD instrument are discussed below, along with the rationale for selecting the various components.

The light source for an FD instrument can be almost any continuous-wave (cw) light source or a high-repetition-rate pulse laser. The choice of source is based on the needed wavelengths and power levels. The He–Cd laser is a convenient cw source, providing cw output at 325 and 442 nm. Unfortunately, these wavelengths are not suitable for excitation of protein fluorescence. A very versatile source is the Ar ion laser, which can now provide deep UV lines (~275 nm) for intrinsic fluorescent probes. However, only a limited number of UV wavelengths are available. Studies of protein fluorescence usually require 290 to 300 nm to avoid excitation of tyrosine and to obtain high fundamental anisotropies. These wavelengths are not available from an argon ion laser. The argon ion laser at 514 nm is an ideal source for pumping dye lasers. The 514 nm line can be mode-locked to synchronously pump a picosecond dye laser system (Section 4.4). An Nd:YAG laser can also be the primary source, particularly for pumping dye lasers.

Appropriate electronics are needed to measure the phase angle and modulation at high frequencies. The measurements appear difficult because the resolution of multi-exponential decays requires accuracy near 0.2° in phase and 0.5% (0.005) in modulation, and that this accuracy needs to be maintained from 1 to 200 MHz. In fact, the measurements are surprisingly easy and free of interference because of cross-correlation detection. In cross-correlation detection the gain of the detector is modulated at a frequency offset ($F + \delta F$) from that of the modulated excitation (F). The difference frequency (δF) is typically in the range of 10 to 100 Hz. This results in a low-frequency signal at δF that contains the phase and modulation information in the original high-frequency signal (Section 5.11.2). At all modulation frequencies, the phase and modulation are measured at the same low cross-correlation frequency (δF). The use of cross-correlation detection results in the rejection of harmonics and other sources of noise. The newer FD instruments use signal processing boards that extract the values from the digitized low-frequency signal.

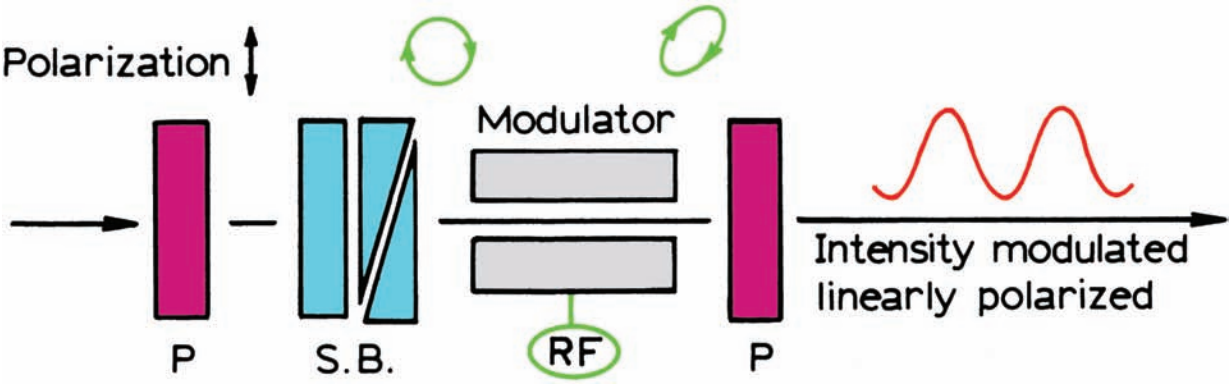

Figure 5.8. Optical arrangement for an electrooptic modulator. P, polarizer; SB, Soliel-Babinet compensator; RF, radio frequency signal. The SB compensator is replaced by an electrical DC voltage in some commercial FD instruments.

The cross-correlation method is surprisingly robust. The harmonic content (frequency components) of almost any excitation profile can be used if it contains frequency components that are synchronized with the detector. Both pulsed lasers and synchrotron radiation have been used as modulated light sources. Pulse lasers provide harmonic content to many gigahertz, so the bandwidth of the frequency-domain instruments is then limited by the detector and not the light modulator (Section 5.6).

5.2.3. Light Modulators

Adjustment of the frequency-domain instruments is aided by understanding the operating principles of light modulators. Light can be modulated with high efficiency using acoustooptic modulators, which diffract light based on a periodic density gradient caused by sound waves. Acoustooptic (AO) modulators are typically resonant devices that operate at only certain frequencies. While broadband or variable frequency AO modulators are known, the active area is usually small, limiting their use to focused laser sources.

A general procedure to modulate light is provided by the use of electrooptic (EO) modulators (Figure 5.8). EO modulators are constructed of materials that rotate polarized light when the material is exposed to an electrical field.[54–56] The modulator is placed between crossed polarizers. In the absence of any voltage there is no effect on the incident light, and no light is transmitted. If a voltage is applied to the modulator, the electric vector of the light is rotated and some light passes through the second polarizer. A voltage is applied to the modulator at the desired modulation frequency.

When an EO modulator is used as just described, without a bias, it provides modulated light at twice the frequency of the electric field applied to the modulator. This occurs because the optical system becomes transmissive whether the voltage is positive or negative (Figure 5.9). However, the amount of light transmitted is rather small. Hence, EO modulators are usually operated with an optical or electri-

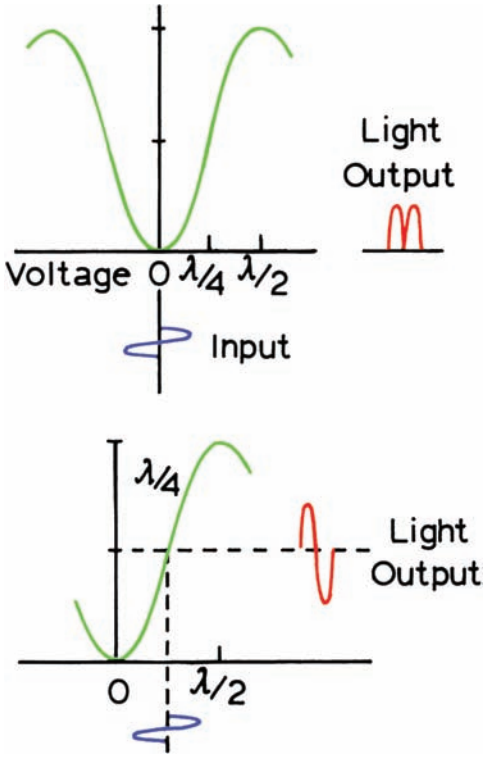

Figure 5.9. Modulated intensity from an electrooptic modulator. The upper drawing shows the modulated intensity without an electrical or optical bias, the lower drawing includes a λ/4 bias.

cal bias, which results in some light transmission when the voltage applied to the modulation is zero. This can be accomplished by the use of an optical bias (Soliel-Babinet compensator) or an electrical bias (DC voltage). This bias converts the linearly polarized light to circular or elliptically polarized light even if no AC voltage is applied to the modulator. This results in partial transmission of the laser beam in the absence of the RF voltage. Application of an RF voltage now results in amplitude modulation of the laser beam at the applied RF frequency (Figure 5.9). The modulated light is polarized according to the orientation of the second polarizer.

The usefulness of the EO modulator results from the ability to rapidly change the electric field across the EO crystal. In practice, adequate RF voltage can be applied up to about 200 MHz, which is also the upper frequency limit of most dynode PMTs. The EO modulators are not resonant devices, and perform equally well at any frequency below the upper frequency limit. However, there are several features of EO modulators that are not ideal for use in a frequency domain fluorometer. Perhaps the most serious limitation is the high half-wave voltage. The half-wave voltage is the voltage needed to rotate the electrical vector by 90° and allow all the light to pass through the second polarizer. Half-wave voltages for commonly used EO modulators are 1 to 7 kV, whereas the maximum practical RF peak-to-peak voltages are near 100 volts. For this reason one can only obtain a relatively small amount of modulation.

In frequency-domain fluorometers the extent of modulation is usually increased by adjusting the optical or electrical bias close to the zero transmission point. This decreases both the AC and DC intensities, but the DC intensity can be decreased to a greater extent, resulting in a larger AC/DC ratio. Because of the large half-wave voltage, crossed polarizers, and a modulator biased near zero transmission, the overall efficiency of light transmission rarely exceeds 10%.

Another disadvantage of the EO modulators is that they generally require collimated light. They are easier to use with lasers than with arc lamp sources. It is possible to obtain useful amounts of modulation with an arc lamp, but the transmission is typically less than 5%. Unfortunately, there does not seem to be any general solution to this problem. As shown in Section 5.6, the limitations of using a light modulator can be avoided by using intrinsically modulated light sources. These include pulsed lasers, laser diodes, and LEDs. LEDs and LDs are now available for FD measurements with output from 370 to 830 nm[56] that can be used to excite many extrinsic fluorophores. A pulsed subnanosecond LED at 280 nm has recently been described for TCSPC,[57] so that modulated LEDs for excitation of intrinsic protein fluorescence should be available in the near future.

Modulators are known that have lower half-wave voltages and higher frequency limits above 1 GHz.[54] These include the longitudinal field and traveling wave modulators. These devices typically have long narrow light paths and are only suitable for use with lasers. Also, they are sensitive to temperature and RF power. This instability limits their use in frequency-domain instruments.

5.2.4. Cross-Correlation Detection

The use of cross-correlation detection is an essential feature of the frequency-domain measurements. The basic idea is to modulate the gain of the PMT at a frequency offset (δF) from the light modulation frequency. The result is a low-frequency signal from the PMT at frequency δF that contains the phase and modulation information. The phase shift and modulation of the low-frequency signal is the same as one would have observed at high frequency. The phase and modulation of the low-frequency signal is easily measured using either analog or digital methods. Some FD instruments use zero crossing detectors and a ratio voltmeter (DVM) to measure these values, as was done in the early instruments.[41] In newer FD instruments the low-frequency signal is digitized and analyzed by a fast Fourier transform.[58–60] It seems that digital data acquisition of the low-frequency signal decreases the noise in the phase and modulation data by about twofold compared to the analog circuits. The equations describing cross-correlation detection are provided in Section 5.11.2.

Cross-correlation detection provides a significant advantage in addition to allowing low-frequency measurements. The process of cross-correlation suppresses harmonic or other frequencies, so that the modulation of the light or PMT gain need not be a pure sine wave. In fact, the excitation waveform can be almost any repetitive waveform, even a laser pulse train. After cross-correlation, the phase and modulation values are the values that would have been observed if the modulation were perfectly sinusoidal. This feature of harmonic suppression makes the frequency-domain instruments easy to use. One need not be concerned about the shape of the modulated signals, as this will be corrected by cross-correlation.

5.2.5. Frequency Synthesizers

The use of cross-correlation distributions requires two frequencies that are synchronized but different by a small frequency δF. The cross-correlation frequency δF can be any value, and is generally selected to be between 10 and 100 Hz. The synthesizer must provide frequencies to 200 MHz or higher, with 1 or 0.1 Hz resolution, which is not difficult with modern electronics. The requirements for frequency resolution in the synthesizer can be relaxed if one uses higher cross-correlation frequencies,[61] and schemes are being developed that use only one high-stability frequency source.[62] It seems clear that the cost of frequency-domain instrumentation will continue to decrease.

5.2.6. Radio Frequency Amplifiers

The electrooptic modulator requires the highest reasonable voltage, preferably 1500 volts peak-to-peak over a wide frequency range. Unfortunately, this is not practical. In order to obtain variable frequency operation the circuit is usually terminated with a 50-ohm (Ω) power resistor. A 25-watt amplifier provides only about 100 volts into 50 Ω, which is why overall light transmission is low. One can usually remove the 50-Ω terminating resistor, which results in a twofold increase in voltage. The RF amplifier should be protected from reflected power. It is important to avoid standing waves in the amplifier to modulator cable, which should be less than 30 cm long.

In contrast to the high power required by the light modulator, relatively little power is needed to modulate the gain of the PMT. This amplifier is typically near 1 watt, and can be less. In fact, we often directly use the output of the frequency synthesizer without amplification for gain modulation of the PMT.

5.2.7. Photomultiplier Tubes

The detector of choice for FD measurements is a PMT. The upper frequency limit of a PMT is determined by its transient time spread, so that the same detectors that are useful in TCSPC are useful in FD fluorometry. There is a slight difference in that the most important feature for TCSPC is the rise time of the pulse. For FD measurements the PMTs with the highest frequency limits are those with the narrowest pulses for each photoelectron. While fast rise times usually imply narrow photoelectron pulse widths, some detectors can have fast rise times with long tails.

The approximate upper frequency limits of commonly used PMTs are listed in Table 4.1. These values are estimated based on our experience and product literature. The upper frequency limit of the side window R928 is near 200 MHz. Much higher-frequency measurements are possible with MCP PMTs (Section 5.7), but special circuits are needed for cross-correlation outside of the PMT.

It is informative to examine the PMT electronics used in a frequency-domain fluorometer (Figure 5.10), in this case for an R928 PMT. The circuit starts with a high negative voltage of the photocathode. There is a Zener diode (Z_1) between the photocathode and first dynode. This diode maintains a constant high 250-volt potential. With the use of a constant high potential, the wavelength- and position-dependent time response of the PMT is minimized. The next dynodes are all linked by simple resistors. This allows the gain of the PMT to be varied by changes in applied voltage. Capacitors are included to maintain the voltage difference during periods of transiently high illumination.

Cross-correlation is accomplished by injection of a small RF signal at dynode 9 (D_9). The voltage between D_8 and D_9 is held constant by the Zener diode (Z_2). The average voltage between D_9 and ground is adjusted by bias

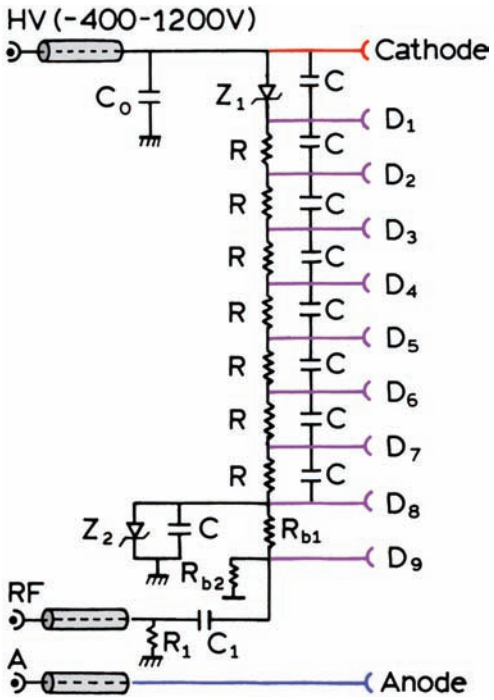

Figure 5.10. Dynode chain for an R928 photomultiplier tube used in a frequency-domain fluorometer. Revised from [1] and reprinted with permission from the Biophysical Society.

resistors R_{b1} and R_{b2}. A few volts of RF signal are adequate to obtain nearly 100% gain modulation of the PMT.

5.2.8. Frequency-Domain Measurements

When performing frequency-domain measurements it is valuable to understand what is being measured. One performs a comparison of the sample emission and scattered light, similar to the comparison in TCSPC. The FD instruments typically contain two detectors, one for the sample and one that serves as a timing reference (Figure 5.7). The reference PMT typically observes reflected light, scattered light, or the emission from a short-lifetime standard. The sample PMT is exposed alternately to the emission from either the sample or to scattered light. The sample and scattering solutions are usually in a rotating sample holder (turret) that precisely positions each solution in the same location. Since everything else in the measurement remains the same, any change in relative phase or modulation is due to the intensity decay of the sample.

Because the scatterer and sample are not observed at the same time, the phase difference and relative modulation cannot be measured at the same time. Instead, all measurements are performed relative to the reference PMT (Figure 5.11). First, the phase shift between the scatterer and reference PMT is measured. These signals are shifted by an arbitrary phase angle (ϕ_1) due to the inevitable time delays in the cables and electronic circuits. The second measurement is the phase of the sample relative to the reference PMT. This phase angle (ϕ_2) contains both the arbitrary phase shift ϕ_1 and the value of interest, ϕ_ω. The actual phase shift is then calculated from $\phi_\omega = \phi_2 - \phi_1$.

The modulation is measured in a similar way, except that one typically does not measure the modulation of the reference PMT is not measured. The modulation is determined from the AC and DC components of the sample (B/A) and scatterer (b/a), as shown in Figure 5.2. For measurement of the modulation it does not matter if one measures the peak-to-peak or RMS voltage of the modulated signal, as the method of measurement cancels in the ratio. The modulation at the reference PMT can be used as a correction for modulation drifts in the instrument. In this case all measured modulation values are divided by the value at the reference PMT during each particular measurement. This procedure is useful if the extent of modulation is changing during the measurement due to instabilities in the modulator or light source.

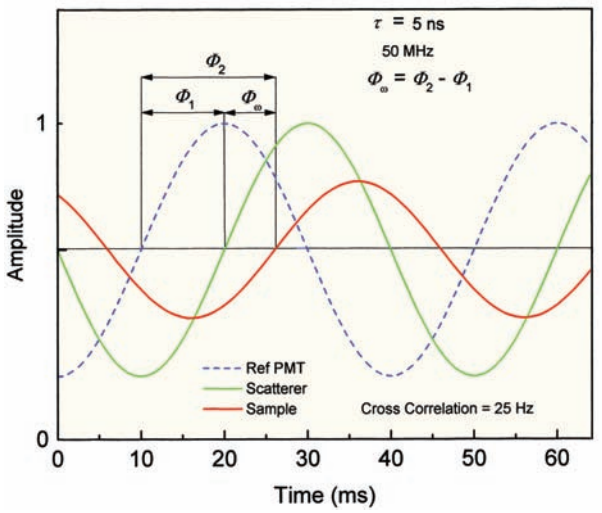

Figure 5.11. Measurement of phase shift and modulation for a modulation frequency of 50 MHz, a lifetime of 5 ns, and a cross-correlation frequency of 25 Hz. The phase angle is 57.5° and the modulation 0.54.

As described in Chapter 4 for time-domain measurements, it is important to consider the effects of rotational diffusion on the measured intensity decays. Rotational diffusion can also affect the frequency-domain measurements (Chapter 11). The use of an excitation and/or emission monochromator results in either partially polarized excitation or selective observation of one of the polarized components of the emission. If the decay rate is comparable to the rate of rotational diffusion, which is a situation frequently encountered for fluorophores bound to biological macromolecules, then the decay of the individual polarized components of the emission is multi-exponential. This effect is unimportant if the rate of rotational diffusion is either much slower or faster than the decay rate. These effects can be canceled by use of vertically polarized excitation and an emission polarizer oriented at 54.7° to the vertical.

5.3. COLOR EFFECTS AND BACKGROUND FLUORESCENCE

5.3.1. Color Effects in Frequency-Domain Measurements

Photomultiplier tubes can display a wavelength-dependent time response (Section 4.6.4), which can affect the frequency-domain measurements.[63–68] In frequency-domain measurements the effects are somewhat more difficult to under-

stand. There can be systematic errors in the phase or modulation values, and the direction of the errors is not always intuitively obvious. Fortunately, the color effects are minor with presently used side-window dynode PMTs, and the effect appears to be negligible with microchannel plate PMTs. Although no reports have appeared, it is likely that color effects are minimal with the TO-8 compact PMTs (Section 4.6.3.). Systematic errors due to the wavelength-dependent time response are easily corrected using lifetime standards.

In order to correct for a wavelength-dependent response one uses a lifetime standard in place of the scatterer in the sample turret (Figure 5.7). The standard should display a single-exponential decay of known lifetime τ_R. The lifetime of the standard should be as short as possible, typically near 1 ns, to avoid demodulation that results in decreased precision of the phase-angle measurements. Another advantage of short-lifetime standards is the minimal effect of dissolved oxygen on the lifetimes. Short lifetimes can be obtained with collisional quenching, but this is not recommended because such samples display non-exponential decays. Lifetime standards are summarized in Appendix II. The chosen standard should absorb and emit at wavelengths comparable to the sample, so that the sample and reference can be observed with the same emission filter and/or monochromator setting. Under these conditions the PMT observes essentially the same wavelength for both sample and reference measurements, so the color effects are eliminated.

The decay time of the reference results in a phase delay (ϕ_R) and demodulation (m_R) of the reference emission compared to that which would have been observed using a scatterer with a lifetime of zero. Of course, ϕ_R and m_R depend on the modulation frequency. The measured values (ϕ_ω^{obs} and m_ω^{obs}) need to be corrected for this effect. The corrected values are given by

$$\phi_\omega = \phi_\omega^{obs} + \phi_R \tag{5.16}$$

$$m_\omega = m_\omega^{obs} \cdot m_R = m_\omega^{obs} / \sqrt{1 + \omega^2 \tau_R^2} \tag{5.17}$$

where ϕ_ω^{obs} and m_ω^{obs} are the observed values measured relative to the lifetime standard. These equations can be understood by noting that the observed phase angle is smaller than the actual phase angle due to the phase angle of the reference ($\phi_\omega^{obs} = \phi_\omega - \phi_R$). Similarly, the observed modulation is the ratio of the modulation of the sample relative to the reference ($m_\omega^{obs} = m_\omega / m_R$). We find this simple approach adequate for all samples we have encountered. Somewhat different methods have also been proposed.[67–68]

5.3.2. Background Correction in Frequency-Domain Measurements

Correction for background fluorescence from the sample is somewhat complex when using the FD method.[69–70] In time-domain measurements, correction for autofluorescence can be accomplished by a relatively straightforward subtraction of the data file measured for the blank from that measured for the sample, with error propagation of Poisson noise if the background level is high. In the frequency domain it is not possible to perform a simple subtraction of the background signal. The background may be due to scattered light with a zero decay time, due to impurities with finite lifetimes, or a combination of scattered light and autofluorescence. The phase ($\phi_{\omega B}$) and modulation ($m_{\omega B}$) of the background can be measured at each light modulation frequency. However, the measured values $\phi_{\omega B}$ and $m_{\omega B}$ cannot be subtracted from the sample data unless the intensities are known and the correction is properly weighted.

Background correction of the FD data is possible, but the procedure is somewhat complex and degrades the resolution of the measurements. It is preferable to perform the FD measurements under conditions where background correction is not necessary. If needed, the correction is performed by measuring the frequency response of the background, and its fractional contribution (f_B) to the steady-state intensity of the sample. If the background level is low, then the values of $\phi_{\omega B}$ and $m_{\omega B}$ have large uncertainties due to the weak signals. However, this is not usually a problem because if the background is low its weighted contribution to the sample data is small, so that minimal additional uncertainty is added to the data. If the background is larger, its significance is greater, but it can also be measured with higher precision.

A data file corrected for background is created by the following procedure.[66] Let

$$N_{\omega B} = m_{\omega B} \sin \phi_{\omega B} \tag{5.18}$$

$$D_{\omega B} = m_{\omega B} \cos \phi_{\omega B} \tag{5.19}$$

represent the sine and cosine transforms. In these equations $\phi_{\omega B}$ and $m_{\omega B}$ represent the measured values for the phase

and modulation of the background. A least-squares fit of the phase and modulation data for the background is performed and for the parameter values to calculate $\phi_{\omega B}$ and $m_{\omega B}$. This latter procedure is useful if the background file is not measured at the same modulation frequencies as the sample. In the presence of background the observed values of N_ω^{obs} and D_ω^{obs} are given by

$$N_\omega^{obs} = (1 - f_B)m_\omega \sin\phi_\omega + f_B m_{\omega B} \sin\phi_{\omega B} \quad (5.20)$$

$$D_\omega^{obs} = (1 - f_B)\, m_\omega \cos\phi_\omega + f_B\, m_{\omega B} \sin\phi_{\omega B} \quad (5.21)$$

In these equations f_B is the fraction of the total signal due to the background, and ϕ_ω and m_ω are the correct phase and modulation values in the absence of background. The corrected values of N_ω and D_ω are given by

$$N_\omega = \frac{N_\omega^{obs} - f_B N_{\omega B}}{1 - f_B} \quad (5.22)$$

$$D_\omega = \frac{D_\omega^{obs} - f_B D_{\omega B}}{1 - f_B} \quad (5.23)$$

In using these expressions the values of $\phi_{\omega B}$ and $m_{\omega B}$ are known from the measured frequency response of the background. The value of f_B is found from the relative steady-state intensity of the blank measured under the same instrumental conditions and gain as the sample. Except for adjusting the gain and/or intensity, the values of $\phi_{\omega B}$ and $m_{\omega B}$ should be measured under the same conditions as the sample. The corrected values of N_ω and D_ω can be used in eqs. 5.9 and 5.10 to calculate the corrected phase and modulation values. An important part of this procedure is propagation of errors into the corrected data file. Error propagation is straightforward but complex to describe in detail.[69]

5.4. REPRESENTATIVE FREQUENCY-DOMAIN INTENSITY DECAYS

5.4.1. Exponential Decays

It is informative to examine some typical frequency-domain measurements.[71] Frequency-domain intensity decays for anthracene (AN) and 9-cyanoanthracene (9-CA) are shown in Figure 5.12. The samples were in equilibrium with atmospheric oxygen. The emission was observed through a long pass filter to reject scattered light. Magic-angle polarizer conditions were used, but this is unnecessary for such samples where the emission is completely depolarized. The excitation at 295 nm was obtained from the frequency-doubled output of a rhodamine 6G dye laser, cavity dumped at 3.8 MHz. This pulse train provides intrinsically modulated excitation over a wide range of frequencies (Section 5.6).

Experimental FD data are shown in Figure 5.12 (upper panel). The increasing values are the frequency-dependent phase angles (ϕ_ω) and the decreasing values are the modulation values (m_ω). The solid lines are calculated curves for the best single-decay-time fits. In the single-exponential model the decay time is the only variable parameter. The shape of a single-decay-time frequency response is always the same, except that the response is shifted to higher frequencies for shorter decay times.

The lower panels show the deviations between the data (●, ○) and the fitted curve (solid line). In this case the deviations are presented in units of degrees and percentage modulation. For calculation of χ_R^2 the standard errors were taken as $\delta\phi = 0.2$ and $\delta m = 0.005$. The fact that the values of χ_R^2 are close to unity reflects an appropriate choice for the values of $\delta\phi$ and δm. In analysis of the FD data the absolute values of χ_R^2 are variable due to the unknown

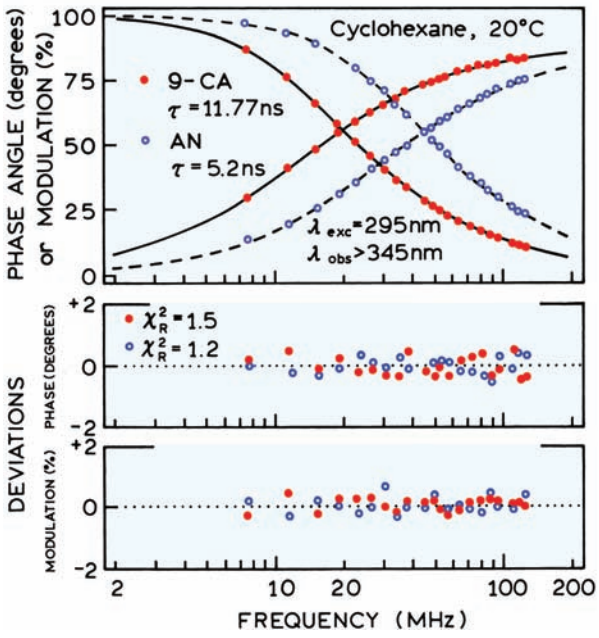

Figure 5.12. Single-exponential decays of anthracene (AN) and 9-cyanoanthracene (9-CA). Samples were equilibrated with atmospheric oxygen. $\delta\phi = 0.2$ and $\delta m = 0.005$. From [71].

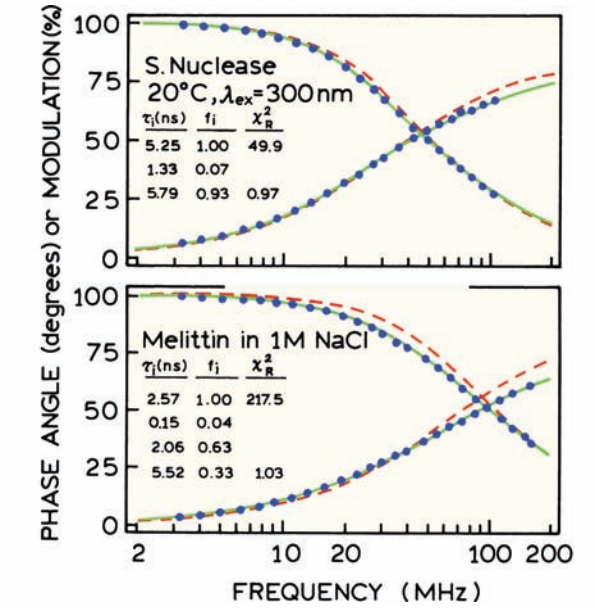

Figure 5.13. Frequency responses of staph nuclease and melittin tetramer. The data are the solid dots. The best single- (dashed) and double- or triple-exponential fits (solid) are shown.

amounts of noise. The ratio of the χ_R^2 is used for testing various models. For anthracene and 9-cyanoanthracene, the values of χ_R^2 did not decrease for the two-decay-time model, so the single-exponential model was accepted.

5.4.2. Multi-Exponential Decays of Staphylococcal Nuclease and Melittin

Most single-tryptophan proteins display multi-exponential intensity decays. This is illustrated for two proteins in Figure 5.13.[70] The intensity decay of trp-140 in staph nuclease is at least a double exponential. The intensity decay of trp-19 in melittin is at least a triple-exponential decay. Under these experimental conditions (1 M NaCl) melittin is a tetramer, with the monomers each in the α-helical state. The frequency responses and recovered lifetimes in Figure 5.13 are typical of many single- and multi-tryptophan proteins.

5.4.3. Green Fluorescent Protein: One- and Two-Photon Excitation

Green fluorescent protein (GFP) is of wide interest because it can be used to follow gene expression. GFP spontaneously forms a highly fluorescent fluorophore after the amino-acid backbone is synthesized. GFP is widely used in optical microscopy and cellular imaging. In these applications GFP is frequently excited by two-photon absorption (Chapter 18). In this process a fluorophore simultaneously absorbs two or more long-wavelength photons to reach the first singlet excited state. Two-photon excitation occurs when there is reasonable probability of two photons being in the same place at the same time, and thus the power density must be rather high. Multi-photon excitation requires locally intense excitation, and there is often concern about the stability of the fluorophores. The stability of GFP under these conditions was investigated by measuring the intensity decays with one- and two-photon excitation.

Since GFP is a modest-sized protein (≈28 kDa) the emission is expected to be polarized. For this reason the intensity decays were measured with magic-angle polarizer conditions. Excitation was obtained using fs pulses from a Ti:sapphire laser.[72] A pulse picker was used to reduce the repetition rate to near 4 MHz. For one-photon excitation the laser pulses were frequency doubled to 400 nm. For two-photon excitation the 800-nm output from the Ti:sapphire laser was used directly to excite the sample. These measurements used the harmonic content of the pulse train (Section 5.6). It is essential to select emission filters that reject scattered light at both 400 and 800 nm. The emission was observed through a 510-nm interference filter and a Corning 4-96 colored glass filter.

Intensity decays of proteins and labeled macromolecules are typically dependent on the conformation, and any perturbation of the structure is expected to alter the decay times. The intensity decays of GFP were found to be essentially identical for one- and two-photon excitation (Figure 5.14). This indicated that GFP was not perturbed by the intense illumination at 800 nm. The values of χ_R^2 are somewhat high, but did not decrease when using the two-decay-time model. The single-decay-time model was thus accepted for GFP, in agreement with one-photon excitation results from other laboratories.[73]

5.4.4. SPQ: Collisional Quenching of a Chloride Sensor

Collisional quenching decreases the lifetime of the quenched fluorophore (Chapter 8). This suggests that the lifetimes can be used to determine the concentration of quenchers. The probe SPQ (6-methoxy-N-[3-sulfopropyl]-quinoline) is sensitive to quenching by chloride,[74–76] probably by photoinduced electron transfer (Chapter 9).

Absorption and emission spectra of SPQ were shown in Chapter 3. Frequency responses of SPQ are shown in

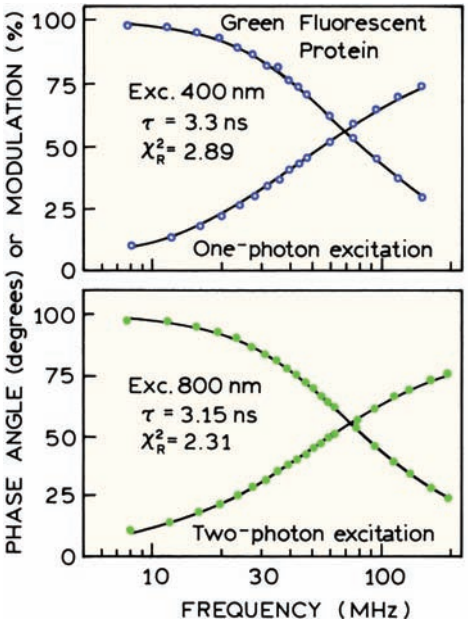

Figure 5.14. Frequency-domain intensity decay data for GFPuv in 0.05 M phosphate buffer, pH = 7, for one-photon excitation at 400 nm, and for two-photon excitation at 800 nm. From [72].

Figure 5.15. The frequency responses shift to higher frequencies with increasing amounts of chloride, indicating a decrease in lifetime. One can use the data to calculate the decay times at each chloride concentration. These lifetimes are 25.5, 11.3, 5.3, and 2.7 ns, for 0, 10, 30, and 70 mM chloride, respectively (Problem 5.1).

5.4.5. Intensity Decay of NADH

Reduced nicotinamide adenine dinucleotide (NADH) is known to display a subnanosecond decay time near 0.4 ns.

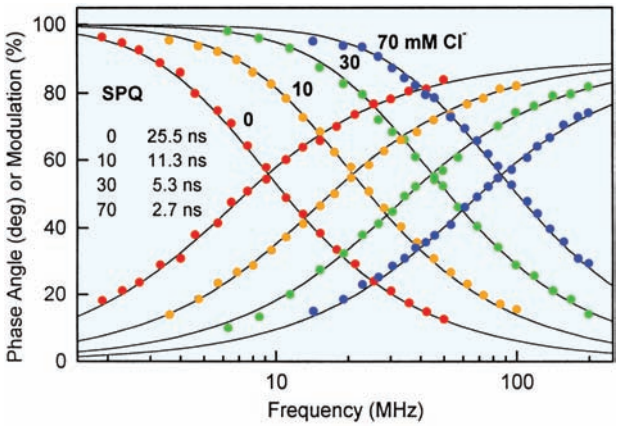

Figure 5.15. Frequency-domain intensity decays of SPQ in the presence of 0, 10, 40, and 70 mM chloride.

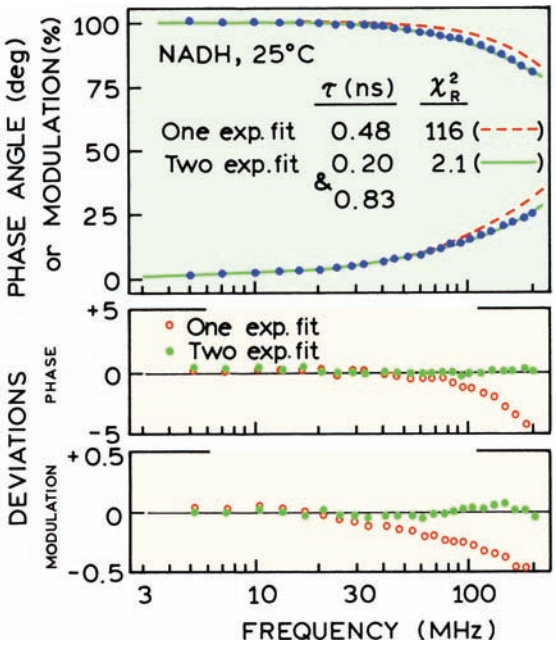

Figure 5.16. Frequency response of NADH dissolved in 0.02 M Tris (pH 8) 25°C. The excitation wavelength was 325 nm from an HeCd laser, which was modulated with an electrooptic modulator. The emission filter was a Corning 0-52. For the two-component analysis f_1 = 0.57 and f_2 = 0.43. Revised and reprinted from [2], Copyright © 1985, with permission from Elsevier Science.

Its intensity decay is complex, with decay times near 0.3 and 0.8 ns.[77] Frequency-domain data for NADH are shown in Figure 5.16. The presence of more than one lifetime is immediately evident from the failure of the single exponential fit (– – –) and the systematic deviations (○). Use of the two decay time model resulted in a 50-fold decrease of χ_R^2. The frequency-domain data for NADH illustrate a limitation of the commercially available instruments. An upper frequency of 200 MHz is too low to determine the entire frequency response of NADH or other subnanosecond intensity decays. For this reason FD instruments were developed to allow measurements at higher modulation frequencies.

5.4.6. Effect of Scattered Light

A critical component of any frequency-domain or time-domain experiment should be collection of emission spectra. One possible artifact is illustrated in Figure 5.17, which shows the emission spectrum of 9,10-diphenylanthracene (DPA) in a solution that also scattered light.[69] 9,10-Diphenylanthracene was dissolved in ethanol that contained a small amount of Ludox scatterer. When the emission is

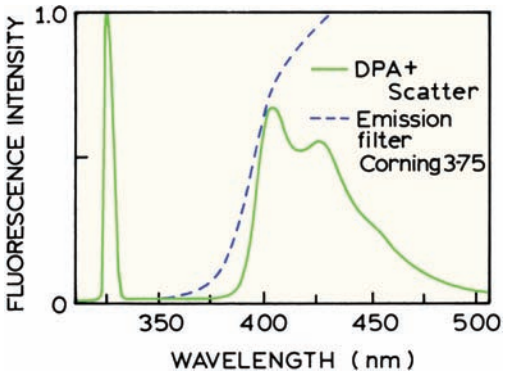

Figure 5.17. Emission spectra of 9,10-diphenylanthracene (DPA) in ethanol for excitation at 325 nm from a helium–cadmium laser. The solvent contained a small amount of Ludox colloidal silica as the scatterer. The dashed line is the transmission of the Corning 3-75 filter. Revised from [69].

observed without an emission filter (solid) there is a large peak due to scattered light at the excitation wavelength of 325 nm. The presence of this scattered component would not be recognized without measurement of the emission spectrum, and would result in an incorrect intensity decay.

Scattered light is typically rejected from the detector by using emission filters. In this case we used a Corning 3-75 filter, which transmits above 360 nm (dashed). As a control measurement one should always record the emission spectrum of the blank sample through the emission filter to ensure scattered light is rejected. Alternatively, one can measure the intensity of the blank through the filter to determine that the blank contribution is negligible. In such control measurements it is important that the blank scatters light to the same extent as the sample. Frequently, buffer blanks do not scatter as strongly as the sample containing the macromolecules because of the inner filter effect present in the sample.

It is useful to understand how scattered light can corrupt the frequency-domain data. Frequency responses for the DPA solution are shown in Figure 5.18. For these measurements the excitation source was a helium-cadmium (HeCd) laser at 325 nm. The cw output of this laser was modulated with an electrooptic modulator, as shown in Figure 5.8. The effect of scattered light is visually evident in the frequency-domain data. When measured without an emission filter, the phase angles (○) are considerably smaller than expected for the single exponential decay of DPA (●). The phase angle error becomes larger at higher frequencies. It should be noted that the fractional intensity of the background is only 15% (f_B = 0.15), so that significant

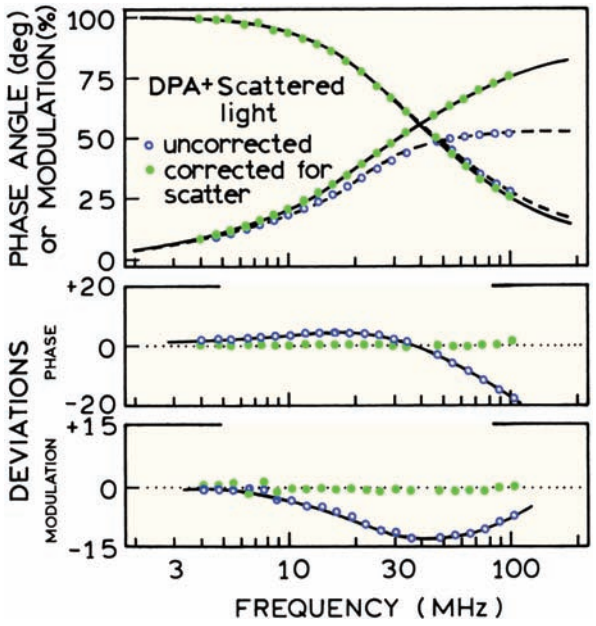

Figure 5.18. Frequency-domain intensity decay of 9,10-diphenylanthracene in ethanol with a scatterer. The sample was in equilibrium with dissolved oxygen. Data were measured without an emission filter (○) and then corrected (●) for the scattered light using eqs. 5.18–5.23. Bottom panels: deviations from the best single exponential fits for the data with (○), and corrected for (●) scattered light. Revised from [69].

errors in phase angle are expected for even small amounts of scattered light.

It is possible to correct for background from the sample. The solid dots represent the data corrected according to eqs. 5.18–5.23. The corrected data can be fit to a single decay time with τ = 6.01 ns. An alternative approach is to fit the data with scattered light to include a second component with a lifetime near zero. This also results in a good fit to the data, with a decay time near zero associated with f_B = 0.15. However, this procedure is only appropriate if the background is only due to scattered light. In general autofluorescence will display nonzero lifetimes and nonzero phase angles.

5.5. SIMPLE FREQUENCY-DOMAIN INSTRUMENTS

A large fraction of the cost of a frequency-domain instrument is the light source and/or modulation optics. In TCSPC these expensive light sources are being replaced by LDs and LEDs. This substitution is also occurring with frequency-domain instruments. For most experiments the

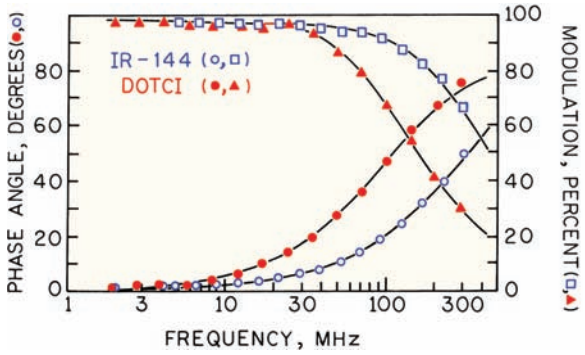

Figure 5.19. Frequency response for IR-144 in ethanol (open symbols) and DOTCI in ethanol (filled symbols). Best one-component fits to each data are indicated by the lines. IR-144 and DOTCI were excited with laser diodes at 790 and 670 nm, respectively. Revised and reprinted with permission from [79], Copyright © 1992, American Chemical Society.

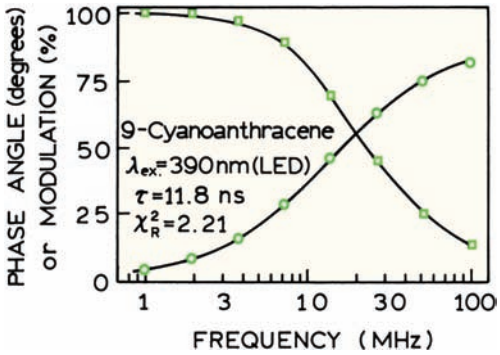

Figure 5.20. Intensity decay of 9-cyanoanthracene in ethanol using the 390-nm output of a UV LED as the excitation source. Revised from [85].

complex laser source can be replaced with laser diodes,[78–79] and light-emitting diodes.[80–86] Frequency-domain measurements have also been accomplished with electroluminescent devices,[87] and even a modulated deuterium lamp.[88] Given the rapid advances with pulsed LDs and LEDs these devices are likely to be the dominant excitation source for FD measurements in the near future.

5.5.1. Laser Diode Excitation

The output of laser diodes can be modulated up to several GHz. Hence, laser diodes can be used for FD excitation without the use of a modulator. Data are shown in Figure 5.19 for two laser dyes—IR-144 and DOTCI—which were excited with 791- or 670-nm laser diodes, respectively (Figure 5.19). Frequency-doubled laser diodes have also been used to obtain shorter excitation wavelengths near 400 nm.[89] However, the need for frequency-doubled LDs has diminished given the availability of LDs and LEDs with fundamental outputs ranging from 280 to 820 nm.

5.5.2. LED Excitation

It is now known that LEDs can be modulated to several hundred MHz.[85–86] Hence, LEDs are becoming an alternative to modulated arc lamps. The modulated output of a 390-nm LED output was used to measure the 3.2-ns decay time of green fluorescent protein (not shown) and the 11.8-ns lifetime of 9-cyanoanthracene[85] (Figure 5.20).

The use of a simple light source such as an LED is likely to find use in analytical chemistry and clinical chemistry.[84–85] This is illustrated in Figure 5.21 for the potassium-sensitive probe CD 222. This probe has a lifetime of 0.15 ns in the absence of potassium and 0.67 ns in the presence of bound potassium. The frequency response could be measured up to 300 MHz using a modulated UV LED at 373 nm. The possibility of measuring nanosecond decay times using modulated LEDs, and the availability of a wide range of wavelengths, suggests these light sources will be used for low-cost FD instruments in the near future.

Another application of LEDs will be for excitation of the longer-lived metal–ligand complexes (Chapter 20). The LEDs are ideal because the 450-nm output is centered on the 450-nm charge-transfer absorption of the ruthenium complexes. The shorter wavelengths are suitable for excitation of the higher-quantum-yield rhenium complexes (Figure 5.22). In this case the entire frequency response of $[Re(dpphen)(CO)_3)\ (4\text{-}COOHPy)]^+$ was measured in the absence (10.24 μs) or presence of oxygen (598 ns).[84]

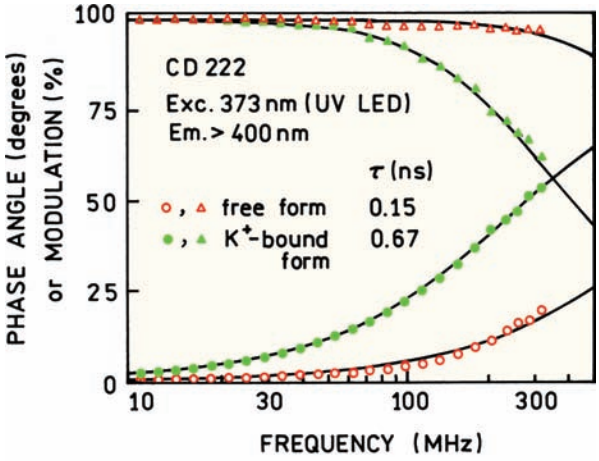

Figure 5.21. Frequency response of the potassium probe CD 222 measured with a 373-nm LED (○). From [84].

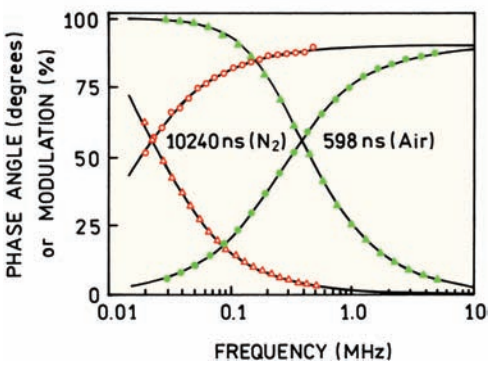

Figure 5.22. Frequency-domain intensity decays of [Re(dpphen)-$(CO)_3$(4-COOHPy)]$^+$ in methanol; dpphen is 4,7-diphenyl-1,10-phenanthroline, Py is pyridine. Excitation was 373 nm from the UV LED. From [84].

Given the simplicity of such light sources, one can imagine the frequency-domain fluorometer built on a card in a personal computer. pH can be measured using lifetimes either in standard cuvette measurements,[90] or through optical fibers.[91] LEDs have been used in phase fluorometric sensors for oxygen[92–93] and carbon dioxide.[94] Phase-modulation lifetimes have been used in HPLC to assist in the identification and quantitation of polynuclear aromatic hydrocarbons.[95–97] Phase-modulation lifetime measurements have already been used to quantify a wide variety of clinically important analytes.[98] Several companies are already designing simple phase-modulation instruments for use in analytical applications. Frequency-domain fluorometry can now be accomplished with components no more complex than consumer electronics.

5.6. GIGAHERTZ FREQUENCY-DOMAIN FLUOROMETRY

In frequency-domain measurements it is desirable to measure over the widest possible range of frequencies, so as to examine the entire frequency response of the sample. Most FD instruments are limited to an upper frequency near 200 MHz. This limitation arises from two components. First, it is difficult to obtain light modulation above 200 MHz. This limitation is due in part to the large half-wave voltages of most electrooptic modulators. Second, many PMTs have an upper frequency limit near 200 MHz.

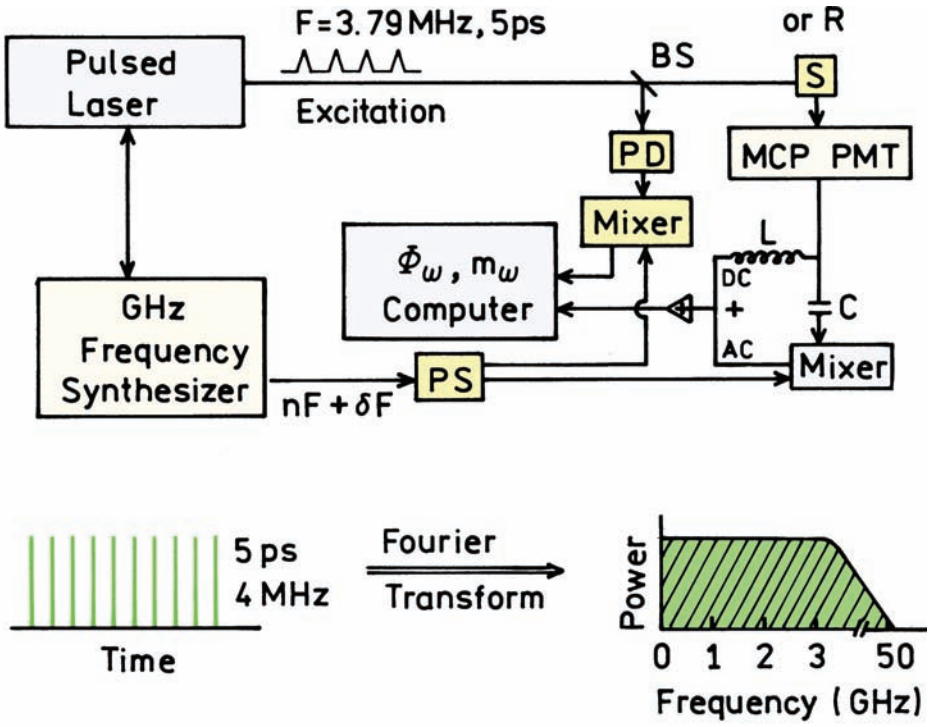

Figure 5.23. Harmonic content frequency-domain fluorometer. PD, high speed photodiode; PS, power splitter; MCP PMT, microchannel plate photomultiplier tube; BS, beam splitter; F, pulse repetition rate of the cavity dumped dye laser; δF, cross-correlation frequency; n, number of the harmonic; S, sample; R, reference or scatterer. The lower panel shows a laser pulse train and its Fourier transform. Revised from [106].

Alternative technologies are available to obtain FD measurements at frequencies above 200 MHz. The need for a light modulator can be eliminated by using the harmonic frequency content of a laser pulse train. Suppose the light source consists of a mode-locked argon ion laser and a cavity-dumped ps dye laser. This source provides 5-ps pulses with a repetition rate near 4 MHz. In the frequency domain this source is intrinsically modulated to many gigahertz, as shown by the schematic Fourier transform in Figure 5.23 (lower panel). The idea of using the harmonic content of a pulse train was originally proposed for pulsed lasers[99] and later for synchrotron radiation.[100–102] Pulse sources provide intrinsically modulated excitation at each integer multiple of the repetition rate, up to about the reciprocal of the pulse width.[103–104] For a ps dye laser the 4-MHz pulse train can be used for frequency domain measurements at 4, 8, 12, 16 MHz, etc. These harmonics extend to GHz frequencies, which are higher than the upper frequency limit of most detectors.

There are significant advantages in using the pulses from a ps laser. The cavity-dumped output of dye lasers is rather easy to frequency double because of the high peak power. Frequency doubling provides wavelengths for excitation of proteins and other extrinsic probes absorbing in the UV. Importantly, when using a ps dye laser source it is no longer necessary to use an electrooptic modulator and nearly crossed polarizers, which results in a significant attenuation of the incident light. There appears to be no detectable increase in noise up to 10 GHz, suggesting that there is no multiplication of phase noise at the higher harmonics.

The second obstacle to higher frequency measurements was the detector. The PMT in the 200-MHz instrument (Figure 5.7) is replaced with a microchannel plate (MCP) PMT.[105–108] These devices are 10- to 20-fold faster than a standard PMT, and hence a multi-gigahertz bandwidth was expected. As presently designed, the MCP PMTs do not allow internal cross-correlation, which is essential for an adequate signal-to-noise ratio. This problem was circumvented by designing an external mixing circuit,[105–106] which allows cross-correlation and preserves both the phase and the modulation data. The basic idea is analogous to Figure 5.10, except that mixing with the low-frequency signal is accomplished after the signal exits the MCP PMT. External cross-correlation was found to perform well without any noticeable increase in noise.

What range of frequencies can be expected with a pulsed-laser light source and an MCP PMT detector? For Lorentzian-shaped pulses the harmonic content decreases to half the low-frequency intensity at a frequency $\omega_2 = 2 \ln 2/\Delta t$, where Δt is the pulse width.[104] For 5-ps pulses the harmonics extend to 280 GHz, higher than the upper frequency limit of any available detector. Hence for the foreseeable future the measurements will be limited by the detector.

The upper frequency of a detector is limited by the pulse width due to a single photoelectron, or equivalently the transit time spread. Hence, one expects the highest modulation frequencies to be measurable with MCP PMTs that have the smallest transit time spread (Table 4.1). The relative power at various frequencies can be measured with a spectrum analyzer. This was done for several PMTs using a ps pulse train with its high harmonic content as the light source. These results show that the side-window R928 is most useful below 200 MHz (Figure 5.24), and cannot be used for measurements much above about 400 MHz. The R-1564U is a 6-micron MCP PMT, and shows a useful response to 2 GHz. This PMT was used in the first 2-GHz instrument.[105]

To obtain frequencies above 2 GHz it was necessary to use a specially designed MCP PMT, the R-2566. The data in Figure 5.25 are for the 6-micron version of the R-2566, which provides measurable power to 10 GHz, and allowed construction of a 10-GHz FD instrument.[106] This MCP PMT possesses a grid between the microchannel plates and the anode, which serves to decrease the width of the photoelectron pulses. In the frequency domain the upper limit of the detector is determined by the reciprocal of the pulse width. In TCSPC the time resolution is determined by the rise time of the PMT, and the overall pulse width is less important.

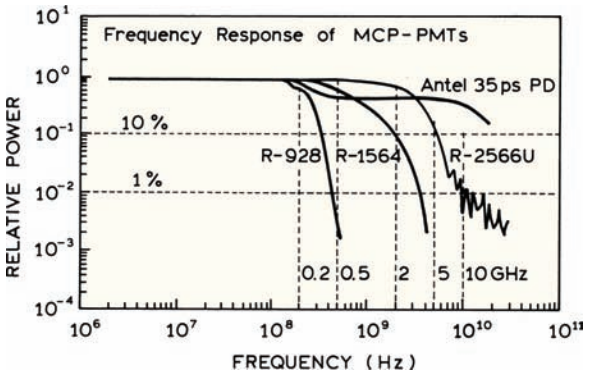

Figure 5.24. Measured frequency-response of several PMTs, and a fast photodiode (PD). Data from [107] and [108], and technical literature from Hamamatsu Inc.

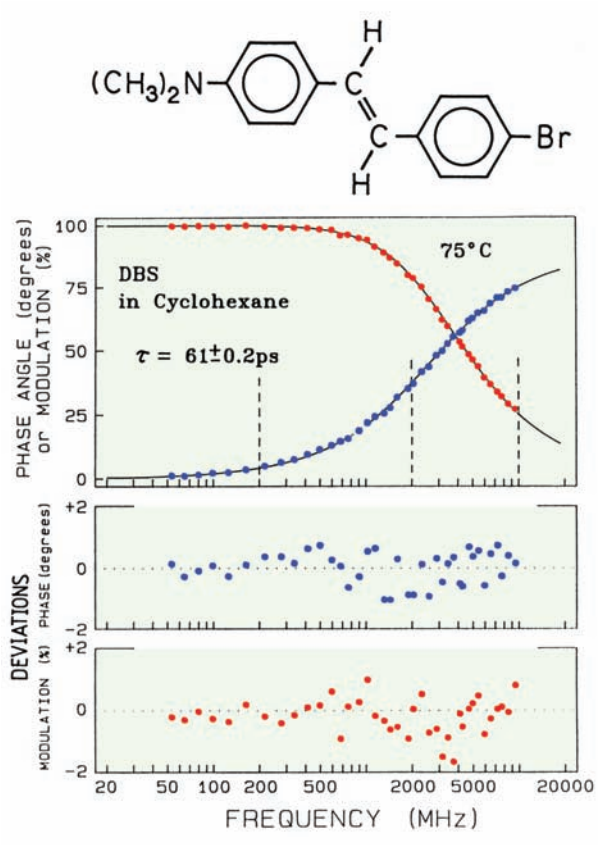

Figure 5.25. Frequency response of 4-dimethylamino-4'-bromostilbene (DBS) up to 10 GHz. The vertical dashed lines are at 200 MHz, 2 GHz, and 10 GHz. From [3].

Figure 5.24 shows that the photodiode provides a higher bandwidth than does any of the MCP PMTs. In fact, photodiode detectors were used in several phase fluorometers for measurements at high frequencies.[109–112] Unfortunately, the small active area of photodiodes results in low sensitivity, so that photodiodes are rarely used for fluorescence spectroscopy.

The schematic for the 10-GHz instrument shown in Figure 5.23 incorporates a ps laser as an intrinsically modulated light source, and an MCP PMT as the detector. A photodiode (PD) is adequate as the reference detector because the laser beam can be focused on its small active area. The use of cross-correlation allows measurement over the entire frequency range from 1 MHz to 10 GHz without any noticeable increase in noise. Cross-correlation allows measurements at any modulation frequency at the same low cross-correlation frequency, and avoids the need to measure phase angles and modulation at high frequencies. A valuable feature of cross-correlation is that the entire signal appears at the measured frequency. Contrary to intuition, one is not selecting one harmonic component out of many, which would result in low signal levels. The use of cross-correlation provides absolute phase and modulation values as if the excitation and detector were both modulated as sine waves. A final favorable feature of this instrument is that the modulation can be higher than 1.0, which is the limit for sine wave modulation. At low frequencies where the detector is fully responsive, the modulation can be as high as 2.0. To understand this unusual result one needs to examine the Fourier components for a pulse train.

5.6.1. Gigahertz FD Measurements

Several examples of gigahertz FD measurements will illustrate the value of a wide range of frequencies. Short decay times are needed to utilize the high-frequency capabilities.[113] Otherwise, the emission is demodulated prior to reaching the upper frequency limit. A short decay time was obtained using 4-dimethylamino-4'-bromostilbene (DBS) in cyclohexane at 75°C (Figure 5.25). Because of the short 61-ps lifetime the phase and modulation data could be measured to 10 GHz. The intensity decay was found to be a single exponential.[3] The vertical dashed lines illustrate how only a fraction of the frequency response could be explored if the upper limit was 200 MHz, or even 2 GHz. It would be difficult to detect additional components in the intensity decay if the data stopped at 200 MHz, which would display a maximum phase angle of 4.4°. An important aspect of these measurements is that no measurable color effect has been observed in the 10 GHz measurements.[106]

5.6.2. Biochemical Examples of Gigahertz FD Data

GHz measurements may seem exotic, but such data are often needed for studies of routine biochemical samples. One example is NADH. At 200 MHz the data only sampled part of the frequency response (Figure 5.16). When measured to higher frequencies one can more dramatically see the difference between the one and two decay time fits (Figure 5.26). The decrease in χ_R^2 for the two decay time model is 400-fold. While we have not performed a support plane analysis on these data, the α_i and τ_i values will be more closely determined using the data extending above 200 MHz.

Another biochemical example is provided by the peptide hormone vasopressin, which acts as an antidiuretic and

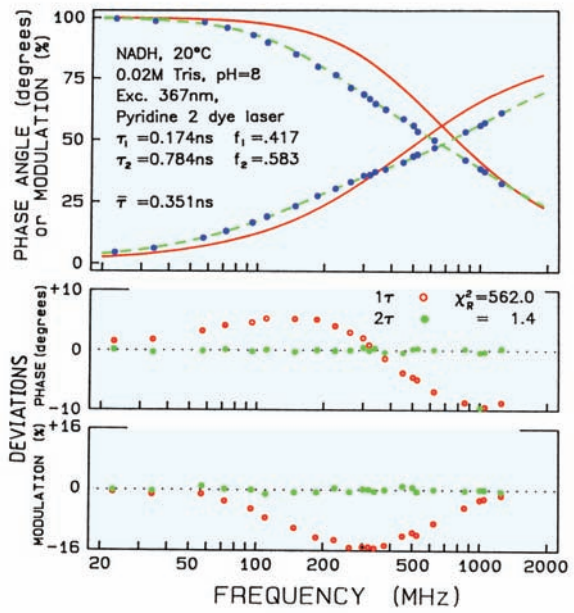

Figure 5.26. Frequency-domain measurements of the intensity decay of NADH up to 2-GHz. From [3].

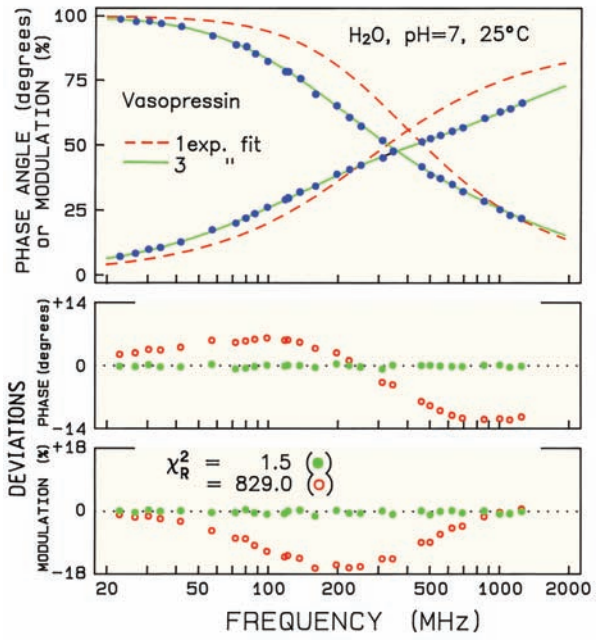

Figure 5.27. Phase and modulation data for the vasopressin tyrosine fluorescence intensity decay. The dashed line is the best single-exponential fit, and the solid line is the best three-exponential fit. From [114].

a vasoconstrictor. Vasopressin is a cyclic polypeptide that contains 9 amino acids including a single tyrosine residue at position 2. Oxytocin has a similar structure, but has a distinct physiological activity of stimulating smooth muscle contraction. Hence there have been many efforts to use the tyrosine emission to learn about the solution conformation of these peptide hormones. The frequency-domain data for vasopressin reveal a complex intensity decay (Figure 5.27).[114] The decay is not even closely approximated by the single exponential model (dashed). Fitting the data requires three decay times of 0.17, 0.75, and 1.60 ns. These multiple decay times could probably not be recovered if the data were limited to 200 MHz.

MCP PMTs are moderately expensive, and their use in FD measurements requires special circuits for cross-correlation. However, the advantages of high-frequency FD data may become available without the use of MCP PMTs. Examination of Figures 5.26 and 5.27 indicates that considerable data can be obtained if the data were available to just 1 GHz. This frequency limit can probably be reached with the new compact PMTs, which show short transit time spreads (Table 4.1). A dynode PMT (H5023) has already been used up to 1 GHz.[115] It seems likely that a compact PMT such as the R74000 will be useful up to 900 MHz. Laser diodes with 30-ps pulse widths will provide useful harmonics up to 40 GHz.

In the near future gigahertz FD instruments will be available based on pulsed-laser diodes and compact PMTs.

5.7. ANALYSIS OF FREQUENCY-DOMAIN DATA

Frequency-domain data is often analyzed in terms of the multi-exponential model. As described in Chapter 4, the amplitudes (α_i) and decay times (τ_i) are usually strongly correlated, so that there can be considerable uncertainty in the values of the recovered parameters. In this section we describe examples that show correlation between the parameter values.

5.7.1. Resolution of Two Widely Spaced Lifetimes

The analysis of frequency-domain data can be illustrated using a mixture of p-terphenyl and indole. This same mixture was used in Chapter 4 for TCSPC data (Figures 4.46–4.49). The same 292-nm excitation and 330-nm emission wavelengths were used for the frequency-domain measurements as for the time-domain measurements. The decay times of the individual fluorophores are 0.93 and 3.58 ns for p-terphenyl and indole, respectively. For this mixture the decay times are spaced 3.8-fold, making this a moderately

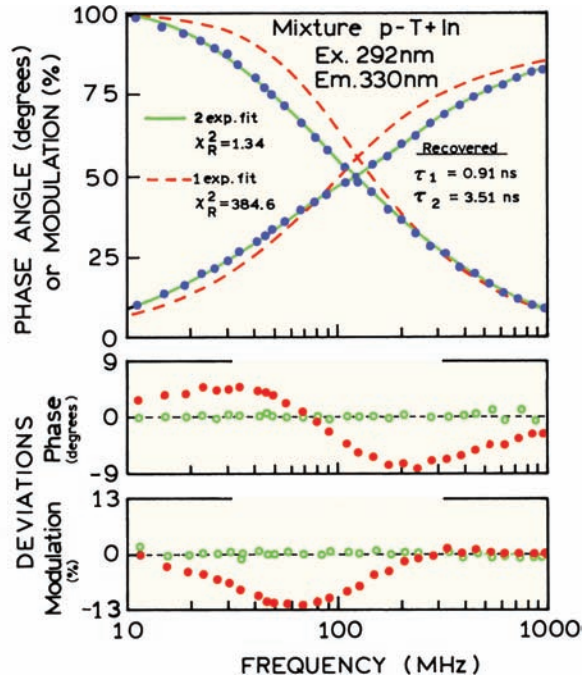

Figure 5.28. Frequency-domain intensity decay data of a two-component mixture of p-terphenyl (p-T) and indole (In) in ethanol, 20°C. Magic-angle polarization conditions were used. The sample was in equilibrium with air. The repetition rate was 1.9 MHz from a frequency-doubled rhodamine 6G dye laser. Emission at 330 nm was isolated with a monochromator. The dashed line (top panel) and closed circles (lower panels) show the best fit with one decay time. The solid curves (top) and open circles (bottom) show the best fit with two decay times. From [116].

easy resolution. Frequency-domain intensity decay data are shown in Figure 5.28. The presence of more than a single decay time is evident from the shape of the frequency response, which appears to be stretched out along the frequency axis. The fact that the decay is more complex than a single exponential is immediately evident from the attempt to fit the data to a single decay time. The best single decay time fit (dashed) is very poor and the deviations are large and systematic (●, lower panels). Also, the value of $\chi_R^2 = 384.6$ is easily rejected as being too large.

Use of a two-decay-time model results in a good fit of the calculated frequency response (Figure 5.28, solid) to the measured phase and modulation values (●). Also, the value of χ_R^2 decreases to 1.34. Use of the three-decay-time model results in a modest reduction of χ_R^2 to 1.24, so that the two-decay-time model is accepted. For this mixture the recovered decay times of 0.91 and 3.51 ns closely match the lifetimes measured for the individual fluorophores. The recovered amplitudes and fractional intensities suggest that about 64% of the emission at 330 nm is from the indole with a decay time of 3.51 ns (Table 5.1).

An important part of data analysis is estimating this confidence intervals for each parameter. Most computer programs report the asymptotic standard errors (ASEs), which are the uncertainties calculated under the assumption that the parameters are not correlated. The range of possible parameters are usually 2- to 10-fold larger than that estimated from the ASEs. For this reason, examination of the χ_R^2 surfaces is preferred. The upper and lower limits of each parameter are determined from the χ_R^2 ratio as the parameter value is held fixed around the optimal value. The least-squares analysis is then run again to obtain the lowest value of χ_R^2 consistent with the fixed parameter value. This allows calculation of the χ_R^2 ratios:

$$F_\chi = \frac{\chi_R^2\,(\text{par})}{\chi_R^2\,(\text{min})} = 1 + \frac{p}{m - p} F(p,\nu,P) \tag{5.24}$$

where χ_R^2(par) is the value of χ_R^2 with a parameter value held fixed at a value different from that yielding the minimum value of χ_R^2(min). The upper and lower bounds of each parameter are selected as those where the χ_R^2 ratio intercepts with the F_χ value for one standard deviation (P = 0.32) and the number of parameters (p) and degrees of free-

Table 5.1. Multi-Exponential Analysis of a Two-Component Mixture of p-Terphenyl and Indole

	Lifetime (ns)		Pre-exponential factors		Fractional intensity		χ_R^2	
Sample	τ_1	τ_2	α_1	α_2	f_1	f_2	1[a]	2[a]
p-Terphenyl	0.93	–	1.0	–	1.0	-	1.38	1.42
Indole	–	3.58	–	1.0	–	1.0	1.10	1.13
Mixture	0.91	3.51	0.686	0.314	0.36	0.64	384.6	1.34[b]

[a]Refers to a two- or one-component fit. $\delta\phi = 0.2$ and $\delta m = 0.005$. From [116].
[b]The value of χ_R^2 for the three-decay-time fit for the mixture was 1.24.

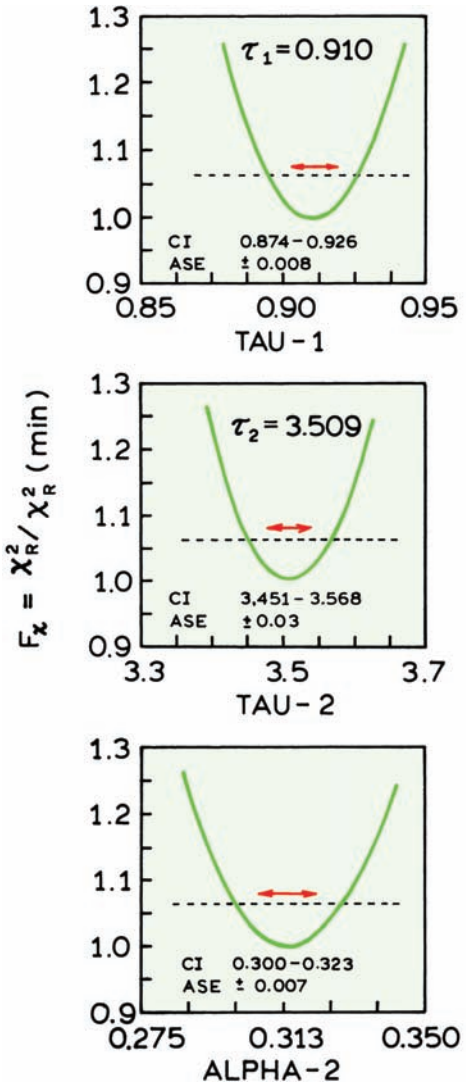

Figure 5.29. χ_R^2 surfaces for the two-component mixture of p-terphenyl and indole. The horizontal arrows show the asymptotic standard errors (ASE), and the dashed lines are at the appropriate F_χ values. From [116].

dom ($\nu = m - p$). It is useful to consider some representative values for the ratio of χ_R^2 values. For the two-component mixture of p-terphenyl and indole there are 29 frequencies and 58 datapoints. The two-decay-time model has three variable parameters. The F statistic for $p = 3$ and $m = 60$ can be found from Table 4.4 and is 1.19. Hence, the F_χ value used for the confidence interval of each parameter is 1.06. As described in Section 4.10.3, there is some disagreement in the statistics literature as to the exact equation for finding the confidence intervals. We will use eq. 5.24, but its correctness has not yet been proven.

The χ_R^2 surfaces for the two-component mixture are shown in Figure 5.29. The confidence intervals (CI) are determined from the intercept of the χ_R^2 surfaces with the χ_R^2 ratio appropriate for the number of parameters and degrees of freedom. The arrows in Figure 5.29 show the asymptotic standard errors. The ASEs are about twofold smaller than the confidence intervals. The decay times in this mixture are widely spaced. For more closely spaced decay times it becomes even more important to consider parameter correlation in the calculation of confidence intervals, and the ASEs can grossly underestimate the true confidence intervals.

5.7.2. Resolution of Two Closely Spaced Lifetimes

The resolution of multi-exponential decays becomes more difficult as the decay times become more closely spaced. It was previously noted that two decay times spaced by a factor of 1.4 represents the practical resolution limit for double exponential decay.[12] It is instructive to examine data for such a mixture because the analysis illustrates the difficulties encountered at the limits of resolution.

To illustrate a sample with two closely spaced decay times we have chosen the mixture of anthranilic acid (AA, $\tau = 8.5$ ns) and 2-aminopurine (2-AP, $\tau = 11.3$ ns). This may seem to be an easy resolution, but it is difficult to resolve decay times which are less than two-fold different. Emission spectra are shown in Figure 5.30. Frequency-domain data for the individual fluorophores and for the mixture are

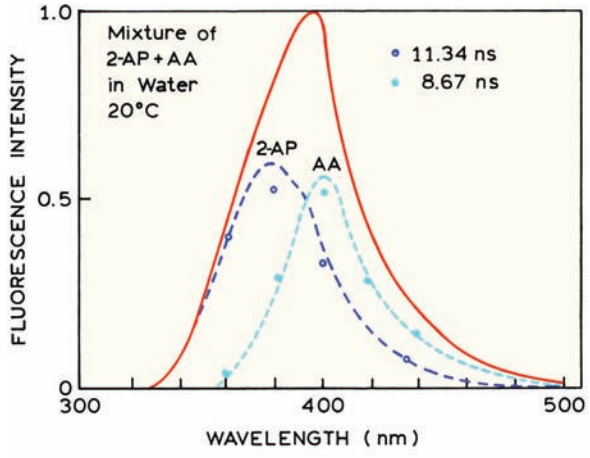

Figure 5.30. Emission spectra of a two-component mixture of anthranilic acid (AA) and 2-aminopurine (2-AP). Also shown are the amplitudes recovered from the global analysis (Figure 5.33). From [116].

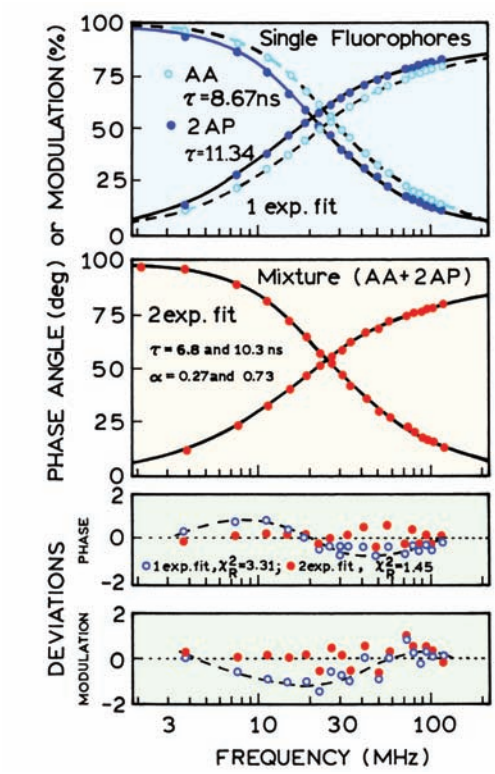

Figure 5.31. Frequency-domain intensity decays for 2-aminopurine (2-AP) and anthranilic acid (AA). Top: single fluorophore data at 400 nm. Middle: the two component mixture measured at 400 nm. Bottom: deviations for fits to the two component mixture. The value of χ_R^2 for the one- and two-component fits are 3.31 and 1.45, respectively. From [116].

shown in Figure 5.31. Each of the single fluorophores displays a frequency response characteristic of a single decay time. The values of χ_R^2 for the single-decay-time fits were acceptably low, and were not improved by using a two-decay-time model. The 40% difference in decay time results in only a modest shift on the frequency axis. Figure 5.31 (middle panel) also shows the frequency-domain data for the two component mixture of AA and 2-AP. Frequency-domain data were measured through a 400-nm interference filter. At this wavelength both fluorophores contribute almost equally to the measured intensities. For these two closely spaced lifetimes, it is difficult to see a difference between the calculated curves for the one and two decay time fits. The deviation plots (lower panels) show larger and systematic deviations for the one component fit. Also, χ_R^2 decreases from 3.3 for the one-decay-time fit to 1.45 for the one- and two-decay-time fits. For these measurements we have approximately 40 degrees of freedom. The F value of 2.3 is seen to be significant at the 1% level (Table 4.3), and there is less than a 0.1% probability that random noise is the origin of the elevated χ_R^2 value for the one-decay-time fit (Table 4.2).

In general we accept the more complex model if χ_R^2 decreases by at least 50%, preferably twofold. Occasionally, the value of χ_R^2 is larger than expected, but χ_R^2 does not decrease for the next more complex model. In these cases the elevated χ_R^2 is usually due to systematic errors in the measurements. It is fortunate that in many cases systematic errors cannot be accounted for by another decay time component in the model.

The twofold reduction in χ_R^2 for the two-decay-time mixture seems reasonable, but the recovered parameter values have considerable uncertainty. At 400 nm the two-component analysis returns a fractional intensity of 80% for the longer lifetime, and decay times of 6.82 and 10.29 ns (Table 5.2). These values are considerably different from the expected fractional intensity near 40% for the longer decay time component. Also, the recovered decay times of 6.82 and 10.29 ns are different from the expected decay times of

Table 5.2. Resolution of a Two-Component Mixture of Anthranilic Acid and 2-Aminopurine, Observed at a Single Wavelength

Observation wavelength (nm)	Lifetimes (ns)		Pre-exponential factors		Fractional intensity		χ_R^2	
	τ_1	τ_2	α_1	α_2	f_1	f_2	2[a]	1[a]
360	6.18	11.00	0.037	0.963	0.021	0.979	0.95	1.07
380	8.99	12.26	0.725	0.275	0.659	0.341	1.24	2.06
400	6.82	10.29	0.268	0.732	0.195	0.805	1.54	3.44
420	8.44	12.15	0.832	0.168	0.775	0.225	1.36	2.22
440	7.69	9.73	0.479	0.521	0.421	0.579	1.69	2.01

[a]Refers to a two- or one-component fit. $\delta\phi = 0.2$ and $\delta m = 0.005$. From [116].

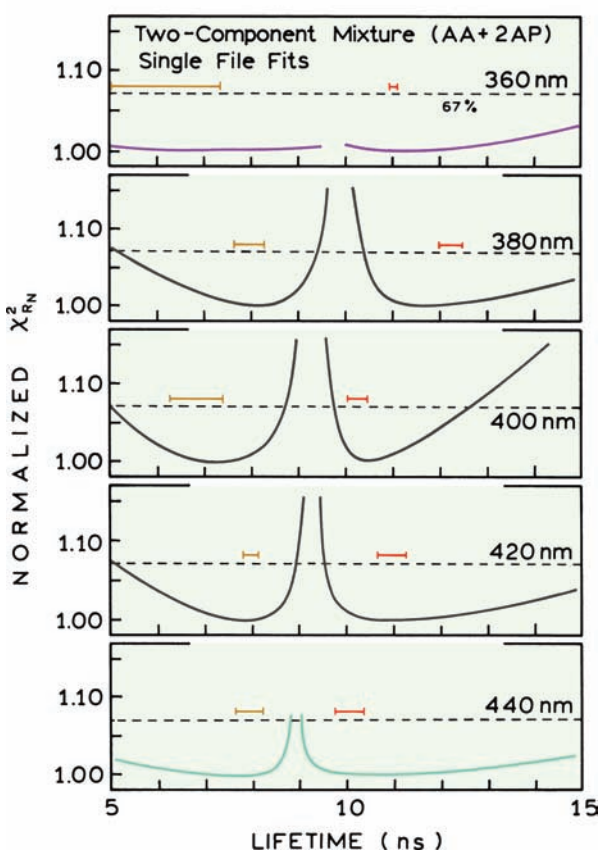

Figure 5.32. Lifetime χ_R^2 surfaces for the mixture of anthranilic acid (AA) and 2-aminopurine (2-AP) for single observation wavelengths. The solid bars (|——|) show the asymptotic standard errors. From [116].

8.5 and 11.3 ns. Analysis of the intensity decays at other wavelengths reveals considerable variability in the recovered lifetimes and fractional intensities. This can be seen in Figure 5.32 from the range of lifetimes consistent with the data from the χ_R^2 surfaces. At different emission wavelengths the lifetime of the shorter decay time ranges from 6.18 to 8.99 ns, and the lifetime of the longer component ranges from 9.73 to 12.26 ns (Table 5.2). The amplitudes and fractional intensities recovered from the measurements at different wavelengths do not accurately represent the emission spectra of the two fluorophores. This is seen at 400 nm, where the amplitude of AA is expected to be dominant, but a low value was recovered (0.195, Table 5.2). Such variability is typical in the analysis of closely spaced decay times, whether the measurements are performed in the frequency domain or in the time domain.

The uncertainties in the recovered lifetimes is best determined from the χ_R^2 surfaces (Figure 5.32). These surfaces for the mixture of AA and 2-AP are wide due to the closely spaced lifetimes and correlation between the lifetimes and amplitudes. The lack of resolution is especially apparent for observation at 360 nm. In this case the emission is due primarily to just one of the fluorophores (AA). The lifetime of one component can be fixed near 12 ns without an elevation in χ_R^2, even when the dominant lifetime is near 8 ns. This probably occurs because the amplitude of the 12-ns component can be decreased as the new χ_R^2 values are calculated. At observation wavelengths where both AA and 2-AP emit there are modest minima in the χ_R^2 surfaces (Figure 5.32). However, the confidence intervals are large, and in some cases the desired χ_R^2 increase is not reached for any reasonable value of the decay times. The confidence intervals, which are the range of parameter values consistent with the data, are not symmetrical about the best-fit values.

5.7.3. Global Analysis of a Two-Component Mixture

The resolution of complex intensity decays can be dramatically enhanced by global analysis, which is the simultaneous analysis of multiple data sets measured under slightly different conditions. For the two-component mixture of AA and 2-AP, data were measured for five emission wavelengths (Figure 5.33, 360 to 440 nm). The decay time of each fluorophore is expected to be independent of emission

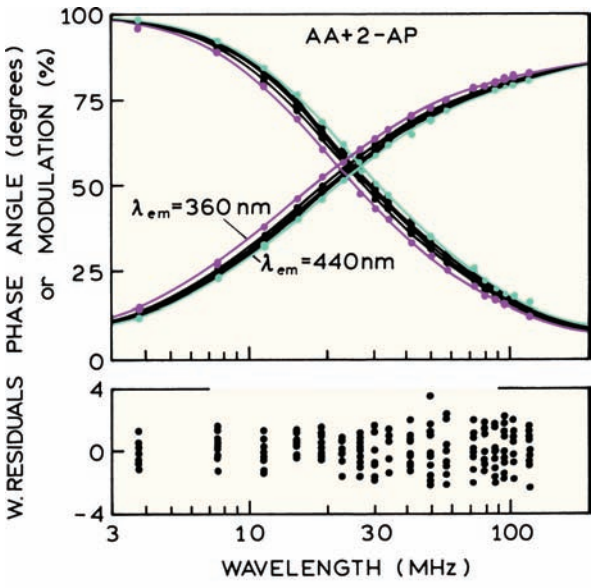

Figure 5.33. Global analysis of the two-component mixtures of AA and 2-AP. From left to right, the data are for 360, 380, 400, 420, and 440 nm. The values of χ_R^2 for the global one- and two-component fits are 37.4 and 1.33, respectively. From [116].

Table 5.3. Global Analysis of a Two-Component Mixture of Anthranilic Acid and 2-Aminopurine Measured at Five Emission Wavelengths[a,b]

Observation wavelength (nm)	2-AP τ_1 = 8.19 ns α_1	2-AP f_1	AA[c] τ_2 = 11.18 ns α_2	AA[c] f_2
360	0.117	0.089	0.883	0.911
380	0.431	0.357	0.569	0.643
400	0.604	0.528	0.396	0.472
420	0.708	0.640	0.292	0.360
440	0.810	0.758	0.190	0.242

[a]Analysis of the data in Figure 5.33. f = 0.2 and δm = 0.005. From [116].

[b]For the one-component fit χ_R^2 = 37.4, for the two-component fit χ_R^2 = 1.33.

[c]Lifetimes assigned to these fluorophores based on measurements of the individual fluorophores (Figure 5.31).

wavelength. Hence the global analysis is performed as described in eqs. 5.13 to 5.15, where the $\alpha_i(\lambda)$ values are assumed to be different at each wavelength, but the τ_i values were assumed to be independent of wavelength.

Results of the global analysis are shown in Figure 5.33 and Table 5.3. The value of χ_R^2 = 37.4 for the one-component fit is easily rejected. Use of the two-component model results in a decrease of χ_R^2 to 1.33. For the global analysis, the frequency responses at each emission wavelength are in good agreement with the calculated curves when using two wavelength-independent decay times. Use of three decay times does not improve χ_R^2, so the two-decay-times model is accepted.

Global analysis results in less uncertainty in the recovered parameters. The lifetime χ_R^2 surfaces from the global analysis are much steeper when calculated using the data at six emission wavelengths (Figure 5.34, ——). The elevated values of χ_R^2 are more significant because of the larger degrees of freedom. For this global analysis there are approximately 200 datapoints, and seven variable parameters. Hence the F statistic is 1.16 (Table 4.4), and the F_ξ value is 1.04 (eq. 5.24). Global analysis also results in improved estimates of the amplitudes. The fractional intensities (f_i) and decay times (τ_i) recovered from the global analysis closely match those expected from the spectral properties of the individual fluorophores (Figure 5.30).

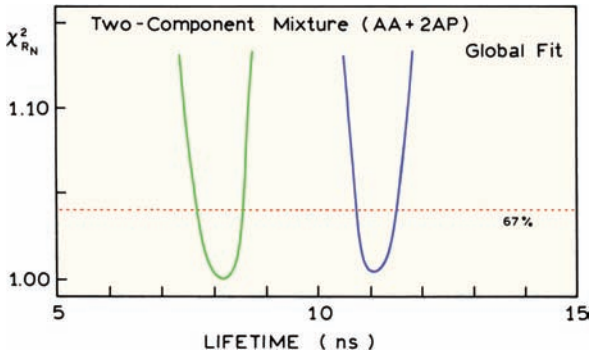

Figure 5.34. Lifetime χ_R^2 surfaces for the mixture of anthranilic acid (AA) and 2-aminopurine (2-AP). The 67% line refers to the F_χ values for global analysis. From [116].

5.7.4. Analysis of a Three Component Mixture: Limits of Resolution

A three-component mixture with less than a threefold range in lifetime represents the practical limit of resolution for both time and frequency domain measurements. Analysis of the data from such a sample illustrates important considerations in data analysis at the limits of resolution. Frequency-domain intensity decay data for the mixture of indole (IN, 4.41 ns), anthranilic acid (AA, 8.53 ns) and 2-aminopurine (2-AP, 11.27 ns) are shown in Figure 5.35. The data cannot be fit to a single decay time, resulting in χ_R^2 = 54.2, so this model is easily rejected. The situation is less clear for the two- and three-decay-time fits, for which the values

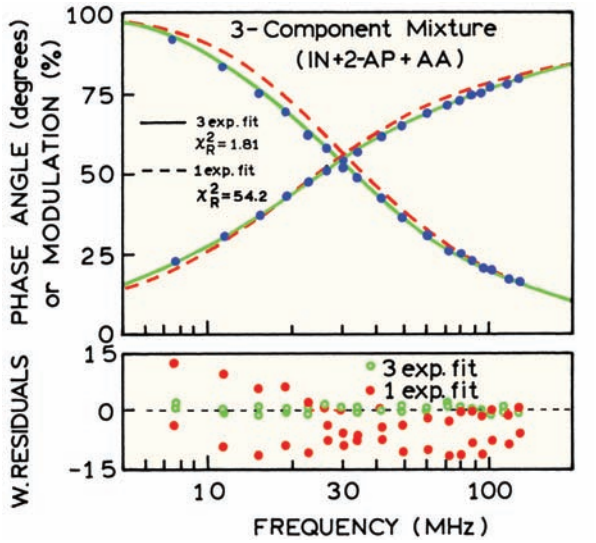

Figure 5.35. Frequency-domain intensity decay for a three-component mixture of indole (IN), 2-aminopurine (2-AP), and anthranilic acid (AA) in water, 20°C, pH 7, observed at 380 nm. The χ_R^2 values for one-, two-, and three-decay-time fits are 54.2, 1.71, and 1.81, respectively. From [116].

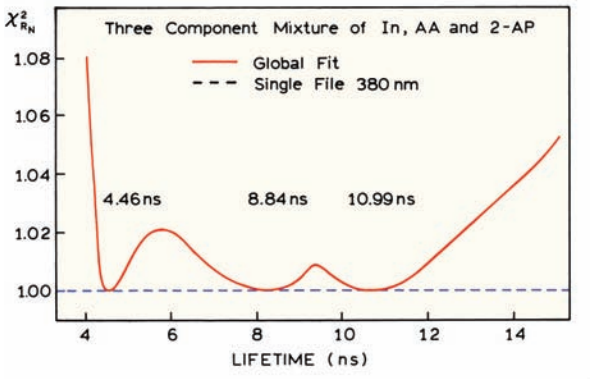

Figure 5.36. Lifetime χ_R^2 surfaces for the three component mixtures of In, AA, and 2-AP; dashed, 380 nm; solid, global fit at 360, 380, 400, 420, and 440 nm. From [116].

of χ_R^2 are 1.71 and 1.81, respectively. At first glance it seems that χ_R^2 has increased for the three-exponential fit. However, the increase in χ_R^2 for the three-decay-time model is a result of the larger number of variable parameters and the smaller number of degrees of freedom. The value of χ^2, which is the sum of the squared deviations, for these three fits is 2006, 59.7, and 59.6, for the one-, two-, and three-decay-time fits. Hence, the fit is not worse for the three-decay-time fit, but is essentially equivalent to the two-decay-time model.

Samples such as this three-component mixture are difficult to analyze. In this case we know there are three decay times, and the three decay times are correctly determined by the analysis. However, obtaining the correct values required that the starting parameter values are close to the correct values. Otherwise, the program stopped at incorrect values, apparently trapped in local χ_R^2 minima. Additionally, the χ_R^2 surface is almost independent of lifetime, as shown in Figure 5.36 for the data measured at 380 nm (dashed). Without prior knowledge of the presence of three decay times, it would be difficult to know whether to accept the two or three decay time fit.

At this point in the analysis there is little reason for proceeding further. If the information is not present in the data, no amount of analysis will create new information. One can either add new experimental data, or add information by restricting parameters based on separate knowledge about the sample. If one or more of the lifetimes are known, these can be held constant during the least-square fit. Similarly, one of the amplitudes could be fixed. However, the best approach is to add new data and perform a global analysis.

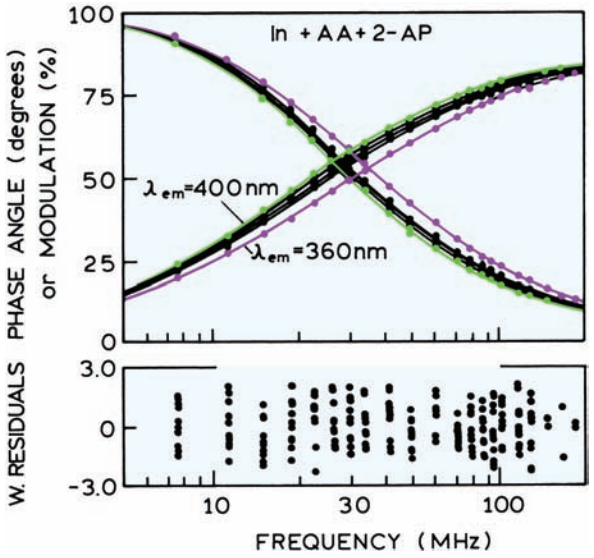

Figure 5.37. Frequency-domain intensity decays of the three-component mixture observed at 360, 380, 400, 420, and 440 nm. The lines are for the best fit to three global decay times and non-global amplitudes. The values of χ_R^2 for the one-, two-, and three-decay-time fit are 109.8, 2.3, and 1.1, respectively. From [116].

The emission from the three-component mixture was measured at five wavelengths: 360, 380, 400, 420 and 440 nm (Figure 5.37). At each wavelength each fluorophore displays the same decay time, but a different fractional amplitude based on its emission spectrum (Figure 5.38). Because of the different amplitudes at each wavelength, the frequency responses are wavelength dependent (Figure 5.37). The

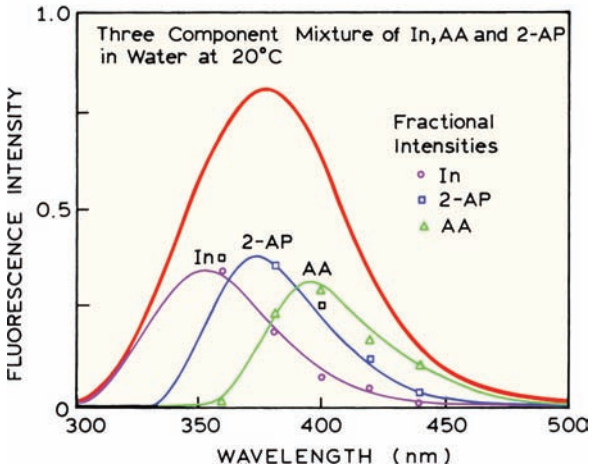

Figure 5.38. Emission spectra of the three-component mixture of indole, anthranilic acid, and 2-aminopurine. Also shown are the fractional intensities recovered from global analysis of the frequency-domain data. From [116].

Table 5.4. Global Analysis of the Frequency-Domain Data for a Three-Component Mixture of Indole, Anthranilic Acid, and 2-Aminopurine[a]

Observation wavelength (nm)	τ_1 = 4.46 ns		τ_2 = 8.84 ns		τ_3 = 10.99 ns	
	α_1	f_1	α_2	f_2	α_3	f_3
360	0.700	0.488	0.008	0.011	0.292	0.501
380	0.434	0.254	0.244	0.282	0.322	0.464
400	0.235	0.123	0.429	0.444	0.336	0.433
420	0.306	0.169	0.430	0.471	0.264	0.360
440	0.219	0.121	0.687	0.752	0.094	0.127

[a]$\delta\phi$ = 0.2 and δm = 0.005. From [116]. χ_R^2 = 1.19, 2.30, and 109.8 for the three-, two-, and one-component fits, respectively.

relative position of these curves can be understood by recognizing that indole (4.41 ns) displays the shortest lifetime and emits towards shorter wavelengths. The mean lifetime is expected to be largest near 380 nm, which is the emission maximum of 2-AP (11.27 ns). The mean lifetime decreases at longer wavelengths as the emission becomes dominated by AA (8.53 ns).

Figure 5.38 and Table 5.4 show the results of global analysis of the wavelength-dependent data. The one- and two-component fits are easily rejected on the basis of the χ_R^2 values of 109.8 and 2.3, respectively, which are both significantly larger than χ_R^2 = 1.2 for the three-decay-time fit. The uncertainties in the parameter values can be found by examining χ_R^2 surfaces (Figure 5.36). For the single-wavelength data at 380 nm the value of χ_R^2 was insensitive to fixing any of the three decay times. When this occurs, recovery of the correct decay times should be regarded as a fortunate coincidence rather than evidence for the resolution obtainable from the data. For the global data the χ_R^2 surfaces display distinct minima at the correct lifetimes, providing good estimates of the values and range consistent with the data. Also, the recovered amplitudes now closely match those expected from the known emission spectra of the fluorophores (Figure 5.38). By performing additional measurements at different wavelengths, and global analysis, a sample that had been unresolvable became a readily resolvable mixture. The magnitude of the χ_R^2 ratio is larger for the more widely spaced decay times. The ratio increases to 1.02 between the 4.46- and 8.84-ns lifetimes, and to only 1.01 between the 8.84 and 10.99-ns lifetimes. This effect illustrates why it is more difficult to resolve more closely spaced lifetimes. Finally, it is interesting to consider the F_χ value appropriate for this analysis. There are approximately 200 datapoints and 13 parameters. The χ_R^2 ratio is 1.15, so F_χ = 1.08. Hence, the confidence intervals overlap for the three lifetimes.

5.7.5. Resolution of a Three-Component Mixture with a Tenfold Range of Decay Times

The ability to resolve a three-component mixture increases rapidly if the decay times are more widely spaced. A mixture with a tenfold range of lifetimes is provided by POPOP (1.32 ns), 9-methylanthracene (4.44 ns), and 9-cyanoanthracene (12.12 ns). The relative value of χ_R^2 decreased 20-fold for the three-decay-time fit relative to the two-decay-time fit (Figure 5.39). For this mixture the calculated phase and modulation values for the two-decay-time model (○) differ systematically from the data, whereas the deviations from the three-decay-time model (●) are randomly distributed (Figure 5.39). In this analysis the value of χ_R^2 = 0.26 for the three-decay-time fit seems too small. This is not an error, but indicates the assumed values of $\delta\phi$ = 0.3 and δm = 0.003 are too large, and that the actual uncertainties are smaller. From these results we see that three decay times with a tenfold range are easily recovered, but three lifetimes with a threefold range are difficult to resolve.

5.7.6. Maximum Entropy Analysis of FD Data

The maximum entropy method (MEM) has also been used to analyze frequency-domain data. However, there are relatively few papers on this topic,[117–121] so it is difficult to judge the usefulness of the MEM for FD data. The published results give the impression that the MEM is less robust with FD data than with TD data, but a detailed comparison has not been published.

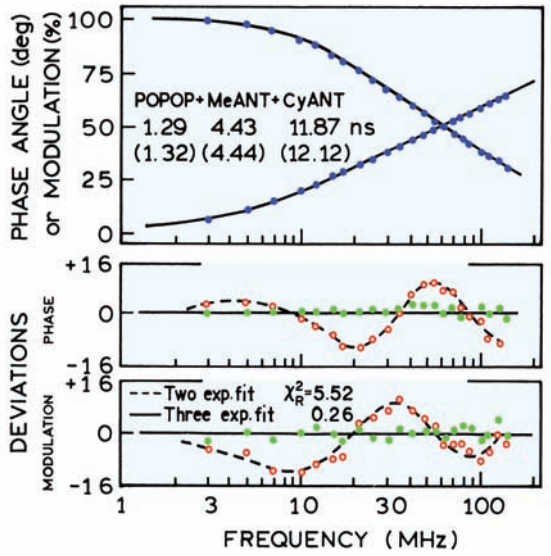

Figure 5.39. Phase and modulation data for a three-component mixture of POPOP, 9-methylanthracene (MeANT), and 9-cyanoanthracene (CyANT) in ethanol at 20°C, in equilibrium with air. The values shown are recovered from the three-component fit, and the values in parentheses are from separate measurement of the pure compounds. The fractional intensities of the three components were equal ($f_1 = f_2 = f_3 = 1/3$). The excitation wavelength was 325 nm and the emission filter a Corning 0-52. The measurements were performed relative to a POPOP reference solution with a reference lifetime of 1.32 ns. $\delta\phi = 0.3°$ and $\delta m = 0.003$. Revised from [13] and reprinted with permission from the Biophysical Society.

5.8. BIOCHEMICAL EXAMPLES OF FREQUENCY-DOMAIN INTENSITY DECAYS

5.8.1. DNA Labeled with DAPI

The probe DAPI (4',6-diamidino-2-phenylindole) is widely used to study DNA.[122–126] DAPI binds to the minor groove of DNA and shows preferential binding to AT-rich regions of DNA. DAPI is only weakly fluorescent in water (Figure 5.40), and displays an increase in quantum yield upon binding to DNA.[126] The increase in quantum yield is minimal for binding to poly d(GC). A more significant enhancement in DAPI fluorescence is found upon binding to DNA containing both GC and AT pairs (circular and linear DNA in Figure 5.40). The largest enhancement of DAPI fluorescence is found for binding of DAPI to poly d(A)-poly d(T) or to poly d(AT). The dependence of DAPI fluorescence on the base composition of DNA suggests that DAPI will display complex decay kinetics when bound to DNA because the DAPI will be near both AT and GC base pairs.

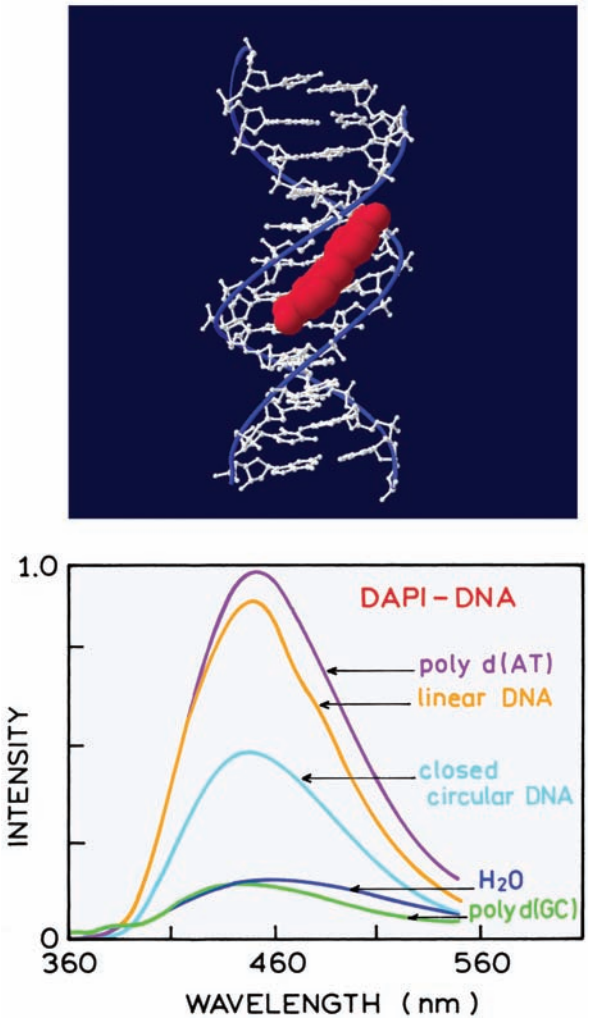

Figure 5.40. **Top**: Structure of a DAPI–DNA complex. **Bottom**: Emission spectra (x20) of DAPI in water at pH 7.1, and complexed with poly d(GC) (x20), closed circular DNA (x10), linear DNA and to polyd (AT). Excitation at 340 nm. Lower panel revised from [126].

Frequency-domain intensity decays of DAPI are shown in Figure 5.41. Excitation was at 325 nm from an HeCd laser. For the intensity decay measurements the entire emission was observed using an RG370 longpass filter. Measurements were performed using POPOP in ethanol as a reference, with a lifetime of 1.35 ns. The frequency responses are visually heterogeneous for DAPI bound to poly d(GC) and to linear DNA, indicating that DAPI is bound in more than one environment with different decay times. The average lifetime is longest when DAPI is bound to poly d(A)-poly d(T), as seen from the frequency response shifted to the lowest frequencies.

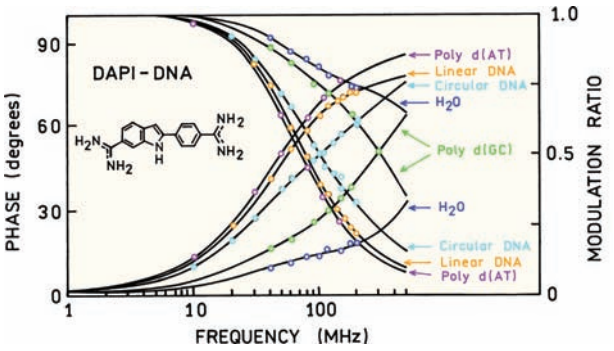

Figure 5.41. Frequency-domain intensity decays of various DNAs labeled with DAPI. DAPI in water at pH 7.1, and complexed with polyd(GC), linear DNA, circular DNA, and AT polymers. The solid lines correspond to the best fits using a double-exponential model. Revised from [126].

The intensity decays could be fit to the two decay time model (Table 5.5). In the absence of DNA, the intensity is dominated by a 0.19-ns component. The decay is nearly unchanged by the presence of poly d(GC), except for an increase in the decay time of the short component to 0.6 ns. Substantial changes in the intensity decay are found upon binding to the other DNAs, where the decays are dominated by a 3.8–3.9-ns component. Linear and closed circular (CC) DNA has both AT and GC base pairs. In these cases the intensity decay is heterogeneous due to the presence of DAPI bound to both types of base pairs. Binding of DAPI to a homogeneous DNA, either poly d(AT) or poly d(A)-poly d(T), results in a homogeneous decay. These results show how the time-resolved decays can be used to learn about the presence of more than one type of binding site for a fluorophore.

As discussed in Section 5.10, the lifetimes calculated from the phase and modulation at a single frequency are only apparent values. The heterogeneous decay of DAPI in water illustrates this effect.[126] For an observation wavelength of 470 nm, and a modulation frequency of 100 MHz, the apparent phase and modulation lifetimes are $\tau_\phi^{app} = 0.47$ ns and $\tau_m^{app} = 1.24$ ns. The fact that $\tau_\phi < \tau_m$ indicates that the decay is heterogeneous.

5.8.2. Mag-Quin-2: A Lifetime-Based Sensor for Magnesium

Ion-sensitive fluorophores are widely used in cell biology to measure intracellular calcium concentrations. While most calcium and magnesium measurements are based on intensity or wavelength-ratiometric measurements, one can also use intensity decay measurements. Lifetime measurements offer the advantage of being independent of the total fluorescence intensity, and can thus be used in fluorescence microscopy where quantitative intensity measurements are difficult. Probes that display changes in lifetime can be used for fluorescence-lifetime imaging microscopy (Chapter 22).

The use of a magnesium probe as lifetime-based sensors requires an understanding of how the decay times change in response to Mg^{2+}. One example is shown in Figure 5.42 for Mag-Quin-2.[127] The mean decay time of Mag-Quin-2 increases from 0.84 ns in the absence of Mg^{2+} to 8.16 ns in the presence of Mg^{2+}. This increase in lifetime results in a dramatic shift of the frequency response to lower frequencies. At intermediate Mg^{2+} concentrations, where Mag-Quin-2 is partially saturated with Mg^{2+}, one can visually see that the frequency response is heterogeneous and one can see the contributions of the short and long decay times of Mag-Quin-2.

Data of the type shown in Figure 5.42 are ideal for a global analysis. The two decay times are expected to be constant at all Mg^{2+} concentrations, and the amplitudes are expected to depend on magnesium. An alternative approach to improving the resolution is to fix the decay times. In this case the lifetimes in the absence and presence of saturating

Table 5.5. Intensity Decays of DAPI Bound to Various DNAs[a]

DNA[b]	τ_1 (ns)	τ_2 (ns)	f_1	f_2
None, in water at pH 7.1[c]	0.19	2.80	0.73	0.27
Poly d(GC)[b]	0.6	2.9	0.71	0.29
CC-DNA[d]	0.4	3.8	0.05	0.95
Linear DNA	0.5	3.8	0.20	0.80
Poly d(AT)	–	3.9	–	1.00
Poly d(A)-poly d(T)	–	3.9	–	1.00

[a]From [126]. The DNA phosphate:DAPI ratio was 60.
[b]The measurements with DNA were at pH 7.2 in 0.1 M tris with 0.1 M NaCl.
[c]DAPI in water at pH 7.1.
[d]Closed circular DNA-CoEl plasmid DNA.

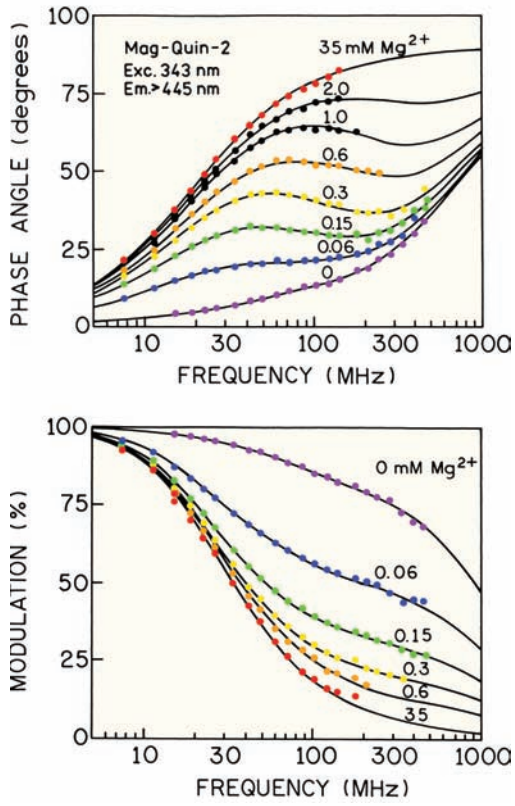

Figure 5.42. Frequency response of the magnesium indicator Mag-Quin-2 with increasing amounts of magnesium. Revised from [127].

Mg^{2+} can be used as known values. Analysis of the frequency-domain data at one Mg^{2+} concentration can then be used to recover the amplitudes with less uncertainty than if the lifetimes were variable parameters.

5.8.3. Recovery of Lifetime Distributions from Frequency-Domain Data

Frequency-domain data can be used to recover lifetime distributions. For a distribution of lifetimes the intensity decay is given by

$$I(t) = \int_0^\infty \alpha(\tau)\ \exp^{(-t/\tau)} \tag{5.25}$$

where the lifetime distribution $\alpha(\tau)$ can be a unimodal or multimodal distribution:

$$\alpha(\tau) = \sum_i \alpha_i(\tau) \tag{5.26}$$

For a lifetime distribution the transforms are given by

$$N_\omega J = \int_{t=0}^{\infty} \int_{\tau=0}^{\infty} \alpha(\tau) e^{-t/\tau} d\tau \sin\omega t\, dt \tag{5.27}$$

$$D_\omega J = \int_{t=0}^{\infty} \int_{\tau=0}^{\infty} \alpha(\tau) e^{-t/\tau} d\tau \cos\ \omega t\, dt \tag{5.28}$$

where

$$J = \int_{\tau=0}^{\infty} \alpha(\tau)\tau\ d\tau \tag{5.29}$$

It is not easy to write analytical expressions for the sine and cosine transforms. Hence, the sine and cosine transforms are calculated numerically. This is not a problem with modern computers, which can rapidly do the required numerical integrations. It is important to recognize that it is difficult to recover all the parameters of a multimodal lifetime distribution, and that in general a lifetime distribution cannot be distinguished from a multi-exponential distribution.[128–129]

5.8.4. Cross-Fitting of Models: Lifetime Distributions of Melittin

When analyzing data in terms of lifetime distribution it is difficult to know is the results are unique. In such cases we suggest cross-fitting of models to determine whether the recovered distributions are statistically different. This procedure is illustrated by the intensity decay of melittin. Frequency-domain data for the single tryptophan protein melittin are shown in Figure 5.43. In a mixture of 20% water and 80% methanol, melittin exists as α-helical monomers. The data could be fit to a bimodal Lorentzian,[130] which is shown in the lower panel of Figure 5.44. The lifetime distributions found for melittin are consistent with the notion of protein structure being an origin of the complex intensity decays of proteins. When dissolved in 6 M guanidine hydrochloride (GuHCl), which eliminates all structure, the intensity decay becomes equivalent to a double exponential decay (Figure 5.44, top). In water, melittin is known to have a small amount of residual structure. Under these conditions one

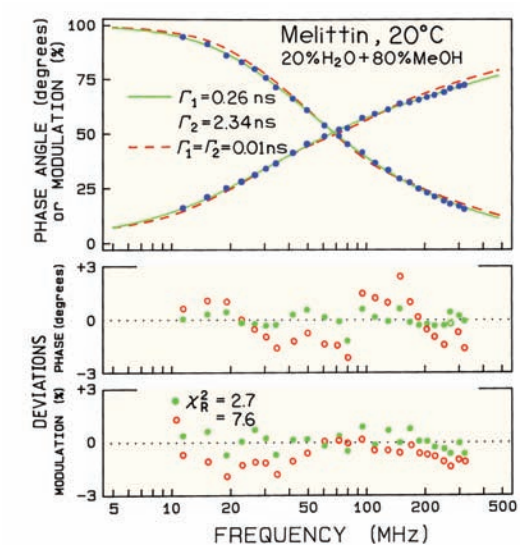

Figure 5.43. Phase and modulation data for synthetic melittin in 20% H_2O + 80% MeOH. The solid line and filled circles show the best fit to a bimodal Lorentzian. The dashed line and open circles show the best fit when the widths of the distribution Γ_1 and Γ_2 were held constant at the narrow value of 0.01 ns. From [130].

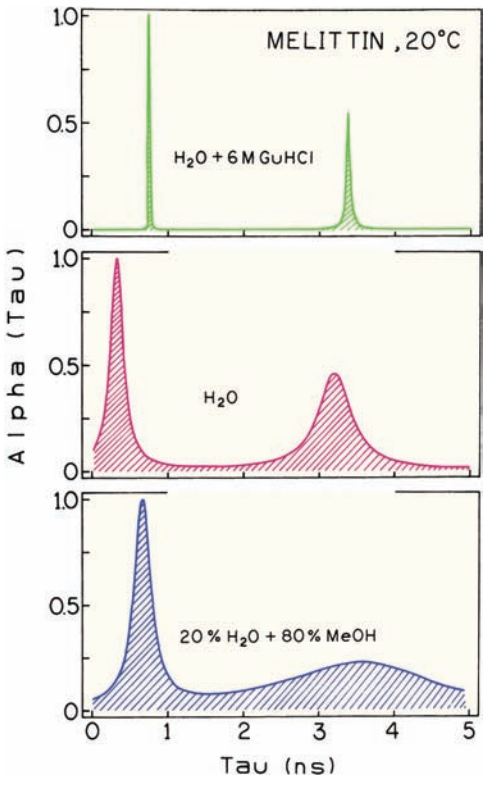

Figure 5.44. Lifetime distributions for synthetic melittin in H_2O with 6 M GuHCl (top), H_2O (middle), and a mixture of 20% H_2O + 80% MeOH (bottom). From [130].

notices that the lifetime distributions become broader (Figure 5.44, middle and lower panels).

While lifetime distributions can be recovered from the FD data, it is important to ask whether the various distributions are distinct within the resolution limits of the data, or cannot be distinguished from the data. We answer this question by fitting the data with some of the fixed parameter values. In this case we asked whether the data for melittin in 80% methanol (broad distribution) could be fit with narrow Lorentzian half widths ($\Gamma_1 = \Gamma_2 = 0.01$ ns). The mean lifetimes and amplitudes of the Lorentzian were still variable parameters. The forced fit results in an approximate threefold elevation of χ_R^2, indicating that the intensity decay of melittin in 80% methanol is not consistent with two lifetimes and narrow distributions. A less rigorous test would be to cross-fit the data with all the parameters fixed, which results in easier rejection of the alternate decay law. The cross-fitting procedure is recommended whenever one is trying to distinguish between two similar models.

5.8.5. Frequency-Domain Fluorescence Microscopy with an LED Light Source

Frequency-domain measurements are finding use in fluorescence microscopy, for both single point measurements[131–135] and for imaging (Chapter 22). Figure 5.45 shows fluorescence images of mouse 3T3 fibroblasts stained with three different fluorophores, with widely varying lifetimes.[134] The images show that an LED can be used as the excitation source for steady-state fluorescence microscopy. Coum-Eu is a europium chelate with a submillisecond decay time. $Ru(bpy)_2phe–C_{12}$ is a lipophilic ruthenium metal–ligand complex and Syto 14 is a nuclear stain. The mean lifetimes of these probes when bound to the fibroblasts were 1.01 ms, 0.95 μs, and 2.57 ns, respectively. These results show that a wide range of decay times can be readily measured using the FD method. In contrast to TCSPC, the FD measurements are not restricted to a small number of photons per time interval, allowing short and long decay times to be measured using the same apparatus.

5.9. PHASE-ANGLE AND MODULATION SPECTRA — Advanced Topic

In all the preceding sections we emphasized FD measurements at a single emission wavelength. When using phase-modulation methods it is also possible to record the phase and modulation data as the emission wavelength is

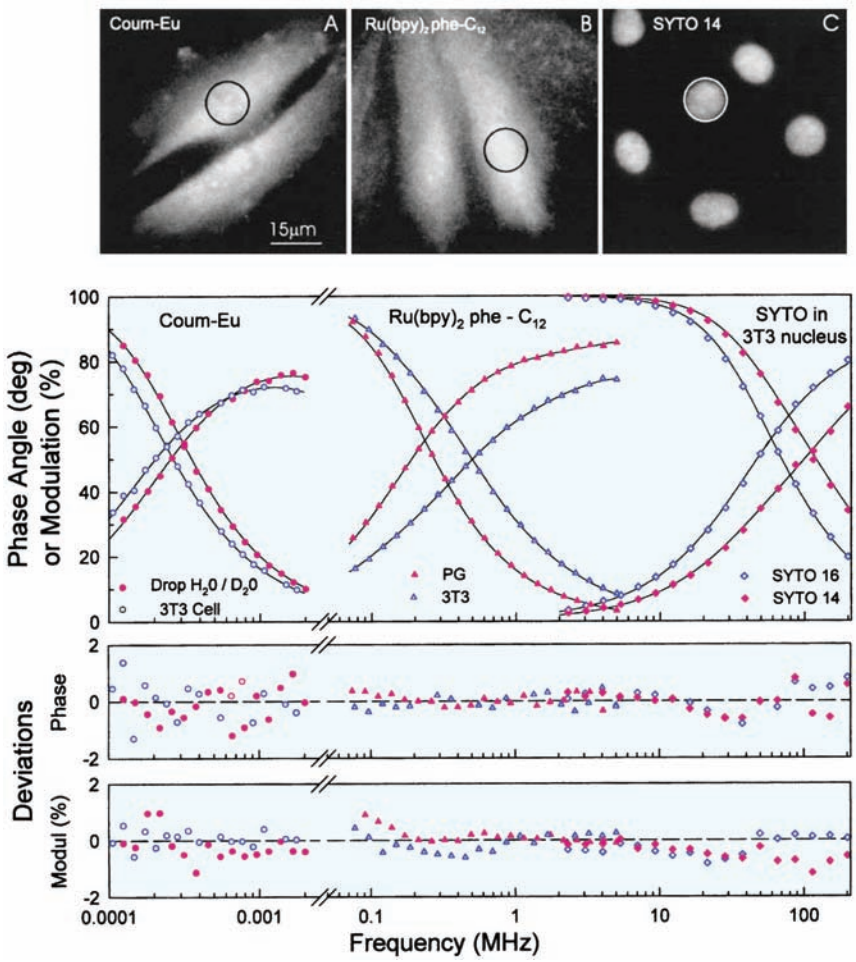

Figure 5.45. Fluorescence images of mouse 3T3 fibroblasts labeled with a europium chelate, a ruthenium metal–ligand complex and syto 14. The lower panels show the frequency responses obtained using a modulated 460 nm LED as the excitation source, in solvents and in cells. Revised from [134].

scanned.[135–136] Such data can be referred to as phase-angle or modulation spectra. Given the stability of modern FD instruments, this procedure is quite reliable. For very short decay times one may need to correct for the wavelength-dependent transit time through the monochromator and/or PMT. For ns-timescale measurements such corrections are not necessary.

The use of phase-modulation spectra can be illustrated by a mixture of fluorophores, acriflavine (ACF, 4.0 ns), and 3-aminofluoranthene (AFA, 11.7 ns) (Figure 5.46). Phase-angle and modulation spectra were recorded using the 325-nm output of an HeCd laser modulated by the Lasermetrics 1024 modulator, and detected through a monochromator with an R928 PMT. Phase and modulation spectra were collected at various modulation frequencies (Figure 5.47). The phase angles increase with wavelength (top) and the modulation decreases (bottom). These effects are due to the increase in mean lifetime as the relative contribution of the 11.7-ns decay time of AFA increases at longer wavelengths.

The phase-modulation spectra can be used to recover the emission spectra and lifetime of each component in the mixture. This is accomplished by a global analysis of the phase-modulation spectra measured at various frequencies. Except for a change in the nature of the data files, the analysis is performed according to eqs. 5.12 to 5.15. The emission spectra associated with each fluorophore can be calculated from the recovered values of $\alpha_i(\lambda)$ and the steady-state spectrum of the mixture $I(\lambda)$. The fractional intensity of each fluorophore at wavelength λ is given by

$$f_i(\lambda) = \frac{\alpha_i(\lambda)\,\tau_i}{\sum_j \alpha_j(\lambda)\,\tau_j} \tag{5.30}$$

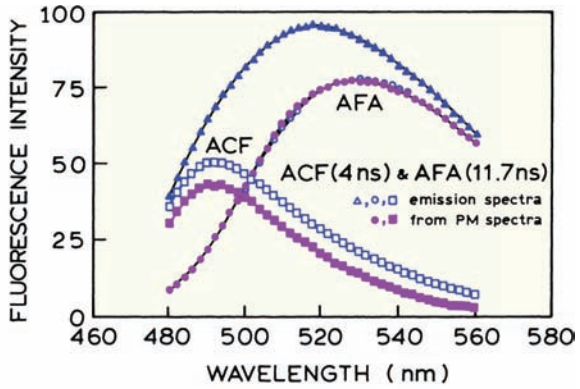

Figure 5.46. Emission spectra and recovered spectra for a mixture of ACF and AFA in propylene glycol at 20°C. Emission spectra are shown for the mixture (closed inverted triangles), of the individual components (open squares, open circles), and recovered from the phase-modulation spectra (closed squares, closed circles). [ACF] = 5 x 10^{-7} M, [AFA] = 2 x 10^{-5} M. Revised and reprinted with permission from [135], Copyright © 1990, American Chemical Society.

and the emission spectrum of each component is given by

$$I_i(\lambda) = f_i(\lambda) I(\lambda) \tag{5.31}$$

The fractional contribution of each fluorophore to the total intensity of the sample is given by

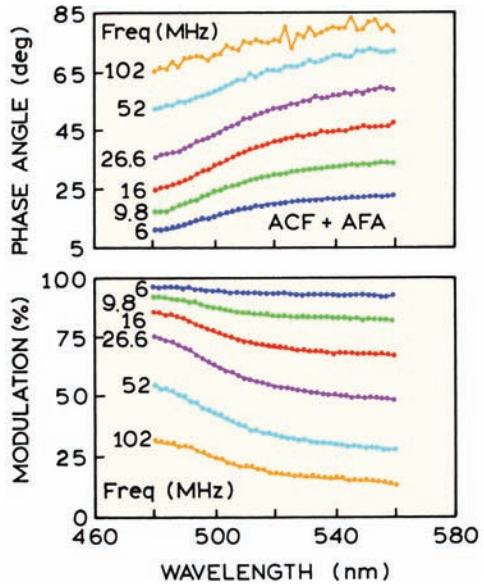

Figure 5.47. Representative phase-angle (top) and modulation spectra (bottom) for a mixture of ACF and AFA. The complete data set consisted of spectra at 20 modulation frequencies. Revised and reprinted with permission from [135], Copyright © 1990, American Chemical Society.

$$F_i = \frac{1}{N} \sum_{\lambda} f_i(\lambda) \tag{5.32}$$

where N is the number of emission wavelengths. The emission spectra recovered from the analysis were in good agreement with those known from the sample preparation (Figure 5.46). For samples such as ACF and AFA there is little advantage in using phase and modulation spectra, as compared with frequency-swept measurements at a single wavelength followed by changing the wavelength. However, phase and modulation spectra can be more convenient if the fluorophores show highly structured emission spectra. In these cases it may be easier to scan wavelength than to measure at discrete wavelengths adequate to determine the individual emission spectra.

5.10. APPARENT PHASE AND MODULATION LIFETIMES

Prior to the availability of variable-frequency instruments most phase-modulation fluorometers operated at one or a few fixed modulation frequencies. During this time it became standard practice to report the apparent phase and modulation lifetimes, which are the values calculated from the data at a single modulation frequency. These values are given by

$$\tau_\phi^{app} = \frac{1}{\omega} \tan \phi_\omega \tag{5.33}$$

$$\tau_m^{app} = \frac{1}{\omega} \left[\frac{1}{m_\omega^2} - 1 \right]^{1/2} \tag{5.34}$$

where we have dropped the indicator of wavelength for simplicity.

There are several characteristics of the phase and modulation lifetimes that are valuable to know.[41,137] The apparent values are equal only if the intensity decay is a single exponential, for which case

$$\tau_\phi^{app} = \tau_m^{app} = \tau \tag{5.35}$$

For multi-exponential or non-exponential decays the apparent phase lifetimes are shorter than the apparent modulation lifetimes ($\tau_\phi^{app} < \tau_m^{app}$). Also, τ_ϕ^{app} and τ_m^{app} generally decrease at higher modulation frequencies. Hence, their

apparent lifetimes depend on the method of measurement, and are not true molecular parameters.

The relationship of τ_ϕ^{app} and τ_m^{app} are most easily seen by consideration of a double exponential decay. Using eqs. 5.7 and 5.8 one obtains

$$N_\omega(\alpha_1\tau_1 + \alpha_2\tau_2) = \frac{\alpha_1\omega\tau_1^2}{1 + \omega^2\tau_1^2} + \frac{\alpha_2\omega\tau_2^2}{1 + \omega^2\tau_2^2} \tag{5.36}$$

$$D_\omega(\alpha_1\tau_1 + \alpha_2\tau_2) = \frac{\alpha_1\tau_1}{1 + \omega^2\tau_1^2} + \frac{\alpha_2\tau_2}{1 + \omega^2\tau_2^2} \tag{5.37}$$

Using eqs. 5.9 and 5.33, the apparent phase lifetime is given by

$$\tau_\phi^{app} = \frac{\Sigma_i\alpha_i\tau_i^2/(1 + \omega^2\tau_i^2)}{\Sigma_i\alpha_i\tau_i/(1 + \omega^2\tau_i^2)} \tag{5.38}$$

Recall that the average lifetime is given by

$$\bar{\tau} = \frac{\Sigma_i\alpha_i\tau_i^2}{\Sigma_j\alpha_j\tau_j} = \Sigma_i f_i\tau_i = \frac{\alpha_1\tau_1^2 + \alpha_2\tau_2^2}{\alpha_1\tau_1 + \alpha_2\tau_2} \tag{5.39}$$

Comparison of eqs. 5.38 and 5.39 shows that in τ_ϕ^{app} each decay time is weighted by a factor $\alpha_i\tau_i/(1 + \omega^2\tau_i^2)$ rather than a factor $\alpha_i\tau_i = f_i$. For this reason the components with shorter decay times are weighted more strongly in τ_ϕ^{app} than in $\bar{\tau}$. Increasing the modulation frequency increases the relative contribution of the short-lived component and hence decreases the value of τ_ϕ^{app}. Using similar reasoning but more complex equations,[41] one can demonstrate that the apparent modulation lifetime is longer than the average lifetime.

An example of the use of apparent phase and modulation lifetimes is given in Figure 5.48, for the mixture of ACF and AFA. This figure shows the phase-angle and modulation spectra in terms of τ_ϕ^{app} and τ_m^{app}. The fact that $\tau_\phi^{app} < \tau_m^{app}$ for a heterogeneous decay is evident by comparison of the upper and lower panels. Also, one immediately notices that the apparent lifetime by phase or modulation depends on modulation frequency, and that higher frequencies result in shorter apparent lifetimes. Hence, the apparent lifetimes depend on the method of measurement (phase or modulation) and on the frequency, and it is difficult to interpret these values in terms of molecular features of the sample.

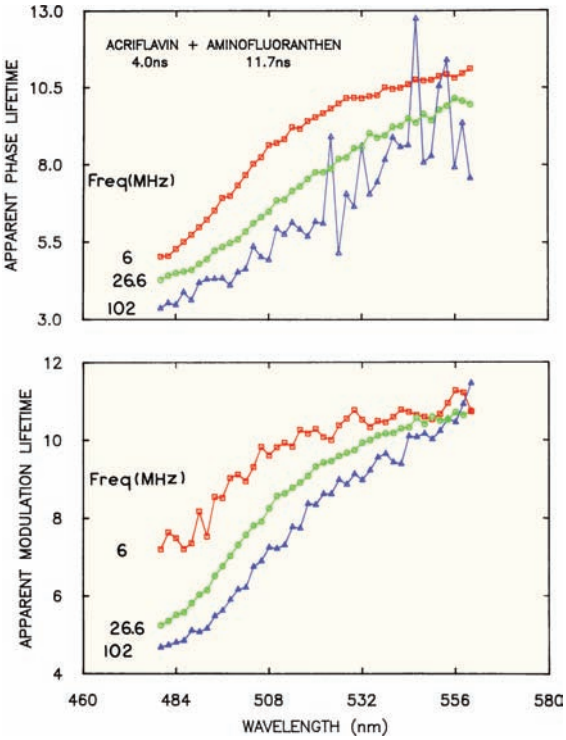

Figure 5.48. Apparent phase (top) and modulation (bottom) lifetimes for a mixture of ACF and AFA. Revised and reprinted with permission from [135], Copyright © 1990, American Chemical Society.

It is always possible to interpret the phase and modulation values in terms of the apparent lifetimes. However, the use of apparent phase and modulation lifetimes is no longer recommended. These are only apparent values that are the result of a complex weighting of the individual decay times and amplitudes, which depend on the experimental conditions. Also, one does not actually measure apparent lifetimes. These values are interpretations of the measurable quantities, which are the phase and modulation values.

Supplemental Material

5.11. DERIVATION OF THE EQUATIONS FOR PHASE-MODULATION FLUORESCENCE

5.11.1. Relationship of the Lifetime to the Phase Angle and Modulation

The equations relating the phase and modulation values to the apparent lifetimes (eqs. 5.3 and 5.4) are widely known,

but the derivation is rarely given. These expressions have been derived by several routes.[41,138–139] The simplest approach uses the kinetic equations and algebraic manipulation.[41,138] The excitation is assumed to be sinusoidally modulated light

$$L(t) = a + b\sin\omega t \tag{5.40}$$

so that $b/a = m_L$ is the modulation of the incident light. The fluorescence emission is forced to respond with the same frequency, but the phase shift and modulation will be different. One can assume the excited-state population is given as follows:

$$N(t) = A + B\sin(\omega t - \phi) \tag{5.41}$$

and determine the relationship between fluorescence lifetime and the phase shift (ϕ) and the demodulation (m). The intensity $I(t)$ at any time is proportional to the number of molecules in the excited state $N(t)$.

Suppose the intensity decay following δ-function excitation is a single exponential:

$$I(t) = I_0 \exp(-t/\tau) \tag{5.42}$$

For a single-exponential decay the differential equation describing the time-dependent excited-state population is

$$\frac{dI(t)}{dt} = -\frac{1}{\tau}I(t) + L(t) \tag{5.43}$$

Substitution of 5.41 into eq. 5.43 yields

$$\omega B\cos(\omega t - \phi) =$$

$$-\frac{1}{\tau}[A + B\sin(\omega t - \phi)] + a + b\sin\omega t \tag{5.44}$$

This equation must be valid for all times. The relationship between the values of a, b, A, and B and the fluorescence lifetime τ can be obtained by expansion of the sine and cosine functions, followed by equating of the constant terms and terms in sin ωt and cos ωt. This yields

$$a - (1/\tau)A = 0 \tag{5.45}$$

$$\omega\cos\phi - (1/\tau)\sin\phi = 0 \tag{5.46}$$

$$\omega\sin\phi + (1/\tau)\cos\phi = b/B \tag{5.47}$$

From eq. 5.46 one obtains the familiar relationship

$$\frac{\sin\phi}{\cos\phi} = \tan\phi = \omega\tau_\phi \tag{5.48}$$

Squaring eqs. 5.46 and 5.47, followed by addition, yields

$$[\omega^2 + (1/\tau)^2] = (b/B)^2 \tag{5.49}$$

Recalling that $A = a\tau$ [eq. 5.45], one obtains

$$m = \frac{B/A}{b/a} = [1 + \omega^2\tau_m^2]^{-1/2} \tag{5.50}$$

which is the usual relationship between the lifetime and the demodulation factor.

An alternative derivation is by the convolution integral.[134] The time-dependent intensity $I(t)$ is given by the convolution of excitation function (eq. 5.40) with the impulse response function (eq. 5.42):

$$I(t) = \int_0^\infty L(t')I(t - t')dt' \tag{5.51}$$

Substitution of eqs. 5.40 and 5.42 yields

$$I(t) = I_0\int_0^\infty \exp(-t'/\tau)\,[a + b\cos(\omega t - \omega t')]dt' \tag{5.52}$$

These integrals can be calculated by recalling the identities

$$\cos(x - y) = \cos x\cos y + \sin x\sin y \tag{5.53}$$

$$\int_0^\infty \exp(-kx)\sin mx\,dx = \frac{m}{k^2 + m^2} \tag{5.54}$$

$$\int_0^\infty \exp(-kx)\cos mx\,dx = \frac{a}{k^2 + m^2} \tag{5.55}$$

Using these identities yields

$$\int_0^\infty \exp(-t'/\tau)\cos\omega(t-t')\,dt' = \tag{5.56}$$

$$= \frac{\tau}{\sqrt{1+\omega^2\tau^2}}\left\{\frac{\cos\omega t}{\sqrt{1+\omega^2\tau^2}} + \frac{\omega t\sin\omega t}{\sqrt{1+\omega^2\tau^2}}\right\} \tag{5.57}$$

$$= \frac{\tau}{\sqrt{1+\omega^2\tau^2}}\cos(\omega t-\phi) \tag{5.58}$$

Equation 5.58 was obtained using

$$\cos\phi = (1+\omega^2\tau^2)^{-1/2} \tag{5.59}$$

$$\tan\phi = \frac{\sin\phi}{\cos\phi} \tag{5.60}$$

Hence, the time dependent intensity is given by

$$I(t) = I_0\tau\left\{a + \frac{b}{\sqrt{1+\omega^2\tau^2}}\cos(\omega t-\phi)\right\} \tag{5.61}$$

This expression shows that the emission is demodulated by a factor $(1+\omega^2\tau^2)^{-1/2}$ relative to the excitation and that the emission is delayed by an angle ϕ relative to the excitation.

5.11.2. Cross-Correlation Detection

The use of cross-correlation detection transforms the high-frequency emission to a low-frequency signal while preserving the meaning of the phase and modulation values. This can be seen by considering the nature of the signals. The high-frequency time-dependent intensity is given by

$$I(t) = I_0[1 + m\cos(\omega t-\phi)] \tag{5.62}$$

This signal is multiplied by the sinusoidal gain modulation of the detector:[138]

$$G(t) = G_0[1 + m_c\cos(\omega_c t+\phi_c)] \tag{5.63}$$

where G_0 is the average value of the function, and m_c, ω_c, and ϕ_c are the modulation, frequency, and phase of the cross-correlation signal. Multiplication of eqs. 5.62 to 5.63 yields

$$S(t) = N_0G_0[1 + m\cos(\omega t+\phi) + m_c\cos(\omega_c t+\phi_c) + mm_c\cos(\omega t+\phi)\cos(\omega_c t+\phi_c)] \tag{5.64}$$

Using trigonometric identities the last term becomes

$$\frac{mm_c}{2}[\cos(\Delta\omega t+\Delta\phi) + \cos(\omega_c t+\omega t+\Delta\phi)] \tag{5.65}$$

where $\Delta\omega = \omega_c - \omega$ and $\Delta\phi = \phi_c - \phi$. The frequencies ω_c and ω typically differ by only a small amount. Hence eq. 5.64 contains a constant term plus terms with frequencies, ω, ω_c, $\omega+\omega_c$, and $\Delta\omega$. The $\Delta\omega$ term contains the phase and modulation information. In the electronic filtering process the constant term and terms in ω, ω_c, and $\omega+\omega_c$ all contribute to average intensity, and the term $\Delta\omega$ determines the phase and amplitude of the low-frequency modulated emission. The presence of the phase and modulation information in the low-frequency signal can also be seen by integration of eqs. 5.62 and 5.63 over one measurement cycle.[41]

5.12. PHASE-SENSITIVE EMISSION SPECTRA

The frequency-domain method also allows several other types of measurement that can be useful in special circumstances. One method is measurement of phase-sensitive intensities and/or emission spectra.[140–143] In phase-sensitive detection of fluorescence (PSDF) the measurements are somewhat different than in frequency-domain fluorometers. In PSDF the emission from the sample is analyzed with a phase-sensitive detector, typically a lock-in amplifier. This measurement procedure selectively attenuates the signal from individual fluorophores on the basis of their fluorescence lifetimes, or more precisely, their phase angles relative to the phase of the detector. PSDF allows the emission from any one species to be suppressed, or, more precisely, the emission with any desired angle to be suppressed. Phase suppression is accomplished when the phase of the detector is 90° shifted from the phase angle of the emission. Then, the resulting phase-sensitive emission spectrum represents only the emission from the remaining fluorophores. For a two-component mixture, suppression of the emission from

one component allows the emission spectrum of the second component to be directly recorded. This procedure is experimentally simple and can be used to record the emission spectra of fluorophores with closely spaced lifetimes. PSDF is frequently used in fluorescence lifetime imaging microscopy (Chapter 22).

5.12.1. Theory of Phase-Sensitive Detection of Fluorescence

A phase fluorometer, when coupled with phase-sensitive detection of fluorescence, can be used in a simple manner to resolve heterogeneous fluorescence. Consider a sample containing a single fluorescent species with a lifetime τ. When excited with sinusoidally modulated light the emission is given by

$$F(t) = 1 + m_L m \sin(\omega t - \phi) \qquad (5.66)$$

where m_L is the modulation of the exciting light. In this equation, m and ϕ are related to the lifetime by eqs. 5.3 and 5.4. Since phase-sensitive spectra are typically measured at a single modulation frequency the subscript ω has been dropped for simplicity. If the sample contains more than one fluorophore then the modulated emission at each wavelength (λ) is given by

$$F(\lambda,t) = \sum_i I_i(\lambda) f_i m_i \sin(\omega t - \phi_i) \qquad (5.67)$$

In this expression $I_i(\lambda)$ are the individual emission spectra, f_i are the fractional intensities to the total steady-state intensity, $\Sigma f_i = 1.0$, m_i is the modulation of the ith component, and ϕ_i is its phase angle. Depending upon the needs of the experiment, the steady-state spectra of each species $I_i(\lambda)$ can be replaced by the steady-state spectra of the sample $I(\lambda)$ and the wavelength-dependent fractional intensities:

$$F(\lambda,t) = I(\lambda) \sum_i f_i(\lambda) m_i \sin(\omega t - \phi_i) \qquad (5.68)$$

In eqs. 5.67 and 5.68 we have assumed that the sample contains discrete lifetimes characterized by m_i and ϕ_i, rather than a non-exponential decay or a lifetime distribution.

Phase-sensitive detection is accomplished by multiplying the emission $F(\lambda,t)$ by a square wave, and integrating the result over time to yield a steady-state intensity.[1–9] The square wave is usually regarded as having a value of 0 or 1 depending on the angle within a single period of 2π (Figure 5.49):

$$\begin{cases} = 0 \text{ from } 0 \text{ to } \phi_D \\ = 1 \text{ from } \phi_D \text{ to } \phi_D + \pi \\ = 0 \text{ from } \phi_D \text{ to } \phi_D + 2\pi \end{cases} \qquad (5.69)$$

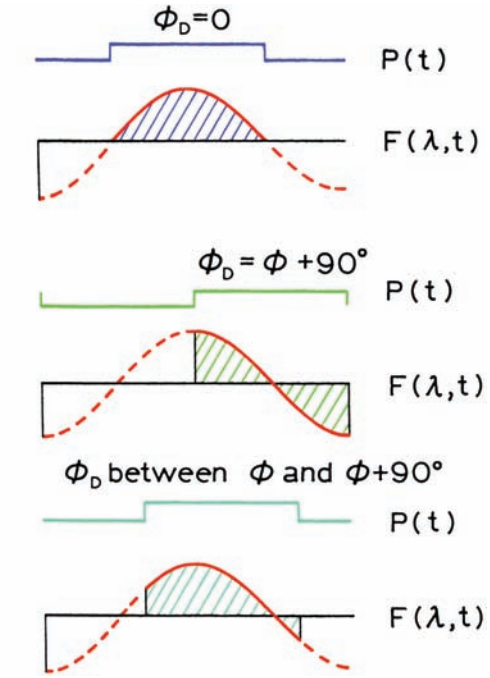

Figure 5.49. Phase-sensitive detection of fluorescence. The detector phase (ϕ_D) can be in phase with the emission $\phi_D = \phi$ (top), out of phase with the emission ($\phi_D = \phi + 90°$, middle), or at some intermediate value (bottom).

Typically the phase angle of the detector (ϕ_D) is varied to integrate the emission over various portions of the 0 to 2π cycle.

The phase-sensitive detector yields a direct current signal proportional to the modulated amplitude and to the cosine of the phase difference between the detector phase ϕ_D and the phase of the sample. If an emission spectrum of a sample containing a single fluorophore (lifetime) is scanned using phase-sensitive detection, one observes a steady-state spectrum whose amplitude depends on the detector phase angle ϕ_D and the phase angle of the fluorophore ϕ_1:

$$F(\lambda, \phi_D) = kF(\lambda) m \cos(\phi_D - \phi_1) \qquad (5.70)$$

where $F(\lambda)$ is the steady-state emission spectrum, λ is the wavelength, and k is a constant that contains the usual sample and instrumental factors and the constant factor m_L. From eq. 5.70 one can predict the appearance of the phase-sensitive spectrum of a single component solution at various detector phase angles. One expects the intensity of the spectra to vary as $\cos(\phi_D - \phi)$, and the spectral distribution to remain unchanged.

The principle and usefulness of phase-sensitive detection is best understood by considering a mixture of two fluorophores, A and B, whose lifetimes (τ_A and τ_B) are each independent of emission wavelength (Figure 5.50). To resolve the spectra of A and B by PSDF the phase angles (ϕ_A and ϕ_B) or lifetimes must be different. We will assume $\tau_A < \tau_B$. The time-dependent emission is given by

$$F(\lambda,t) = F_A(\lambda)m_A \sin(\omega t - \phi_A) + F_B(\lambda)m_B \sin(\omega t - \phi_B) \quad (5.71)$$

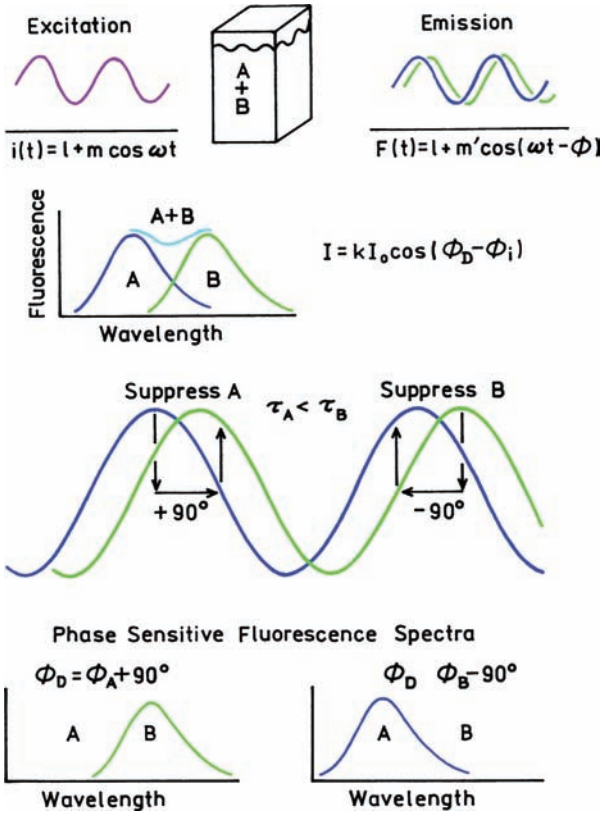

Figure 5.50. Intuitive description of phase-sensitive detection of fluorescence. Reprinted from [140], Copyright © 1981, with permission from Elsevier Science.

where $F_A(\lambda)$ and $F_B(\lambda)$ are the intensities of components A and B at wavelength λ in the steady-state spectrum. An important characteristic of the modulated emission is that it is a superimposition of sine waves of the same frequency but differing phases, each resulting from one of the fluorophores (Figure 5.50). The modulated emission can be conveniently examined with a phase-sensitive detector or lock-in amplifier. The resulting unmodulated signal is given by

$$F(\lambda,\phi_D) = F_A(\lambda)m_A \cos(\phi_D - \phi_A) + F_B(\lambda)m_B \cos(\phi_D - \phi_B) \quad (5.72)$$

For a mixture of two fluorophores one expects the phase-sensitive spectra to contain contributions from both fluorophores, with a fractional contribution dependent on the relative intensities ($F_i(\lambda)$), the modulations (m_i), and, most important, the values of $\phi_D - \phi_i$. The relative contribution of each fluorophore to the phase-sensitive intensity depends on the value of $\cos(\phi_D - \phi_i)$. By selection of $\phi_D - \phi_i = 90°$, the detector can be out of phase with one component in the sample. Then the phase-sensitive spectrum represents the emission spectrum of the other component.

5.12.2. Examples of PSDF and Phase Suppression

Since the initial reports on PSDF, this method has been applied to a variety of samples. These applications are illustrated by two examples: suppression of scattered light and resolution of an excited-state reaction. Scattered light has a zero lifetime, and is thus always out of phase to some extent with the emission. Several laboratories have suggested the use of phase-sensitive detection to suppress scattered light or sample autofluorescence.[145–150] This application is illustrated in Figure 5.51 for a dilute solution of quinine sulfate excited at 355 nm. There is a large peak due to Rayleigh scatter below 370 nm, and a Raman scatter peak at 410 nm. The scattered light could be suppressed by phase-sensitive detection, allowing the emission spectrum of quinine sulfate to be directly recorded.

PSDF can be used to study excited-state reactions, as well as ground state multi-exponential decays.[151–153] This application is illustrated in Figure 5.52 for exciplex formation between anthracene and diethylaniline. In this case the long-wavelength emission forms subsequent to excitation of anthracene, and displays the features of an excited-state reaction. In PSDF it does not matter if the pre-exponential

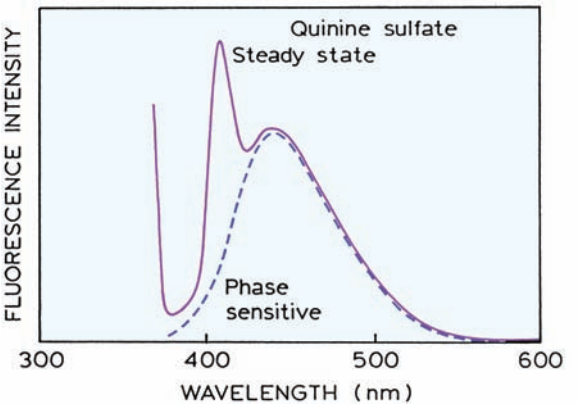

Figure 5.51. Steady-state emission spectrum of quinine sulfate (solid) and the phase-sensitive spectrum with nulling of the scattered light (dashed). Revised from [145].

factors are positive or negative, or if the phase angle exceeds 90°. Adjustment of the detector phase angle to be out of phase with either anthracene or its exciplex allows the emission spectrum of the other species to be recorded (lower panel).

Phase-sensitive spectra of relaxing systems can be informative. PSDF has been used to resolve mixtures of four or more fluorophores[154–159] and to suppress background fluorescence.[160] Phase-sensitive detection has also been used to resolve the emission of fluorophores free in solution and bound to macromolecules,[161–162] and to study binding between antigens and antibodies.[163-165]

5.12.3. High-Frequency or Low-Frequency Phase-Sensitive Detection

To this point we have not described the technical details associated with recording phase-sensitive emission spectra. Do the phase-sensitive spectra need to be recorded using the high-frequency signal prior to cross-correlation,[166] or can phase-sensitive detection be performed using the low-frequency cross-correlation signals? Fortunately, it is not necessary to perform phase-sensitive detection at high frequency. It was found that the modulated emission from individual fluorophores could still be resolved using the low-frequency cross-correlation signals. Such low-frequency detection is easy to perform, and one need not be concerned with the possible perturbation of tuned high-frequency circuits. The reference signal for the phase-sensitive detector is provided by the reference phototube, which observes the emission from a reference fluorophore or scatterer (Figure 5.7). Following selection of the detector phase angle, the phase-sensitive spectra are collected in the usual manner by scanning the emission monochromator.

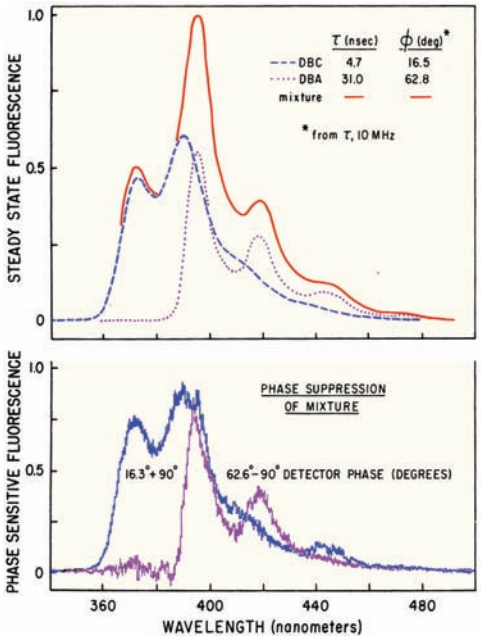

Figure 5.52. Emission spectra of anthracene and its exciplex with diethylaniline. Normalized steady-state spectra are shown in the upper panel. Phase-sensitive fluorescence spectra of anthracene in the presence of diethylaniline are shown in the lower panel. The excitation wavelength was 357 nm, and the excitation and emission bandpasses were 8 nm. The solution was not purged with inert gas. Reprinted from [140], Copyright © 1981, with permission from Elsevier Science.

5.13. PHASE-MODULATION RESOLUTION OF EMISSION SPECTRA

In recent years the use of phase-sensitive detection has diminished, except for its use in lifetime imaging. The phase-sensitive spectra contain less information than the phase angle and modulation spectra. In the time it takes to record the phase-sensitive spectra, one can now record the phase angle and/or modulation across the emission spectra. From these phase-modulation spectra one can compute the phase-resolved spectra.[167–169] Calculation of individual spectra from the phase and modulation spectra has a long history, dating to the early reports by Veselova and coworkers.[170–171] The equations to accomplish these resolutions have been presented in several different forms, which are useful under different circumstances.

5.13.1. Resolution Based on Phase or Modulation Lifetimes

One approach to calculating this phase resolved spectra is based on use of the apparent phase ($\tau_\phi(\lambda)$) or modulation ($\tau_m(\lambda)$) lifetimes at each wavelength.[167] Suppose that the sample contains two species, with fractional steady-state intensities of $f_1(\lambda)$ and $f_2(\lambda)$, and that the two decay times τ_1 and τ_2 are known and are independent of wavelength. Then the ratio of fractional intensities can be calculated from[167]

$$\frac{f_1(\lambda)}{f_2(\lambda)} = \frac{\tau_2 - \tau_\phi(\lambda)}{\tau_\phi(\lambda) - \tau_1}\frac{(1 + \omega^2\tau_1^2)}{(1 + \omega^2\tau_2^2)} \tag{5.73}$$

A similar calculation can be performed using the apparent modulation lifetime:

$$\frac{f_1(\lambda)}{f_2(\lambda)} = \frac{\omega\tau_1 - \left[(1 + \omega^2\tau_1^2)(1 + \omega^2\tau_2^2)/(1 + (\omega\tau_m(\lambda))^2) - 1\right]^{1/2}}{\left[(1 + \omega^2\tau_1^2)(1 + \omega^2\tau_2^2)/(1 + (\tau_m(\lambda))^2) - 1\right]^{1/2} - \omega\tau_2} \tag{5.74}$$

An advantage of this direct calculation procedure is that one can change the assumed values of τ_1 and τ_2 to see how these values affect the calculated spectra. Such further calculations are not possible using the phase-sensitive spectra.

5.13.2. Resolution Based on Phase Angles and Modulations

The equations for spectral resolution based on phase and modulation data can be presented in several ways. For simplicity, we will present these equations for a system with two emitting species. For any decay law the values of $N(\lambda)$ and $D(\lambda)$ are given by[168–169]

$$N(\lambda) = m(\lambda)\sin\phi(\lambda)$$

$$= f_1(\lambda)m_1\sin\phi_1 + f_2(\lambda)\, m_2\sin\phi_2 \tag{5.75}$$

$$D(\lambda) = m(\lambda)\cos\phi(\lambda)$$

$$= f_1(\lambda)m_1\cos\phi_1 + f_2(\lambda)\, m_2\cos\phi_2 \tag{5.76}$$

It is important to understand the meaning of the terms in eqs. 5.74 and 5.75. The values of $m(\lambda)$ and $\phi(\lambda)$ are the experimentally determined data. The values of m_i and ϕ_i are constant terms that will somehow be known or separately measured. If the intensity decay is due to a mixture of fluorophores, each of which displays a single exponential decay, then $m_1 = \cos\phi_1$ and $m_2 = \cos\phi_2$ and

$$N(\lambda) = f_i(\lambda)\sin\phi_1\cos\phi_1 + f_2(\lambda)\sin\phi_2\cos\phi_2 \tag{5.77}$$

$$D(\lambda) = f_i(\lambda)\cos^2\phi_1 + f_2(\lambda)\cos^2\phi_2 \tag{5.78}$$

However, if the decay is non-exponential, then $m_i \pm \cos\phi_i$.

Applications of Cramer's rule to eqs. 5.75 and 5.76, followed by the law for the sine of a difference between two angles, yield

$$f_1(\lambda) = \frac{m(\lambda)\sin(\phi(\lambda) - \phi_2)}{m_1\sin(\phi_1 - \phi_2)} \tag{5.79}$$

$$f_2(\lambda) = \frac{m(\lambda)\sin(\phi_1 - \phi(\lambda))}{m_2\sin(\phi_1 - \phi_2)} \tag{5.80}$$

These expressions were first used by Veselova et al.[170] to calculate the emission spectra of relaxed and unrelaxed fluorophores during spectral relaxation. Alternative forms of eqs. 5.79 and 5.80 can be found by noting that $f_1(\lambda) + f_2(\lambda) = 1.0$:

$$f_1(\lambda) = \frac{m(\lambda)\cos\phi(\lambda) - m_2\cos\phi_2}{m_1\cos\phi_1 - m_2\cos\phi_2} \tag{5.81}$$

$$f_2(\lambda) = \frac{m(\lambda)\cos\phi(\lambda) - m_1\cos\phi_1}{m_2\cos\phi_2 - m_1\cos\phi_1} \tag{5.82}$$

Employing either form of these equations requires knowledge of ϕ_1, ϕ_2, m_1, and m_2, or for a mixture of fluorophores τ_1 and τ_2.

5.13.3. Resolution of Emission Spectra from Phase and Modulation Spectra

Resolution of spectra from the phase and modulation data is illustrated in Figure 5.53. The dashed line shows the emis-

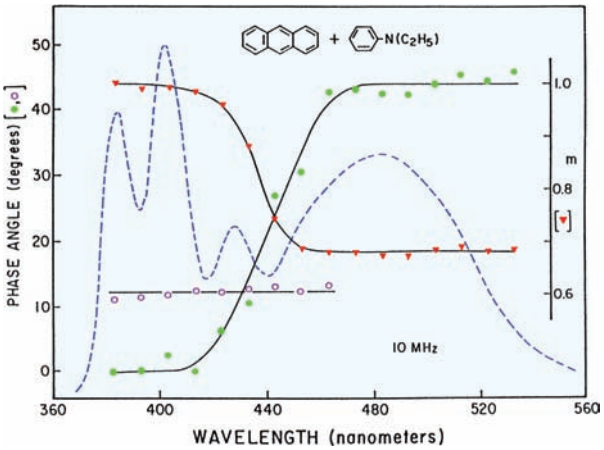

Figure 5.53. Phase angles and demodulation factors for anthracene and its exciplex with diethylaniline. Anthracene was dissolved in toluene and the concentration of diethylaniline was 0.2 M. The excitation was at 357 nm. The solution was not purged with inert gas. Reprinted from [169], Copyright © 1982, with permission from Elsevier Science.

sion spectrum of anthracene in the presence of diethylaniline (DEA). The structured emission is due to anthracene, and the broad long wavelength emission is due to the exciplex formed with DEA. The presence of DEA results in a decrease in the phase angle (●) of anthracene seen near 400 nm and an increased phase angle at long wavelengths where the exciplex emits. The modulation decreases at wavelengths where the exciplex emission contributes to the intensity.

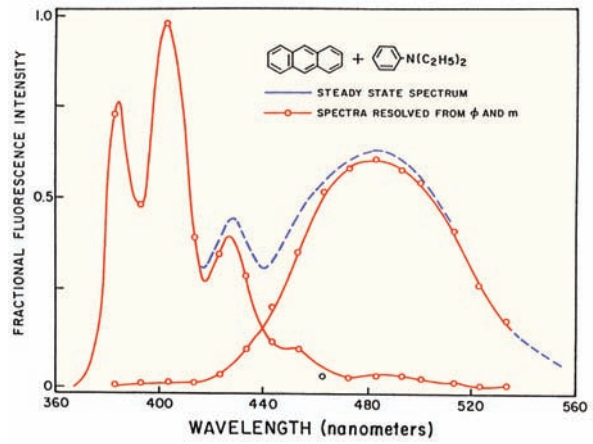

Figure 5.54. Resolution of the monomer and exciplex emission of anthracene. The spectra were calculated using eqs. 5.81 and 5.82 and the data shown in Figure 5.53. Reprinted from [169], Copyright © 1982, with permission from Elsevier Science.

At long and short wavelengths the phase and modulation values are constant, allowing assignment of ϕ_1, ϕ_2, m_1 and m_2. The constant phase angles and modulations indicate the excited-state reaction in a two-state process, rather than a continuous process. In this case of an excited-state reaction it may not be possible to use eqs. 5.73 and 5.74 because the phase angles can exceed 90° and the value of the modulation is not due to a single modulation lifetime. One can use eqs. 5.81 and 5.82 to calculate the fractional intensity at each wavelength. When the $f_i(\lambda)$ values are multiplexed by the steady-state spectrum one can calculate the emission spectra of anthracene and its exciplex (Figure 5.54).

This procedure can also be used when the phase and modulation values do not display constant values on the blue and red sides of the emission. In this case one obtains apparent spectra, whose molecular significance can only be understood with additional information about the sample.[170]

REFERENCES

1. Gratton E, Limkeman M. 1983. A continuously variable frequency cross-correlation phase fluorometer with picosecond resolution. *Biophys J* **44**:315–324.
2. Lakowicz JR, Maliwal BP. 1985. Construction and performance of a variable-frequency phase-modulation fluorometer. *Biophys Chem* **21**:61–78.
3. Lakowicz JR, Gryczynski I. 1991. Frequency-domain fluorescence spectroscopy. In *Topics in fluorescence spectroscopy*. Vol 1: *Techniques*, pp. 293–355. Ed JR Lakowicz. Plenum Press, New York.
4. Gratton E. 1984. The measurement and analysis of heterogeneous emissions by multifrequency phase and modulation fluorometry. *Appl Spectrosc Rev* **20**(1):55–106.
5. Gratton E, Jameson DM, Hall RD. 1984. Multifrequency phase and modulation fluorometry, *Ann Rev Biophys Bioeng* **13**:105–124.
6. Lakowicz JR. 1986. Biochemical applications of frequency-domain fluorometry. In *Applications of fluorescence in the biomedical sciences*, pp. 225–244. Ed D Lansing, AS Waggoner, F Lanni, RF Murphy, RR Birge. Alan R. Liss, New York.
7. Bright FV, Betts TA, Litwiler KS. 1990. Advances in multifrequency phase and modulation fluorescence analysis. *Anal Chem* **21**:389–405.
8. Lakowicz JR. 1985. Frequency-domain fluorometry for resolution of time-dependent fluorescence emission. *Spectroscopy* **1**:28–37.
9. Rabinovich EM, O'Brien M, Srinivasan B, Elliott S, Long X-C, Ravinder KJ. 1998. A compact, LED-based phase fluorimeter-detection system for chemical and biosensor arrays, *SPIE Proc* **3258**:2–10.
10. Bevington PR, Robinson DK. 1992. *Data reduction and error analysis for the physical sciences*. McGraw-Hill, New York.
11. Taylor JR. 1982. *An introduction to error analysis, the study of uncertainties in physical measurements*. University Science Books, Mill Valley, CA.
12. Lakowicz JR, Laczko G, Cherek H, Gratton E, Limkeman M. 1984. Analysis of fluorescence decay kinetics from variable-frequency phase shift and modulation data. *Biophys J* **46**:463–477.

13. Gratton E, Limkeman M, Lakowicz JR, Maliwal B, Cherek H, Laczko G. 1984. Resolution of mixtures of fluorophores using variable-frequency phase and modulation data. *Biophys J* **46**:479–486.
14. Straume M, Frasier-Cadoret SG, Johnson ML. 1991. Least-squares analysis of fluorescence data. In *Topics in fluorescence spectroscopy*. Vol. 2: *Principles*, pp. 177–239. Plenum Press, New York.
15. Johnson ML. 1994. Use of least-squares techniques in biochemistry. *Methods Enzymol* **240**:1–22.
16. Johnson ML, Faunt LM. 1992. Parameter estimation by least-squares methods. *Methods Enzymol* **210**:1–37.
17. Klein UKA. 1984. Picosecond fluorescence decay studied by phase fluorometry and its application to the measurement of rotational diffusion in liquids. *Arabian J Sci Eng* **9**(4):327–344.
18. Gaviola Z. 1926. Ein Fluorometer, apparat zur messung von fluoreszenzabklingungszeiten. *Z Phys* **42**:853–861.
19. Wood RW. 1921. The time interval between absorption and emission of light in fluorescence. *Proc Roy Soc London A* **99**:362–371.
20. Abraham H, Lemoine T. 1899. *C R Hebd Seanas Acad Sci* **129**:206–208. As cited in reference [23].
21. Duschinsky VF. 1933. Der zeitliche intensitatsverlauf von intermittierend angeregter resonanzstrahlung. *Z Phys* **81**:7–22.
22. Szymanowski W. 1935. Verbesserte fluorometermethode zur messung der abklingzeiten der fluoreszensatrahlung. *Z Phys* **95**:440–449.
23. Tumerman LA. 1941. On the law of decay of luminescence of complex molecules. *J Phys (USSR)* **4**:151–166.
24. Maercks VO. 1938. Neuartige fluorometer. *Z Phys* **109**:685–699.
25. Hupfeld VH-H. 1929. Die nachleuchtdauern der J_2-, K_2-, Na_2- und Na-resonanzstrahlung. *Z Phys* **54**:484–497.
26. Schmillen A. 1953. Abklingzeitmessungen an flussigen und festen losungen mit einem neuen fluorometer. *Z Phys* **135**:294–308.
27. Galanin MD. 1950. Duration of the excited state of a molecule and the properties of fluorescent solutions. *Trudy Fiz Inst, Akad Nauk SSSR* **5**:339–386.
28. Birks JB, Little WA. 1953. Photo-fluorescence decay times of organic phosphors. *Proc Phys Soc* **A66**:921–928.
29. Resewitz VE-P, Lippert E. 1974. Ein neuartiges phasenfluorometer. *Ber Bunsenges* **78**:1227-1229.
30. Labhart VH. 1964. Eine experimentelle methode zur ermittlung der singulett-triplett-konversionswahrscheinlichkeit und der triplettspektren von gelosten organischen molekeln messungen an 1,2–benzanthracen. *Fasciculus S* **252**:2279-2288.
31. Bailey EA, Rollefson GK. 1953. The determination of the fluorescence lifetimes of dissolved substances by a phase shift method. *J Chem Phys* **21**:1315–1326.
32. Bonch-Breuvich AM, Kazarin IM, Molchanov VA, Shirokov IV. 1959. An experimental model of a phase fluorometer. *Instrum Exp Technol (USSR)* **2**:231–236.
33. Bauer RK, Rozwadowski M. 1959. A new type of fluorometer: measurements of decay periods of fluorescence of acridine yellow solutions as a function of concentration. *Bull Acad Pol Sci Ser Sci Math Astr Phys* **8**:365–368.
34. Birks JB, Dyson DJ. 1961. Phase and modulation fluorometer. *J Sci Instrum* **38**:282–285.
35. Muller A, Lumry R, Kokubun H. 1965. High-performance phase fluorometer constructed from commercial subunits. *Rev Sci Instrum* **36**:1214–1226.
36. Michelbacher E. 1969. Decay time measurements on pseudo-isocyanine by a phase-fluorometer of 200 Mc modulation frequency. *Z Naturforsch A* **24**:790–796.
37. Demtroder W. 1962. Bestimmung von oszillatorenstarken durch lebensdauermessungen der ersten angeregten niveaus für die elemente Ga, Al, Mg, Tl und Na. *Z Phys* **42**:42–55.
38. Schlag EW, Wessenhoff HV. 1969. Direct timing of the relaxation from selected excited states; beta-naphthylamine. *J Chem Phys* **51**(6):2508–2514.
39. Venetta BD. 1959. Microscope phase fluorometer for determining the fluorescence lifetimes of fluorochromes. *Rev Sci Instrum* **30**(6):450–457.
40. Schaefer VW. 1956. Bestimmung der schwingungsrelaxationszeit in CO/N_2-gasgemischen aus der analyse des frequenzganges eines ultrarot-gasanalysators. *Z Ang Physik* **19**:55–61.
41. Spencer RD, Weber G. 1969. Measurement of subnanosecond fluorescence lifetimes with a cross-correlation phase fluorometer. *Ann NY Acad Sci* **158**:361–376.
42. Debye P, Sears FW. 1932. On the scattering of light by supersonic waves. *Proc Natl Acad Sci USA* **18**:409–414.
43. Lakowicz JR. 1983. *Principles of Fluorescence Spectroscopy*, pp. 76–78. Plenum Press, New York.
44. Hauser M, Heidt G. 1975. Phase fluorometer with a continuously variable frequency. *Rev Sci Instrum* **46**(4):470–471.
45. Salmeen I, Rimal L. 1977. A phase-shift fluorometer using a laser and a transverse electrooptic modulator for subnanosecond lifetime measurements. *Biophys J* **20**:335–342.
46. Menzel ER, Popovic ZD. 1978. Picosecond-resolution fluorescence lifetime measuring system with a cw laser and a radio. *Rev Sci Instrum* **49**(1):39–44.
47. Haar H-P, Hauser M. 1978. Phase fluorometer for measurement of picosecond processes. *Rev Sci Instrum* **49**(5):632–633.
48. Gugger H, Calzaferri G. 1979. Picosecond time resolution by a continuous wave laser amplitude modulation technique, I: a critical investigation. *J Photochem* **13**:21–33.
49. Gugger H, Calzaferri G. 1980. Picosecond time resolution by a continuous wave laser amplitude modulation technique, II: experimental basis. *J Photochem* **13**:295–307.
50. Gugger H, Calzaferri G. 1981. Picosecond time resolution by a continuous wave laser amplitude modulation technique, III: dual-beam luminescence experiment. *J Photochem* **16**:31–41.
51. Baumann J, Calzaferri G. 1983. Development of picosecond time-resolved techniques by continuous-wave laser amplitude modulation, IV: systematic errors. *J Photochem* **22**:297–312.
52. Baumann J, Calzaferri G. 1983. Development of picosecond time-resolved techniques by continuous-wave, V: elimination of r.f. interference problems. *J Photochem* **23**:387–390.
53. Ide G, Engelborghs Y, Persoons A. 1983. Fluorescence lifetime resolution with phase fluorometry. *Rev Sci Instrum* **54**(7):841–844.
54. Kaminov IP. 1984. *An introduction to electrooptic devices*. Academic Press, New York.
55. Wilson J, Hawkes JFB. 1983. *Optoelectronics: an introduction*. Prentice/Hall, London.
56. ISS Inc., Urbana, IL. http://www.ISS.com.
57. McGuinness CD, Sagoo K, McLoskey D, Birch DJS. 2004. A new sub-nanosecond LED at 280 nm: application to protein fluorescence. *Meas Sci Technol* **15**:L1–L4.
58. Fedderson BA, Piston DW, Gratton E. 1989. Digital parallel acquisition in frequency domain fluorimetry. *Rev Sci Instrum* **60**(9):2929–2936.
59. Watkins AN, Ingersoll CM, Baker GA, Bright FV. 1998. A parallel multiharmonic frequency-domain fluorometer for measuring excited-state decay kinetics following one-, two-, or three-photon excitation. *Anal Chem* **70**:3384–3396.
60. Alcala JR. 1991. Comment on "Digital parallel acquisition in frequency domain fluorometry." *Rev Sci Instrum* **62**(6):1672–1673.
61. Barbieri B, De Piccoli F, Gratton E. 1989. Synthesizers' phase noise in frequency-domain fluorometry. *Rev Sci Instrum* **60**(10): 3201–3206.

62. Levy R, Guignon EF, Cobane S, St. Louis E, Fernandez SM. 1997. Compact, rugged and inexpensive frequency-domain fluorometer. *SPIE Proc* **2980**:81–89.
63. Lakowicz JR, Cherek H, Balter A. 1981. Correction of timing errors in photomultiplier tubes used in phase-modulation fluorometry. *J Biochem Biophys Methods* **5**:131–146.
64. Berndt K, Dürr H, Palme D. 1983. Picosecond phase fluorometry and color delay error. *Opt Commun* **47**(5):321–323.
65. Baumann J, Calzaferri G, Forss L, Hungentobler Th. 1985. Wavelength-dependent fluorescence decay: an investigation by multiple-frequency picosecond phase fluorometry. *J Photochem* **28**: 457–473.
66. Pouget J, Mugnier J, Valeur B. 1989. Correction of systematic phase errors in frequency-domain fluorometry. *J Phys E: Sci Instrum* **22**:855–862.
67. Barrow DA, Lentz BR. 1983. The use of isochronal reference standards in phase and modulation fluorescence lifetime measurements. *J Biochem Biophys Methods* **7**:217–234.
68. Thompson RB, Gratton E. 1988. Phase fluorometric method for determination of standard lifetimes. *Anal Chem* **60**:670–674.
69. Lakowicz JR, Jayaweera R, Joshi N, Gryczynski I. 1987. Correction for contaminant fluorescence in frequency-domain fluorometry. *Anal Biochem* **160**:471–479.
70. Reinhart GD, Marzola P, Jameson DM, Gratton E. 1991. A method for on-line background subtraction in frequency domain fluorometry. *J Fluoresc* **1**(3):153–162.
71. Gryczynski I, Malak H. Unpublished observations.
72. Dattelbaum JD, Castellano FN, Gryczynski I, Lakowicz JR. 1998. *Two-photon spectroscopic properties of a mutant green fluorescent protein*. Manuscript in preparation. Biophysical Society Meeting, March 1998. Kansas City, MO, Tu-pos 369.
73. Swaminathan R, Hoang CP, Verkman AS. 1997. Photobleaching recovery and anisotropy decay of green fluorescent protein GFP-S65T in solution and cells: cytoplasmic viscosity probed by green fluorescent protein translational and rotational diffusion. *Biophys J* **72**:1900–1907.
74. Illsley NP, Verkman AS. 1987. Membrane chloride transport measured using a chloride-sensitive fluorescent probe. *Biochemistry* **26**:1215–1219.
75. Verkman AS. 1990. Development and biological applications of chloride-sensitive fluorescent indicators. *Am J Physiol* **253**:C375–C388.
76. Verkman AS, Sellers MC, Chao AC, Leung T, Ketcham R. 1989. Synthesis and characterization of improved chloride-sensitive fluorescent indicators for biological applications. *Anal Biochem* **178**: 355–361.
77. Visser AJWG, van Hoek A. 1981. The fluorescence decay of reduced nicotinamides in aqueous solution after excitation with a UV-mode locked Ar ion laser. *Photochem Photobiol* **33**:35–40.
78. Berndt KW, Gryczynski I, Lakowicz JR. 1990. Phase-modulation fluorometry using a frequency-doubled pulsed laser diode light source. *Rev Sci Instrum* **61**(7):1816–1820.
79. Thompson RB, Frisoli JK, Lakowicz JR. 1992. Phase fluorometry using a continuously modulated laser diode. *Anal Chem* **64**:2075–2078.
80. Sipior J, Carter GM, Lakowicz JR, Rao G. 1996. Single quantum well light-emitting diodes demonstrated as excitation sources for nanosecond phase-modulation fluorescence lifetime measurements. *Rev Sci Instrum* **67**(11):3795–3798.
81. Landgraf S. 2001. Application of semiconductor light sources for investigations of photochemical reactions. *Spectrosc Acta A* **57**:2029–2048.
82. Landgraf S, Grampp G. 1998. Application of laser diodes and ultrabright light-emitting diodes for the determination of fluorescence lifetimes in the nano- and subnanosecond region. *J Inf Rec Mater* **24**:141–148.
83. Landgraf S, Grampp G. 1996. Application of cw-laser diodes for the determination of fluorescence lifetimes. *J Inf Rec Mater* **23**:203–207.
84. Szmacinski H, Chang Q. 2000. Micro- and sub-nanosecond lifetime measurements using a UV light-emitting diode. *Appl Spectrosc* **54**:106–109.
85. Sipior J, Carter GM, Lakowicz JR, Rao G. 1997. Blue light-emitting diode demonstrated as an ultraviolet excitation source for nanosecond phase-modulation fluorescence lifetime measurements. *Rev Sci Instrum* **68**(7):2666–2670.
86. Fantini S, Franceschini MA, Fishkin JB, Barbieri B, Gratton E. 1994. Quantitative determination of the absorption spectra of chromophores in strongly scattering media: a light-emitting diode based technique. *Appl Opt* **33**(22):5204–5213.
87. Berndt KW, Lakowicz JR. 1992. Electroluminescent lamp-based phase fluorometer and oxygen sensor. *Anal Biochem* **201**:319–325.
88. Morgan CG, Hua Y, Mitchell AC, Murray JG, Boardman AD. 1996. A compact frequency domain fluorometer with a directly modulated deuterium light source. *Rev Sci Instrum* **67**(1):41–47.
89. Holavanahali R, Romano MG, Carter GM, Rao G, Sipior J, Lakowicz JR, Bierlein JD. 1996. Directly modulated diode laser frequency doubled in a KTP waveguide as an excitation source for CO_2 and O_2 phase fluorometric sensors. *J Biomed Opt* **1**(1):124–130.
90. Szmacinski H, Lakowicz JR. 1993. Optical measurements of pH using fluorescence lifetimes and phase-modulation fluorometry. *Anal Chem* **65**:1668–1674.
91. Thompson RB, Lakowicz JR. 1993. Fiber optic pH sensor based on phase fluorescence lifetimes. *Anal Chem* **65**:853–856.
92. O'Keefe G, MacCraith BD, McEvoy AK, McDonagh CM, McGilp JF. 1995. Development of an LED-based phase fluorimetric oxygen sensor using evanescent wave excitation of a sol-gel immobilized gel. *Sens Actuators* **29**:226–230.
93. Lippitsch ME, Pasterhofer J, Leiner MJP, Wolfbeis OS. 1988. Fibre-optic oxygen sensor with the fluorescence decay time as the information carrier. *Anal Chim Acta* **205**:1–6.
94. Sipior J, Randers-Eichhorn L, Lakowicz JR, Carter GM, Rao G. 1996. Phase fluorometric optical carbon dioxide gas sensor for fermentation off-gas monitoring. *Biotechnol Prog* **12**:266–271.
95. Cobb WT, McGown LB. 1987. Phase-modulation fluorometry for on-line liquid chromatographic detection and analysis of mixtures of benzo(k)fluoranthene and benzo(b)fluoranthene. *Appl Spectrosc* **41**(8):1275–1279.
96. Cobb WT, McGown LB. 1989. Multifrequency phase-modulation fluorescence lifetime determinations on-the-fly in HPLC. *Appl Spectrosc* **43**(8):1363–1367.
97. Cobb WT, Nithipatikom K, McGown LB. 1988. Multicomponent detection and determination of polycyclic aromatic hydrocarbons using HPLC and a phase-modulation spectrofluorometer. Special Technical Publication, American Society for Testing and Materials, Vol. 1009, pp. 12–25.
98. Szmacinski H, Lakowicz JR. 1994. Lifetime-based sensing. In *Topics in fluorescence spectroscopy*, Vol. 4: *Probe Design and Chemical Sensors*, pp. 295–334. Ed JR Lakowicz. Plenum Press, New York.
99. Merkelo HS, Hartman SR, Mar T, Singhal GS, Govindjee GS. 1969. Mode-locked lasers: measurements of very fast radiative decay in fluorescent systems. *Science* **164**:301–303.
100. Gratton E, Lopez-Delgado R. 1980. Measuring fluorescence decay times by phase-shift and modulation techniques using the high

harmonic content of pulsed light sources. *Nuovo Cimento* **B56**:110–124.
101. Gratton E, Jameson DM, Rosato N, Weber G. 1984. Multifrequency cross-correlation phase fluorometer using synchrotron radiation. *Rev Sci Instrum* **55**:486–494.
102. Gratton E, Delgado RL. 1979. Use of synchrotron radiation for the measurement of fluorescence lifetimes with subpicosecond resolution. *Rev Sci Instrum* **50**(6):789–790.
103. Berndt K, Duerr H, Palme D. 1982. Picosecond phase fluorometry by mode-locked CW lasers. *Opt Commun* **42**:419–422.
104. Gratton E, Barbieri B. 1986. Multifrequency phase fluorometry using pulsed sources: theory and applications. *Spectroscopy* **1**(6): 28–36.
105. Lakowicz JR, Laczko G, Gryczynski I. 1986. 2-GHz frequency-domain fluorometer. *Rev Sci Instrum* **57**(10):2499–2506.
106. Laczko G, Gryczynski I, Gryczynski Z, Wiczk W, Malak H, Lakowicz JR. 1990. A 10-GHz frequency-domain fluorometer. *Rev Sci Instrum* **61**(9):2331–2337.
107. Lakowicz JR, Laczko G, Gryczynski I, Szmacinski H, Wiczk W. 1989. Frequency-domain fluorescence spectroscopy: principles, biochemical applications and future developments. *Ber Bunsenges Phys Chem* **93**:316–327.
108. Lakowicz JR, Laczko G, Gryczynski I, Szmacinski H, Wiczk W. 1988. Gigahertz frequency domain fluorometry: resolution of complex decays, picosecond processes and future developments. *J Photochem Photobiol B: Biol* **2**:295–311.
109. Berndt K, Durr H, Palme D. 1985. Picosecond fluorescence lifetime detector. *Opt Commun* **55**(4):271–276.
110. Berndt K. 1987. Opto-electronic high-frequency cross-correlation using avalanche photodiodes. *Measurement* **5**(4):159–166.
111. Berndt K, Klose E, Schwarz P, Feller K-H, Fassler D. 1984. Time-resolved fluorescence spectroscopy of cyanine dyes. *Z Phys Chem* **265**:1079–1086.
112. Berndt K, Durr H, Feller K-H. 1987. Time resolved fluorescence spectroscopy of cyanine dyes. *Z Phys Chem* **268**:250–256.
113. Lakowicz JR, Gryczynski I, Laczko G, Gloyna D. 1991. Picosecond fluorescence lifetime standards for frequency- and time-domain fluorescence. *J Fluoresc* **1**(2):87–93.
114. Gryczynski I, Szmacinski H, Laczko G, Wiczk W, Johnson ML, Kusba J, Lakowicz JR. 1991. Conformational differences of oxytocin and vasopressin as observed by fluorescence anisotropy decays and transient effects in collisional quenching of tyrosine fluorescence. *J Fluoresc* **1**(3):163–176.
115. Vos R, Strobbe R, Engelborghs Y. 1997. Gigahertz phase fluorometry using a fast high-gain photomultiplier. *J Fluoresc* **7**(1):33S–35S.
116. Gryczynski I. Unpublished observations.
117. Brochon JC, Livesey AK, Pouget J, Valeur B. 1990. Data analysis in frequency-domain fluorometry by the maximum entropy method: recovery of fluorescence lifetime distributions. *Chem Phys Lett* **174**(5):517–522.
118. Shaver JM, McGown LB. 1996. Maximum entropy method for frequency domain fluorescence lifetime analysis, 1: effects of frequency range and random noise. *Anal Chem* **68**:9–17.
119. Shaver JM, McGown LB. 1996. Maximum entropy method for frequency-domain fluorescence lifetime analysis, 2: timing, mismatched intensity, and reference lifetime errors. *Anal Chem* **68**:611–620.
120. He Y, Geng L. 2001. Analysis of heterogeneous fluorescence decays: distribution of pyrene derivatives in an octadecylsilane layer in capillary electrochromatography. *Anal Chem* **73**:5564–5575.
121. Vinogradov SA, Wilson DF. 2000. Recursive maximum entropy algorithm and its application to the luminescence lifetime distribution recovery. *Appl Spectrosc* **54**(6):849–855.
122. Manzini G, Barcellona ML, Avitabile M, Quadrifoglio F. 1983. Interaction of diamidino-2 phenylindole (DAPI) with natural and synthetic nucleic acids. *Nucleic Acids Res* **11**(24):8861–8876.
123. Cavatorta P, Masotti L, Szabo AG. 1985. A time-resolved florescence study of 4',6-diamidino-2-phenylindole dihydrochloride binding to polynucleotides. *Biophys Chem* **22**:11–16.
124. Tanious FA, Veal JM, Buczak H, Ratmeyer LS, Wilson WD. 1992. DAPI (4',6-diamidino-2-phenylindole) binds differently to DNA and RNA: minor-groove binding at AT sites and intercalation at AU sites. *Biochemistry* **31**:3103–3112.
125. Barcellona ML, Gratton E. 1989. Fluorescence lifetime distributions of DNA-4',6-diamidino-2-phenylindole complex. *Biochim Biophys Acta* **993**:174–178.
126. Barcellona ML, Gratton E. 1990. The fluorescence properties of a DNA probe. *Eur Biophys J* **17**:315–323.
127. Szmacinski H, Lakowicz JR. 1996. Fluorescence lifetime characterization of magnesium probes: improvement of Mg^{2+} dynamic range and sensitivity using phase-modulation fluorometry. *J Fluoresc* **6**:83–95.
128. Lakowicz JR, Cherek H, Gryczynski I, Joshi N, Johnson ML. 1987. Analysis of fluorescence decay kinetics measured in the frequency domain using distributions of decay times. *Biophys Chem* **28**:35–50.
129. Alcala JR, Gratton E, Prendergast FG. 1987. Resolvability of fluorescence lifetime distributions using phase fluorometry. *Biophys J* **51**:587–596.
130. Lakowicz JR, Gryczynski I, Wiczk W, Johnson ML. 1994. Distributions of fluorescence decay times for synthetic melittin in water–methanol mixtures and complexed with calmodulin, troponin C, and phospholipids. *J Fluoresc* **4**(2):169–177.
131. Collini M, D'Alfonso L, Baldini G, Oldani A, Cellai L, Giordano C, Barone F, Mazzei F, Chirico G. 2004. Fluorescence anisotropy in the frequency domain by an optical microscope. *Appl Spectrosc* **58**(2):160–165.
132. Despa S, Vecer J, Steels P, Ameloot M. 2000. Fluorescence lifetime microscopy of the Na^+ indicator sodium green in HeLA cells. *Anal Biochem* **281**:159–175.
133. Booth MJ, Wilson T. 2004. Low-cost, frequency-domain, fluorescence lifetime confocal microscopy. *J Microsc* **214**(1):36–42.
134. Herman P, Maliwal BP, Lin H-J, Lakowicz JR. 2001. Frequency-domain fluorescence microscopy with the LED as a light source. *J Microsc* **203**(2):176–181.
135. Lakowicz JR, Jayaweera R, Szmacinski H, Wiczk W. 1990. Resolution of multicomponent fluorescence emission using frequency-dependent phase angle and modulation spectra. *Anal Chem* **62**:2005–2012.
136. Lakowicz JR, Jayaweera R, Szmacinski H, Wiczk W. 1989. Resolution of two emission spectra for tryptophan using frequency-domain phase-modulation spectra. *Photochem Photobiol* **50**(4):541–546.
137. Kilin SF. 1962. The duration of photo- and radioluminescence of organic compounds. *Opt Spectrosc* **12**:414–416.
138. Jameson DM, Gratton E, Hall RD. 1984. The measurement and analysis of heterogeneous emissions by multifrequency phase and modulation fluorometry. *Appl Spectrosc Rev* **20**(1):55–106.
139. Ware WR. 1971. Transient luminescence measurements. In *Creation and detection of the excited state*, pp. 213–302. Ed AA Lamola. Marcel Dekker, New York.

140. Lakowicz JR, Cherek H. 1981. Phase-sensitive fluorescence spectroscopy: a new method to resolve fluorescence lifetimes or emission spectra of components in a mixture of fluorophores. *J Biochem Biophys Methods* **5**:19–35.
141. Lakowicz JR, Cherek H. 1981. Resolution of heterogeneous fluorescence from proteins and aromatic amino acids by phase-sensitive detection of fluorescence. *J Biol Chem* **256**:6348–6353.
142. Lakowicz JR, Cherek H. 1982. Resolution of heterogeneous fluorescence by phase-sensitive fluorescence spectroscopy. *Biophys J* **37**:148–150.
143. Jameson DM, Gratton E, Hall RD. 1984. The measurement and analysis of heterogeneous emissions by multifrequency phase and modulation fluorometry. *Appl Spectrosc Rev* **20**(1):55–106.
144. McGown L, Bright F. 1984. Phase-resolved fluorescence spectroscopy. *Anal Chem* **56**(13):1400–1415.
145. Fugate RD, Bartlett JD, Mattheis JR. 1984. Phase-resolution in spetrofluorometric measurements: applications to biochemical systems. *BioTechniques* **2**(3):174–180.
146. Demas JN, Keller RA. 1985. Enhancement of luminescence and Raman spectroscopy by phase-resolved background suppression. *Anal Chem* **57**:538–545.
147. Nithipatikom K, McGown LB. 1987. Phase-resolved suppression of scattered light in total luminescence spectra. *Appl Spectrosc* **41**(6):1080–1082.
148. Wirth MJ, Chou S-H. 1988. Comparison of time and frequency domain methods for rejecting fluorescence from raman spectra. *Anal Chem* **60**:1882–1886.
149. Nithipatikom K, McGown LB. 1986. Elimination of scatter background in synchronous excitation spectrofluorometry by the use of phase-resolved fluorescence spectroscopy. *Anal Chem* **58**:3145–3147.
150. Crowell E, Geng L. 2001. Reduction of multiexponential background in fluorescence with phase-sensitive detection. *Appl Spectrosc* **55**(12):1709–1716.
151. Lakowicz JR, Balter A. 1982. Direct recording of the initially excited and the solvent relaxed fluorescence emission spectra of tryptophan by phase-sensitive detection of fluorescence. *Photochem Photobiol* **36**:125–132.
152. Lakowicz JR, Balter A. 1982. Detection of the reversibility of an excited-state reaction by phase-modulation fluorometry. *Chem Phys Lett* **92**(2):117–121.
153. Lakowicz JR, Thompson RB, Cherek H. 1983. Phase fluorometric studies of spectral relaxation at the lipid-water interface of phospholipid vesicles. *Biochim Biophys Acta* **734**:295–308.
154. Nithipatikom K, McGown LB. 1987. Five- and six-component determinations using phase-resolved fluorescence spectroscopy and synchronous excitation. *Appl Spectrosc* **41**(3):395–398.
155. Bright FV, McGown LB. 1986. Three-component determinations using fluorescence anisotropy measurements and wavelength selectivity. *Anal Chem* **58**:1424–1427.
156. Bright FV, McGown LB. 1985. Phase-resolved fluorometric determinations of four-component systems using two modulation frequencies. *Anal Chem* **57**:2877–2880.
157. Bright FV, McGown LB. 1985. Four-component determinations using phase-resolved fluorescence spectroscopy. *Anal Chem* **57**:55–59.
158. Vitense KR, McGown LB. 1987. Simultaneous determination of metals in two-component mixtures with 5-sulfo-8-quinolinol by using phase-resolved fluorimetry. *Anal Chim Acta* **193**:119–125.
159. Nithipatikom K, McGown LB. 1986. Multidimensional data formats for phase-resolved fluorometric multicomponent determinations using synchronous excitation and emission spectra. *Anal Chem* **58**:2469–2473.
160. Bright FV, McGown LB. 1984. Elimination of bilirubin interference in fluorometric determination of fluorescein by phase-resolved fluorescence spectrometry. *Anal Chim Acta* **162**:275–283.
161. Lakowicz JR, Keating S. 1983. Binding of an indole derivative to micelles as quantified by phase-sensitive detection of fluorescence. *J Biol Chem* **258**(9):5519–5524.
162. McGown LB. 1984. Phase-resolved fluoroimetric determination of two albumin-bound fluorescein species. *Anal Chim Acta* **157**:327–332.
163. Nithipatikom K, McGown LB. 1989. Studies of the homogeneous immunochemical determination of insulin by using a fluorescent label. *Talanta* **36**(1/2):305–309.
164. Nithipatikom K, McGown LB. 1987. Homogeneous immunochemical technique for determination of human lactoferrin using excitation transfer and phase-resolved fluorometry. *Anal Chem* **59**:423–427.
165. Tahboub YR, McGown LB. 1986. Phase-resolved fluoroimmunoassay of human serum albumin. *Anal Chim Acta* **182**:185–191.
166. Veselova TV, Cherkasov AS, Shirokov VI. 1970. Fluorometric method for individual recording of spectra in systems containing two types of luminescent centers. *Opt Spectrosc* **29**:617–618.
167. Gratton E, Jameson DM. 1985. New approach to phase and modulation resolved spectra. *Anal Chem* **57**:1694–1697.
168. Lakowicz JR, Balter A. 1982. Theory of phase-modulation fluorescence spectroscopy for excited state processes. *Biophys Chem* **16**:99–115.
169. Lakowicz JR, Balter A. 1982. Analysis of excited-state processes by phase-modulation fluorescence spectroscopy. *Biophys Chem* **16**:117–132.
170. Veselova TV, Limareva LA, Cherkasov AS, Shirokov VI. 1965. Fluorometric study of the effect of solvent on the fluorescence spectrum of 3-amino-N-methylphthalimide. *Opt Spectrosc* **19**:39–43.
171. Limareva LA, Cherkasov AS, Shirokov VI. 1968. Evidence of the radiating-centers inhomogeneity of crystalline anthracene in fluorometric phase spectra. *Opt Spectrosc* **25**:132–134.

PROBLEMS

P5.1. *Calculation of the Decay Time of SPQ from Phase and Modulation Data*: Use the data in Figure 5.15 to calculate the decay times of SPQ at each chloride concentration. For convenience, selected phase and modulation values are listed in Table 5.6. Data can also be read from Figure 5.15.

P5.2. *Determination of Chloride Concentrations with SPQ*: Chloride quenches the fluorescence of SPQ, and this intensity can be used to measure chloride concentrations. Suppose one is measuring SPQ fluorescence in a fluorescence microscope, and that the SPQ concentration is not known. Under these conditions it is difficult to use the intensity values to measure the chloride concentrations. Suggest how the phase or modulation data of SPQ (Figure 5.15) could be used to measure chloride concentrations. Assume that the uncertainties in the phase and modulation values are $\pm 0.2^\circ$ and $\pm 0.5\%$, respectively. What is

Table 5.6. Selected Phase and Modulation Values for the Chloride Probe SPQ[a]

Chloride concentration	Frequency (MHz)	Phase angle (degrees)	Modulation
0	10	57.4	0.538
	100	86.3	0.060
10 mM	10	35.1	0.821
	100	82.2	0.141
30 mM	10	18.0	0.954
	100	73.1	0.286
70 mM	10	9.4	0.988
	100	59.1	0.505

[a]The listed values were interpolated using the measured frequency responses (Figure 5.15).

the expected accuracy in the measured chloride concentrations?

P5.3. *Effect of Heterogeneity on Apparent Phase and Modulation Lifetimes*: Suppose you have samples that display a double-exponential-decay low, with lifetimes of 0.5 and 5.0 ns. In one sample the pre-exponential factors are equal ($\alpha_1 = \alpha_2 = 0.5$), and in the other sample the fractional intensities are equal ($f_1 = f_2 = 0.5$). Calculate the apparent phase and modulation lifetimes for these two decay laws at modulation frequencies of 50 and 100 MHz. Explain the relative values of the apparent lifetimes.

P5.4. *Determination of the Excitation Wavelength*: The steady-state emission spectrum of quinine sulfate shows a Raman scatter peak at 410 nm (Figure 5.51). What is the excitation wavelength?

P5.5. *Attenuation of Phase-Sensitive Spectra*: Assume that the lifetime of quinine sulfate is 20 ns, and the light modulation frequency is 10 MHz (Figure 5.51). What detector phase angle was used to suppress the scattered light? What detector phase angle would yield the highest signal for quinine sulfate? What are the relative values of the quinine sulfate intensity for the maximum intensity and when the scattered light is suppressed?

P5.6. *Resolution of a Free and Protein-Bound Fluorophore*: Assume the fluorescent probe 5-dimethylamino-1-naphthalene sulfonic acid (DNS) binds to bovine serum albumin. Assume further that the yield of DNS increases twofold upon binding, and that the lifetime of the free and bound forms are 5 and 10 ns, respectively. Use the following data to calculate the percentage of DNS free in solution and the percentage bound to BSA in the solution containing equimolar concentrations of DNS and BSA. The modulation frequency is 10 MHz. Also, explain the intensity changes between the first two solutions.

Sample	Phase-sensitive intensity at $\phi_D = 17.4 + 90°$	Phase-sensitive intensity at $\phi_D = 3.21 - 90°$
DNS (10^{-5} M)	0	1.0
DNS (10^{-5} M) plus excess BSA	1.776	0
DNS (10^{-5} M) plus 10^{-5} M BSA	0.886	0.50

P5.7. *Phase-Sensitive Spectra and Spectral Relaxation*: Phase-sensitive emission spectra were obtained for N-acetyl-L-tryptophanamide in propylene glycol at various temperatures (Figure 5.55). These spectra were recorded following adjustment of the detector to suppress the emission on the blue or the red side of the emission. Explain the phase-sensitive spectra in Figure 5.55 in terms of the rates of spectral relaxation.

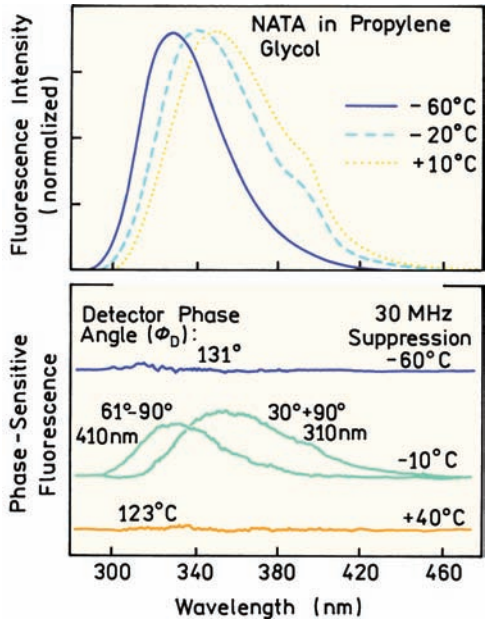

Figure 5.55. Resolution of the initially excited and relaxed states of N-acetyl-L-tryptophanamide by phase-sensitive detection of fluorescence. Excitation was at 280 nm. Emission was observed through a monochromator with a bandpass of 8 nm. Reprinted from [169], Copyright © 1982, with permission from Elsevier Science.